NAVAL POSTGRADUATE SCHOOL

MONTEREY, CALIFORNIA

THESIS

CONJUNCTION OF PHOTOVOLTAIC AND THERMOPHOTOVOLTAIC POWER PRODUCTION IN SPACECRAFT POWER SYSTEMS

by

Matthew J. Thomas

September 2015

Thesis Advisor:	Sherif Michael
Second Reader:	Matthew Porter

Approved for public release; distribution is unlimited

THIS PAGE INTENTIONALLY LEFT BLANK

REPORT DOCUMENTATION PAGE			Form Approved OMB No. 0704-0188
Public reporting burden for this collection of information is estimated to average 1 hour per response, including the time for reviewing instruction, searching existing data sources, gathering and maintaining the data needed, and completing and reviewing the collection of information. Send comments regarding this burden estimate or any other aspect of this collection of information, including suggestions for reducing this burden, to Washington headquarters Services, Directorate for Information Operations and Reports, 1215 Jefferson Davis Highway, Suite 1204, Arlington, VA 22202-4302, and to the Office of Management and Budget, Paperwork Reduction Project (0704-0188) Washington DC 20503.			
1. AGENCY USE ONLY ***(Leave blank)***	**2. REPORT DATE** September 2015	**3. REPORT TYPE AND DATES COVERED** Master's thesis	
4. TITLE AND SUBTITLE CONJUNCTION OF PHOTOVOLTAIC AND THERMOPHOTOVOLTAIC POWER PRODUCTION IN SPACECRAFT POWER SYSTEMS			**5. FUNDING NUMBERS**
6. AUTHOR(S) Thomas, Matthew J.			
7. PERFORMING ORGANIZATION NAME(S) AND ADDRESS(ES) Naval Postgraduate School Monterey, CA 93943-5000			**8. PERFORMING ORGANIZATION REPORT NUMBER**
9. SPONSORING /MONITORING AGENCY NAME(S) AND ADDRESS(ES) N/A			**10. SPONSORING / MONITORING AGENCY REPORT NUMBER**
11. SUPPLEMENTARY NOTES The views expressed in this thesis are those of the author and do not reflect the official policy or position of the Department of Defense or the U.S. Government. IRB Protocol number ____N/A____.			
12a. DISTRIBUTION / AVAILABILITY STATEMENT Approved for public release; distribution is unlimited			**12b. DISTRIBUTION CODE**

13. ABSTRACT (maximum 200 words)

This research examines the potential for the conjunction between photovoltaic (PV) and thermophotovoltaic (TPV) technologies for spacecraft power production. There is sufficient overlap between the sources of energy used for these devices and the function of the devices themselves that either PVs or TPVs could gain improvements in efficiency from the integration of the other type of device, or that a hybrid device could be developed. As a proof of concept, a GaAs PV cell and GaSb TPV cell were modeled in a tandem design using Silvaco ATLAS, with varying PV cell substrate thicknesses, and simulated under the AM0 spectrum to determine the potential range of efficiency gains for a PV device integrated with a TPV device. The same design was then tested under a 2000 K blackbody spectrum—to approximate use in a radioisotope thermoelectric generator (RTG)—to determine if similar efficiency gains could be seen for a TPV device integrated with a PV device. The possible gains with a PV-TPV design under AM0 are clear, potentially resulting in cells with a 30–34% overall efficiency. The possible gains for a PV-TPV device utilizing a blackbody spectrum are less clear, and would benefit from further design and investigation.

14. SUBJECT TERMS photovoltaic, PV, thermophotovoltaic, TPV, gallium arsenide, GaAs, gallium antimonide, GaSb, radioisotope thermoelectric generator, RTG, blackbody spectrum, tandem cell, dual-junction, Silvaco ATLAS			**15. NUMBER OF PAGES** 113
			16. PRICE CODE
17. SECURITY CLASSIFICATION OF REPORT Unclassified	**18. SECURITY CLASSIFICATION OF THIS PAGE** Unclassified	**19. SECURITY CLASSIFICATION OF ABSTRACT** Unclassified	**20. LIMITATION OF ABSTRACT** UU

NSN 7540-01-280-5500

Standard Form 298 (Rev. 2-89)
Prescribed by ANSI Std. 239-18

THIS PAGE INTENTIONALLY LEFT BLANK

Approved for public release; distribution is unlimited

CONJUNCTION OF PHOTOVOLTAIC AND THERMOPHOTOVOLTAIC POWER PRODUCTION IN SPACECRAFT POWER SYSTEMS

Matthew J. Thomas
Lieutenant, United States Navy
B.S., University of Montana, 2006
B.A., University of Montana, 2005

Submitted in partial fulfillment of the
requirements for the degree of

MASTER OF SCIENCE IN SPACE SYSTEMS OPERATIONS

from the

NAVAL POSTGRADUATE SCHOOL
September 2015

Approved by: Sherif Michael. Ph.D.
Thesis Advisor

Matthew Porter
Second Reader

Rudolf Panholzer, Ph.D.
Chair, Space Systems Academic Group

THIS PAGE INTENTIONALLY LEFT BLANK

ABSTRACT

This research examines the potential for the conjunction between photovoltaic (PV) and thermophotovoltaic (TPV) technologies for spacecraft power production. There is sufficient overlap between the sources of energy used for these devices and the function of the devices themselves that either PVs or TPVs could gain improvements in efficiency from the integration of the other type of device, or that a hybrid device could be developed. As a proof of concept, a GaAs PV cell and GaSb TPV cell were modeled in a tandem design using Silvaco ATLAS, with varying PV cell substrate thicknesses, and simulated under the AM0 spectrum to determine the potential range of efficiency gains for a PV device integrated with a TPV device. The same design was then tested under a 2000 K blackbody spectrum—to approximate use in a radioisotope thermoelectric generator (RTG)—to determine if similar efficiency gains could be seen for a TPV device integrated with a PV device. The possible gains with a PV-TPV design under AM0 are clear, potentially resulting in cells with a 30–34% overall efficiency. The possible gains for a PV-TPV device utilizing a blackbody spectrum are less clear, and would benefit from further design and investigation.

THIS PAGE INTENTIONALLY LEFT BLANK

TABLE OF CONTENTS

LIST OF FIGURES

LIST OF TABLES

THIS PAGE INTENTIONALLY LEFT BLANK

LIST OF ACRONYMS AND ABBREVIATIONS

A	area, normally the calculated area of a solar cell
ARC	anti-reflective coating
E_g	energy or band gap
EM	electromagnetic
GaAs	gallium arsenide
GaSb	gallium antimonide
GEO	geostationary orbit
GSO	geosynchronous orbit
GUI	graphical user interface
HD	high doping
HEO	highly elliptical orbit
I	insolation
In	indium
IR	infrared
J	electrical current (sometimes I)
J_{sc}	short-circuit current (sometimes I_{sc})
k	extinction coefficient
K	Kelvin
LD	low doping
LEO	low earth orbit
MEO	medium earth orbit
MOCVD	metalorganic chemical vapor deposition
n	refractive index
NPS	Naval Postgraduate School
NREL	National Renewable Energy Laboratory
P	electrical power
P	phosphorous
PV	photovoltaic

RTG	radioisotope thermoelectric generator
Si	silicon
TCAD	technology computer aided design
TEG	thermoelectric generator
TPV	thermo-photovoltaic
TW	terawatts
USMC	United States Marine Corps
USN	United States Navy
V	voltage
V_{oc}	open-circuit voltage

ACKNOWLEDGMENTS

There are too many people to thank in the brief space available for everything and everyone who has made some contribution to making this work possible, so, though I do not wish to discount the value of any contributions not mentioned here, I must limit myself to those having a direct influence on this works guidance and final accomplishment. First, I would like to thank my thesis advisor, Professor Sherif Michael, for not only garnering my initial interest in the great realm of possibilities associated with photovoltaic technology, but for sharing his immense expertise and guidance while still allowing me to find a line of investigation in this area of research that piqued my interest, and for allowing me the time necessary to investigate the topic to the greatest extent possible. Next, I would like to thank my second reader, Mr. Matthew Porter, who drove me further into the material sciences pertaining to semiconductor devices in general, who's expertise in their modeling was vital to the completion of this work, and who pushed me that one step further, in the overall development of the research, to produce a thesis that was above and beyond what I thought was possible. Last, I would like to thank the faculty and staff of the Space Systems Academic Group—specifically those involved with the Space Systems Operations curriculum—at the Naval Postgraduate School, for providing the educational foundation and directing the justification for this work—which I hope to be of value to the space industry at large—as well as for supporting me through the associated administrative processes. To anyone who reads this, thank you, for your time and attention, and I hope it will be of value to you as well.

THIS PAGE INTENTIONALLY LEFT BLANK

I. INTRODUCTION

A. BACKGROUND

Modern spacecraft power production is dominated by the use of photovoltaic (PV) arrays, which draw electrical energy from the most prominent power source in our solar system, the Sun. These arrays are large, and pose considerable issues with spacecraft control and maneuvering; the larger they are, the more power is required for the spacecraft to maneuver and maintain attitude control. Any potential efficiency gain for these arrays, even as little as 1%, results in significant decrease in the overall array size required, which leads to lower power requirements for maneuvering and attitude control, which in turn leads to the potential for further reduced array size. As the maximum mass that can be sent to any given orbit is limited by current space launch technologies, lower mass requirements in any given spacecraft system, particularly the power system, mean the potential for increased payload mass and functionality. In turn, higher efficiencies in the same size of array also mean more power available for the spacecraft payload, while requiring no or little additional mass, translating to similar potential increases in payload functionality. Thus it can be seen that even a small electrical efficiency increase in PV cell design can result in a cascading improvement to the overall quality or functional potential of a spacecraft.

It is for this reason that various PV cell manufacturers continue to seek even the most minor improvements in efficiency in even the most advanced PV cell designs. Various PV cell technologies have improved in efficiency by as much as 1% from year to year, but many have taken decades to improve a similar amount, and some seem to have leveled off entirely [1]. Increasingly, PV cell designers are looking for ways to merge various technologies or go outside the normal PV design scheme to enhance power production. One potential improvement, associated with developments such as tandem, dual and multi-junction designs, is the use of semiconductor devices with band gaps of a magnitude such that longer wavelengths than PV cells are normally designed to utilize

can be absorbed. Devices that utilize this area of the electromagnetic (EM) spectrum for power production are known as thermo-photovoltaics (TPV) and are not only a relatively new area of exploration in power production, but the use of some materials for TPVs is largely unexplored relative to their use in conjunction with PV materials.

One area where the use of TPVs is being explored vigorously is in relation to radioisotope thermoelectric generators (RTGs), which use heat generated by the decay of radioactive materials to produce electrical power, and are the second most common device used for spacecraft power production. The devices previously utilized for power conversion in these systems, thermo-electric generators (TEGs), require a fairly extreme temperature gradient to operate effectively. Alternatively, the blackbody radiation emitted in these devices can be converted to electricity via TPVs, which have a much higher potential efficiency.

The nature of the majority of photonic energy sources from which either PVs or TPVs draw power is such that the distribution of energy emitted by the source possesses a dominant wavelength, but shows energy distribution across the range of the EM spectrum similar to a normal distribution skewed toward that frequency. This is commonly referred to as a blackbody curve, and this distribution of energy across a black-body curve means that there is a decent quantity of energy distributed across the EM spectrum for any given energy source. A more flexibly designed device employing both PV and TPV technology would not only serve to generate a greater quantity of energy from a given source, but could also be more flexible in the types of sources from which it could generate electricity. Given the consistent drive for improved efficiency in PV power production, and the need for flexible or adaptable power production systems, it would seem clear that this possibility is worthy of investigation.

B. PROBLEM STATEMENT

The commonality between how TPV and PV arrays operate, as well as the potential for improvement for each type of device, involves overall broader access to areas of the EM spectrum normally considered separately or specific to one type of

device or the other, such as visible light being used for PVs and infrared (IR) radiation emitted by the decay of a radioisotope in an RTG being used for TPVs. The fact is that both these areas of the EM spectrum and these technologies have considerable overlap in research and development, and considerable potential for enhancing power production in either type of system. The key to this may simply be the integration of PV and TPV devices into a single PV-TPV cell.

The means for accomplishing this are fairly straightforward, given sufficient knowledge of semiconductor device manufacturing. It essentially involves the layering of one semiconductor device material on top of the other. While there are a variety of manufacturing techniques that could be involved in accomplishing this, they all typically result in one of two major types of design. The first of these is a stacked or tandem design, in which a device composed of one material type is covered by a transparent insulating layer, for electrical isolation, and the other device is then laid on top. This allows power to be generated by the upper device, and then for any EM radiation to which it is transparent to pass through to the lower device. The second major design type is a dual or multi-junction design. This design is essentially a more modern extension of the tandem design in which the semiconductor material layers of one type are deposited or formed directly on top of the other type; though not electrically isolated, per se, the layers are typically separated by two thin intermediary layers of opposite polarity which form a tunnel junction between the two, allowing electrical current to pass through from the upper layers to the lower layers in only one direction.

Given the proper manufacturing facilities, multi-junction designs are typically less expensive to produce than tandem designs; however, their modeling is typically more complex and does not allow for the independent assessment of individual layer or device performance, which can make optimization more difficult. Also, while it may be more expensive to manufacture a tandem design, modeling a tandem design vice a dual-junction design poses no additional cost, and the potential output from a design of a tandem PV, TPV, or PV-TPV cell can be mathematically associated with the potential output for a multi-junction design—where the same cannot be said of a multi-junction

model. To this end, while it might be the more expensive option to manufacture, it would seem that use of a tandem design model would result in the greatest flexibility for overall technology assessment.

C. METHODOLOGY

For the assessment of the potential gains in efficiency and power production to be had by the conjunction of PV and TPV power technologies, a tandem PV-TPV device, in which a PV cell is positioned above a TPV cell, was modeled parametrically using the Silvaco ATLAS technology computer aided design (TCAD) suite to determine the range of potential power output. The material chosen for the PV cell was gallium arsenide (GaAs), which is fairly commonly employed in the PV industry to produce PV cells of relatively high efficiency. The material chosen for the TPV cell was gallium antimonide (GaSb), which has fairly well known and established semiconductor material properties, but has not been widely employed or investigated as a TPV material or as a potential PV material. The assessment of devices modeled using these materials should provide a solid assessment of the potential of PV-TPV devices, as well as a stable overall base from which to draw comparison of future devices employing other materials.

PV and TPV devices were modeled and assessed independently under both the AM1.5 and AM0 spectrums, for validation of the expected output from these models. The devices were then combined into a tandem model for assessment of overall device potential, and various device characteristics such as doping and substrate thickness were varied to determine a range of potential device efficiency and power production, as well as provide a rough approximation of optimal device parameters and an overall assessment of the potential gains from integration of PV and TPV devices. The results of that research are the subject of this thesis, and are provided as follows.

Chapters II and III of this thesis discuss the nature of solar and radioactive energy sources and the means by which the photonic energy from those sources is directly converted to electrical energy, specifically via PVs and TPVs, with some commentary on TEGs—as they are employed in RTGs—and how their performance compares to TPVs.

Chapter IV of this thesis details the modeling software, designs, and assumptions employed in evaluating the potential of PV, TPV, and tandem PV-TPV devices. Chapter V discusses the results of these evaluations, and Chapter VI discusses conclusions drawn from these evaluations and provides recommendations for future work in this area.

THIS PAGE INTENTIONALLY LEFT BLANK

II. ENERGY SOURCES

A. SOLAR RADIATION

The predominant source of energy in our solar system is the sun. In conjunction with the Earth's rotation and the resulting solar gradient, energy from the sun drives thermal atmospheric and ocean currents around the globe. Wind and ocean wave mechanisms have been developed to access the energy that flows through these currents. The cycle of evaporation, atmospheric condensation, precipitation, and water flow across land—commonly referred to as the water cycle—is also driven by solar radiation. Hydroelectric power has been developed to convert the potential energy of water, as it accumulates and cascades through a drainage basin, into kinetic and electric energy. Even fossil fuels are a tertiary conversion of solar energy, having been converted by plants through photosynthesis to carbohydrates and cellulose, sometimes by animals into more carbohydrates and protein, and then being geologically converted by heat, pressure, and time into vast pools and bubbles of hydrocarbons. A bevy of combustion mechanisms and engines, of course, allows us to access this stored energy. One of the most direct methods for converting solar radiation to usable energy, however, is photovoltaics (PV).

The photoelectric effect, the excitement of electrons in a material by incident light, was first discovered in 1839 by Edmund Becquerel [2]. Over the past one-hundred-and-seventy-six years, various endeavors in research and development have transformed this observation into an industry for the design and manufacture of crystalline materials that directly convert the electromagnetic radiation of the sun into electricity.

Terrestrial use of PVs for power production is becoming remarkably widespread, but is still limited in effectiveness by such variables as atmospheric losses of solar irradiance, the terrain, weather, and latitude of the installation, as well as the seasonal cycle and time of day. Figure 1 describes the overall annual impact of some of these variables on direct solar irradiation. The resulting lack of consistency in solar irradiance at any given terrestrial location results in the construction of larger arrays, more extensive

solar energy production facilities, and considerable energy storage facilities to regulate the power available throughout the day, as well as limiting the sites that appear viable for employment of solar technology.

Figure 1. World Map of Direct Normal Solar Irradiation (Insolation)

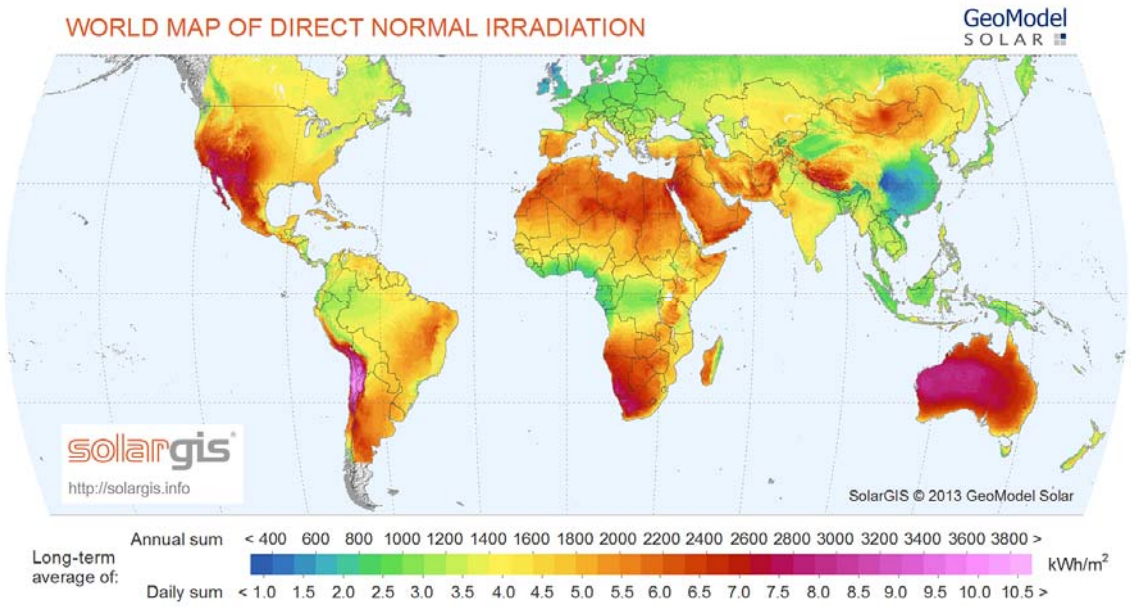

This map describes the considerable variation in annual solar insolation throughout the terrestrial environment. Provided by SolarGIS (solar geographic information system) http://solargis.info/doc/_pics/freemaps/1000px/dni/SolarGIS-Solar-map-DNI-World-map-en.png

By contrast, spacecraft PV power production systems are not so limited. With the exception of spacecraft in low-Earth orbit (LEO)—which frequently pass through the Earth's shadow and have an approximately 60 minute–30 minute day-night cycle—the majority of spacecraft using PV systems, specifically those in geosynchronous, geostationary, and medium earth orbits (GSO, GEO, and MEO, respectively), are able to maintain almost constant power production. Also, the lack of atmospheric losses means that the solar irradiance received by a spacecraft PV system is approximately 30% greater, overall, than that of a terrestrial PV system. The only real limiting factor for a spacecraft PV system is the relationship among the needs of the spacecraft, the lift

capabilities of modern launch systems, and the efficiency of the PV cells used—discussed in depth later—which is the main driver in the overall efficiency of the PV system.

B. RADIOACTIVE DECAY

The second most abundant source of energy in our solar system is heat generated by the decay of radioactive materials. Thirty-eight of the one-hundred-and-eighteen elements on the periodic table are radioactive, and a recent study by the KamLAND Collaboration [3], which employed geo-neutrino flux to determine a more accurate model of the Earth's core, revealed that decay of uranium-238 and thorium-232 may contribute to almost half of the Earth's geothermal heat flux (approximately 20.0 of 44.2 TW). Though this obviously contributes to our use of geothermal energy for heat and electricity production, more direct methods of converting radioactive heat to usable energy have been employed for decades. For example, nuclear power plants use a controlled nuclear reaction, an accelerated form of nuclear decay, to heat water to steam to run a turbine driving an electrical generator. However, direct conversion of heat from spontaneous radioactive decay to electrical energy is the province of thermo-electric generators and thermo-photovoltaics. Both of these technologies have been examined in conjunction with an array of radioactive elements for use in energy production [4], [5], [6], [7].

The process of radioactive decay has simply to do with the breakdown of unstable atoms or unstable isotopes of an atom, through the emission of one of three types of radiation, and the formation of more stable atoms or isotopes thereafter. The three types of radioactive emissions are alpha particles, which are essentially a helium-4 nucleus, beta particles, which are emitted electrons or positrons, and gamma rays, which are extremely high energy photons. Each of these is of progressively higher concern from a safety perspective, as their lower mass or higher energy results in greater potential damage to surrounding materials. As a result, shielding, involving thick layers of dense materials such as lead, through which the radiation will be less likely to penetrate, is typically employed to absorb emitted radiation and protect surrounding personnel and equipment. Electronics are particularly sensitive to radioactive emissions, as the emitted

high energy particles and electrons can cause either permanent damage to micro or nanoscale electronic components or simply cause an upset, or error, in the status or processing of an electronic device. In fact, the abundance of such radiation in the space environment is one of the justifications for the high cost of space-qualified components. These components have to be sufficiently radiation shielded or redundant to survive for the life expectancy of the spacecraft, which can be as much as ten to twenty years.

Despite the apparent concerns over utilizing radioactive materials as a thermal heat source, the practice is not uncommon, particularly in environments or applications where the risk to human health or life is minimal. Some of the more prominent of these applications are as the power source for NASA deep-space craft [8]. These craft are launched for missions sufficiently far from the sun that the intensity of its radiation is significantly diminished, which means a photovoltaic array would need to be ridiculously large relative to the size of the spacecraft in order to provide sufficient power. Likewise, consumable fossil fuel or hydrocarbon sources are of sufficiently low energy density that they cost almost as much, if not more, energy to put into space than they would provide for the space craft, and the volume that could be launched with the craft would not be sufficient to supply it for the duration of its mission. For example, NASA's recently popularized New Horizons mission [9], to Pluto and the Kuiper Belt, was launched in January of 2006, nearly ten years ago, and is expected to operate for at least another five years (through 2020), which is not uncommon for a NASA deep-space mission timeline. The energy density, long life, and consistent energy production of a radioactive heat source make such missions possible.

Radioactive thermal heat sources have even been used by the United States Navy (USN), and investigated for use in forward operating applications by the United States Marine Corps (USMC). Table 1 compares general physical characteristics for various radioactive materials, and Table 2 shows mass and cost comparison statistics for some of the same radioactive elements, the analysis of which was conducted by Langham [4] at NPS in 2013 for a prospective 300 W RTG power supply. It can be seen that some of these elements are more highly available, less expensive, provide a greater power output,

or have a half-life more or less conducive to space applications. Pu-238, one of the radioactive isotopes of Plutonium (Pu), has some of the better characteristics for a long term power supply, and is, in fact the fuel normally used in a NASA deep-space RTG.

Table 1. Radioisotope Data

Isotope	Particle Emitted	Specific Power (W/g)	Density (g/cm3)	Compound Specific Power (W/g)	Half-life (yr)	Cost ($/g)	Availability (kg/100MweY)
Sr-90	Beta	0.96	2.6	0.22	27.7	20	16
Cs-137	Beta/Gamma	0.42	3.42	0.12	30	6.5	36
Po-210	Alpha	141.3	9.298	134	0.379	2800	1
Pu-238	Alpha	0.56	19.86	0.39	87.48	300	15
Cm-242	Alpha	120	13.51	98	0.45	2000	1
Cm-244	Alpha	2.65	13.51	2.27	18.1	170	1
Tm-170	Beta	13.6	9.32	1.2	0.35	136	1
Ru-106	Beta	33.1	12.45	1.1	1	120	2.3
Pm-147	Beta	0.33	7.26	0.27	2.6	75	3.6

This description of characteristics of general concern in relation to a variety of radioactive isotopes is from R. C. Langham. "Feasibility study and system architecture of radioisotope thermoelectric generation power systems for USMC forward operating bases.," M.S. thesis, Dept. Sys. Eng., Naval Postgraduate School, Monterey, CA, 2013

Table 2. Initial Cost and Weight (for a 300 W RTG)

Isotope	Pure isotope mass per 300W (g)	Compound mass per 300W (g)	Estimated cost per 300W ($)	Initial pure mass for 300W at EOL (g)	Initial compound mass for 300W at EOL (g)	Initial estimated cost for 300W at EOL ($)
Sr-90	313	1364	6250	401	1751	8027
Cs-137	714	2500	4642	900	3150	5850
Po-210	2	2	5945	186090003	196227741	521052007084
Pu-238	536	769	160714	580	833	173967
Cm-242	3	3	5000	12231943	14977890	24463887084
Cm-244	113	132	19245	166	194	28225

This table describing the potential mass and cost requirements (as of June 2013) for the radioactive isotope components of a hypothetical 300 W RTG is from R. C. Langham. "Feasibility study and system architecture of radioisotope thermoelectric generation power systems for USMC forward operating bases.," M.S. thesis, Dept. Sys. Eng., Naval Postgraduate School, Monterey, CA, 2013

The heat radiated by these materials can be used in a variety of ways to generate electrical energy, but, the most direct and thereby one of the more efficient ways, is conversion of the blackbody emission of energy proportional to the temperature of the source through the use of thermo-photovoltaics. With selective emitters and thermal concentration techniques, a material radiating sufficient heat could even be used to generate electricity with regular photovoltaics, or a combination of photovoltaics and thermo-photovoltaics.

III. DIRECT ENERGY CONVERSION

A. PHOTOVOLTAICS

Modern photovoltaic cells are essentially large photodiodes intended to maximize the photoelectric effect by increasing the area of the cell exposed to incident light and produce current through the diode and voltage across the diode's p-n junction. They are generally wide, flat, and thin, with a full surface electrical contact on the bottom—which can be mirrored to reflect light back through the cell and generate more current—as well as very thin electrodes on the top—to minimize the light blocked.

As an electrical component, any PV cell has a set of physical characteristics that are used to describe and characterize it, and there are generally agreed upon characteristics that are used throughout PV research and industry to compare them. The more physical of these are the cell's semiconductor materials, including the impurities used to give layers of those materials either an acceptor (P) or donor (N) type, the thickness of the P, N, and other layers, as well as the material, thickness, and arrangement of the devices electrodes. The electrical characteristics are the cells open-circuit voltage (V_{oc}), short-circuit current (J_{sc}), IV-curve, fill-factor, and efficiency. Both the physical and electrical characteristics can be used to compare, and through modeling, optimize various configurations of PV cells.

The electrical characteristics of a PV cell are largely based around the cell's efficiency (η, eta) defined as electrical power out, which is voltage (V) times current (J), divided by the power in, which is based on Insolation (I), or wattage per area of light incident on the cell, and the area of the cell (A).

$$\eta = \frac{P_{out}}{P_{in}}, P_{out} = V * J, P_{in} = I * A_{cell} \quad (1)$$

V_{oc} is the theoretical maximum voltage at which a given PV cell can operate, and J_{sc} is the theoretical maximum current at which a given PV cell can operate. Unfortunately, neither of these two is a practically useful operating parameter, because a

PV cell operating at V_{oc} is also operating with zero current, and a PV cell operating at J_{sc} is operating with zero voltage. The practical range of PV cell voltage and current operation is described by a graph commonly known as its IV-curve, which details the current output from the anode of the cell between zero volts and its V_{oc}, examples of which are provided, for several common PV semiconductor materials, in Figure 2.

Figure 2. IV-Curves for Si, Ge, GaAs, and GaInP Cells.

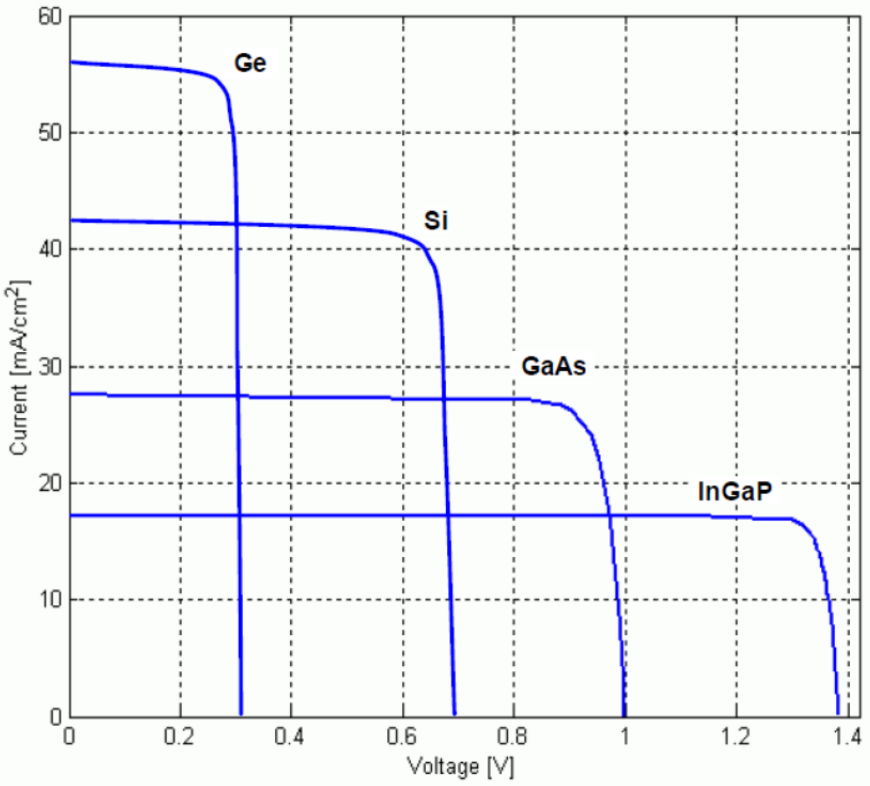

This figure describing the basic IV curves for Germanium (Ge), Silicon (Si), Gallium-Arsenide (GaAs), and Indium-Gallium-Phosphide (InGaP) and demonstrating the variation in J_{sc} and V_{oc} among different semiconductor materials is from P. Michalapoulos. "A novel approach for the development and optimization of state-of-the-art photovoltaic devices using Silvaco," M.S. thesis, Depts. of Com. Sci. and Elec. and Comp. Eng., Naval Postgraduate School, Monterey, CA, 2002

Multiplying the operating voltage on an IV-curve by the associated operating current results in a graph of power over the voltage range for the PV cell. The maximum operating power for the cell, known as P_{Max}, corresponds to a specific voltage and

current, respectively, known as V_{Max} and J_{Max}. These are the ideal operating parameters for a given solar cell, and P_{Max} is generally the described P_{out} from which the PV cell's efficiency is calculated. A PV cell's fill-factor is the area of the IV curve accounted for at P_{Max} and is suggestive of how ideally a cell operates. The IV curve shown in Figure 3, with a graph of Power overlaid on top, graphically demonstrates the relationship among these values.

Figure 3. Sample IV and Power Curves for a Si PV Cell with Other Associated Electrical Parameters

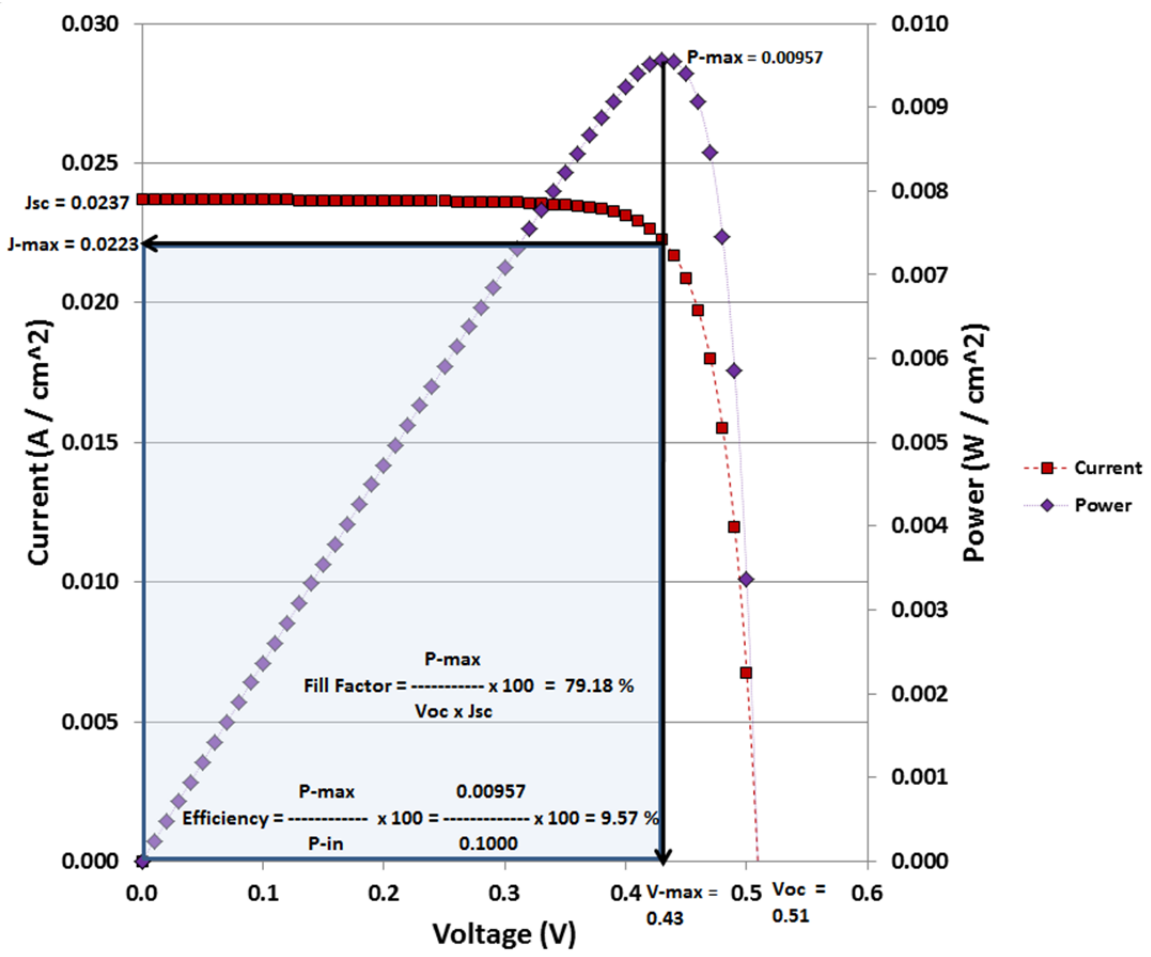

This figure, showing an IV curve overlaid with a Power vs. Voltage curve for a basic Si PV cell, as well as the major electrical characteristics considered representative of a cell's overall performance and how those characteristics are calculated, is from data produced during early model validation for this research

V_{oc} and J_{sc} are somewhat inherent in the semiconductor material or materials utilized in constructing the cell. For example, Silicon (Si) cells generally have a Voc of 0.6 V, and Gallium-Arsenide (GaAs) cells generally have a Voc of 0.9 V. However, even these factors can be varied, within the limitations of the material, by changing the thickness or doping ratio of the semiconductor material. So, the ultimate design of a PV cell can be varied considerably to optimize it for a given application. PV research has led to several general techniques employed to optimize a cell's overall efficiency, largely having to do with countering the major sources of efficiency loss for a PV cell.

One of the greatest potential sources of loss, up to 36%, is reflection of light by the surface of the cell [10]. This is typically countered by the use of an Anti-Reflective Coating (ARC), which is a thin layer of non-conductive material that is transparent at and around the ideal wavelength for that cell. For example, SiO_2 is one potential ARC for silicon solar cells. Though ARCs have been employed in various optics associated industries for quite some time, they continue to be a developing area of research in association with PVs. Modern ARCs can reduce the light reflected by a PV cell's surface to as little as 5% [10]. One part of the losses associated with reflected light is related to light that is at a low angle of incidence to the surface of the PV cell. One solution is the use of a textured surface, to alter average reflective angles of the cells surface. Various implementations of this have led to PV cell efficiency increases as high as 8% [10].

Another major source of loss has to do with the band gap (E_g) of a given semiconductor material. The band gap of a material is the energy necessary to sufficiently excite an electron in the outer shell of its atomic structure such that that electron is free to move through the material. The band gap for conductors is effectively zero and the band gap for insulators tends to be much higher than thermal energy or optical sources can provide. Semiconductors have a band gap that is relatively easily overcome by thermal energy or energy provided by photons; however, there is a minimum energy, the band gap (E_g), required to excite an electron for conduction. Si and GaAs have a E_g of 1.12 eV and 1.42 eV, respectively, which means that a photon with energy lower than that will not have sufficient energy to excite an electron into the material's conductance band. Due to

the differences among their band gaps, different semiconductor materials are only responsive across a certain range of the EM spectrum above the cutoff threshold set by their E_g.

The manufacturing technique addressed to overcoming the limited spectral response of various semiconductor materials is the construction of PV cells with several layers of materials with different band gaps. These cells are known as dual or multi-junction PV cells if the layers are physically integrated or as tandem cells if the layers are physically or electrically isolated. Figures 4 and 5 show the general construction of a multi-junction PV cell, and its associated spectral response. It can be seen that these cells have a much wider range of response to EM energy, and are thus more efficient at converting incident EM energy over a wide range of wavelengths, such as solar radiation.

Figure 4. Sample Multi-Junction PV Cell Design.

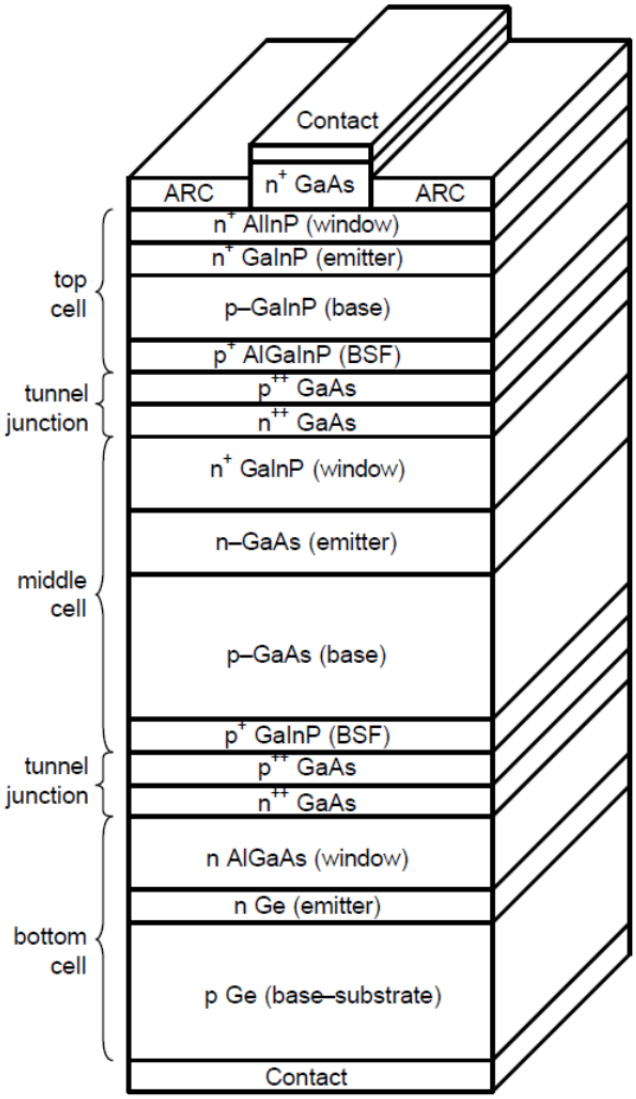

This figure showing the layering employed in a typical multi-junction PV cell, where there are three main P-N junctions, the "top," "middle," and "bottom" cells, and each is separated by a tunnel junction that facilitates the transfer of electric current from one junction to another is from P. Michalapoulos. "A novel approach for the development and optimization of state-of-the-art photovoltaic devices using Silvaco," M.S. thesis, Depts. of Com. Sci. and Elec. and Comp. Eng., Naval Postgraduate School, Monterey, CA, 2002

Figure 5. Spectral Response of a Multi-Junction PV cell, Distinguished by Layer

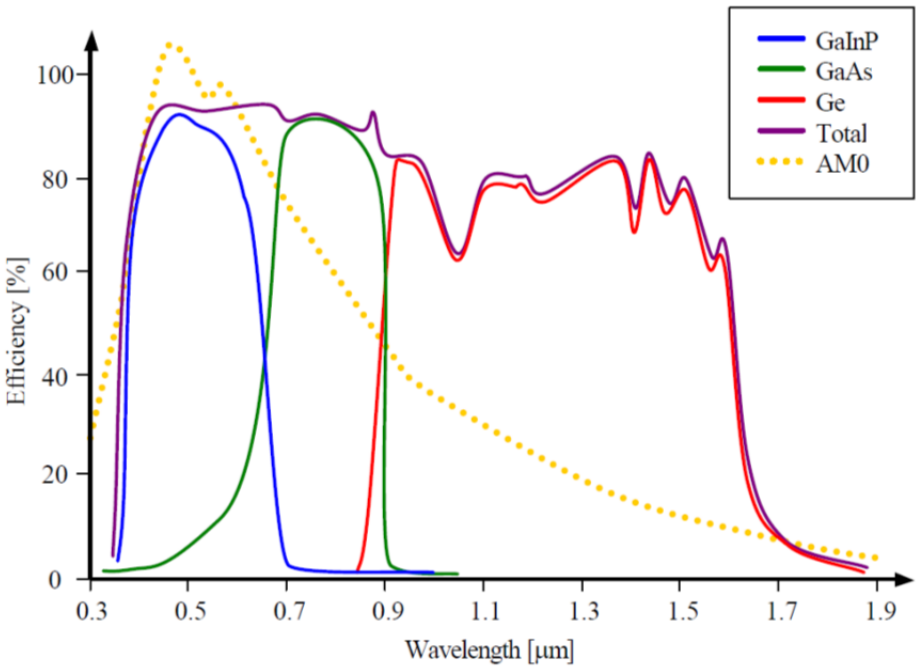

This figure describing the spectral response range for several different semiconductor materials that could be employed in a multi-junction cell, as well as how they overlap and could be employed to manufacture a cell with a wider effective band gap (E_g) is from P. Michalapoulos. "A novel approach for the development and optimization of state-of-the-art photovoltaic devices using Silvaco," M.S. thesis, Depts. of Com. Sci. and Elec. and Comp. Eng., Naval Postgraduate School, Monterey, CA, 2002

More basic manufacturing techniques to improve efficiency include a full surface, mirrored back electrical contact, and the inclusion of a back-surface field. The full-surface mirrored back contact allows for low conduction resistance for potential at the rear of the cell as well as reflectance of incident light that passes through the cell, such that it passes back through the cell and has additional opportunity to excite an electron. The back-surface field is a region of higher doping at the back of the cell, meaning there are more injected charge carriers in that layer, which helps to increase the cell's overall electrical potential. This layer is in addition to the normal P and N layers of the cell, and is typically of the same doping type as the cells lower layer, but with a higher concentration of impurities (e.g., P+ if it is an N on P cell or N+ if it is a P on N cell).

While the overall efficiency improvement from these techniques is not as high as those previously mentioned (1–3% in the case of the mirrored rear contact) [10], it is typically sufficiently substantial to warrant the additional associated cost.

Today there is a significant range of photovoltaic cells in production with an equally significant range of efficiencies. Simple cells that use a single, non-crystalline, semiconductor material with a single p-n junction, can have an efficiency lower than 8%. Multi-junction cells, with a range of semiconductor materials tailored to specific bands, placed under solar concentrators have been independently verified to have an efficiency as high as 46% [11]. Figure 6 is a regularly updated diagram provided by the U.S. National Renewable Energy Laboratory (NREL) that lists a range of photovoltaic technologies and their development over time, with the most recent and highest efficiencies for each technology highlighted at the right of the figure [1].

Figure 6. NREL Best Research-Cell Efficiencies

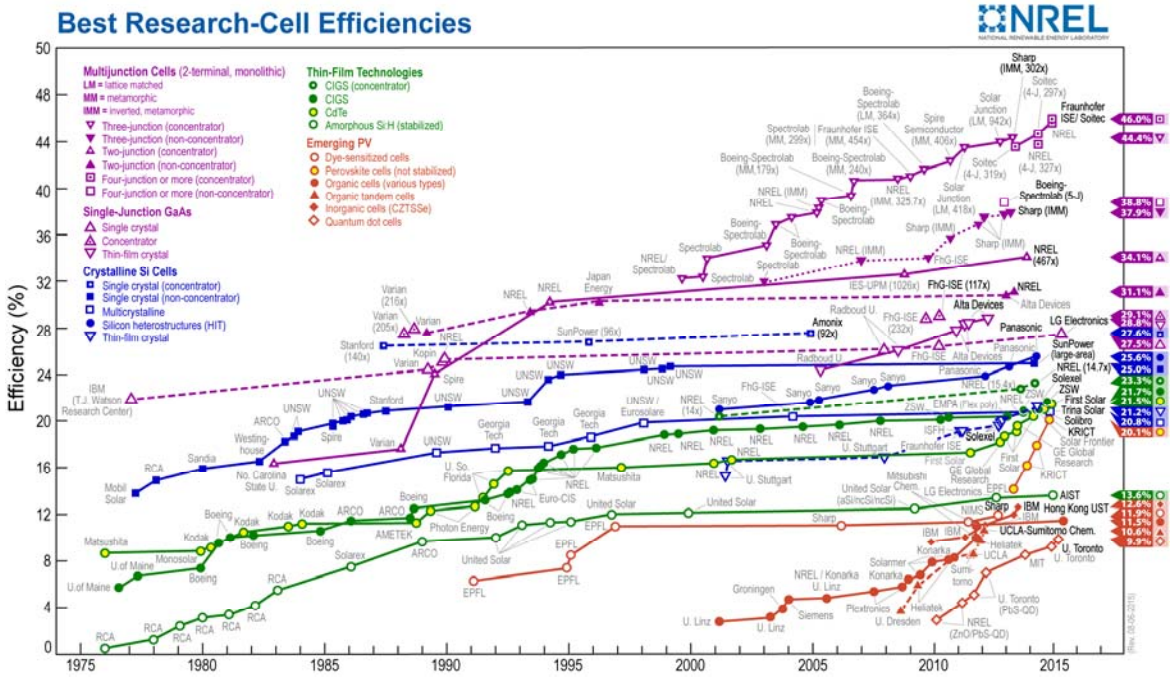

This figure describes the overall best PV cell efficiencies achieved for a given vein of PV technology in a given year and is from Best research-cell efficiencies. (2015). National Renewable Energy Lab. [Online]. Available: http://www.nrel.gov/ncpv/images/efficiency_chart.jpg

The most common PV technologies employ silicon (Si) cells, though this is now largely due to their early development and maturity of manufacturing technology, which is becoming increasingly diverse and widespread. Though less efficient than Si cells during their initial development, gallium-arsenide (GaAs) cells quickly became more efficient [1], and became the technology of choice for use in PV spacecraft electrical power systems. With the development of thin-film technologies and the incorporation of impurities which allow for wider band gap reception (discussed further in Chapter IV), GaAs-based cell technologies seem poised to dominate the regions of the PV market which are focused on overall cell efficiency with fewer concerns for cost [1].

Though current designs are still far from the theoretical limit for PV cell efficiency, which is as high as 86% when the Shockley-Queisser limit is applied to multi-junction cells under concentrated solar radiation [12], the advancements in both design and production implemented for modern cells have allowed PV systems to become considerably more efficient, cost-effective, and widely used.

B. THERMOELECTRIC GENERATORS

Thermoelectric generators (TEGs), are a predecessor to thermo-photovoltaics in various direct heat to electricity conversion systems. TEGs will be discussed here to emphasize the differences in how they are used in a direct energy conversion system vice how thermo-photovoltaics are used. They will not be included as a component of modeling or analysis through the remainder of the thesis.

TEGs were one of the first devices developed for direct conversion of heat to electricity, and are still used today. They utilize the thermo-electric effect—which includes the Seebeck effect (discovered by Thomas Johann Seebeck in 1821), the Peltier effect (discovered by Jean Charles Athanase Peltier in 1834), and Thomson effect (discovered by William Thomson, also known as Lord Kelvin, in 1851) [13].

The Thomson effect describes how a gradient in current density caused by the dissimilarity in temperature at one end of a conducting material and the other will cause electricity to flow from one end of the material to the other. The Seebeck effect describes

how different conducting materials have different current densities at the same temperature, which can result in a voltage flowing between them when they are connected [13]. The proportionality of this difference is related by a material's Seebeck coefficient.

When strands of conducting materials with different Seebeck coefficients are electrically connected in an alternating zig-zag pattern, with one side of the zig-zag, where the dissimilar conductors meet, thermally connected to a cold plate and the other side thermally connected to a hot plate, as seen in Figure 7, a diagram provided by the Naval Power Unit in Port Hueneme, CA [14], this will result in a voltage through the device. Modern thermocouples often use P and N doped semiconductor materials, which can have very high Seebeck coefficients, but very low thermal conductivity, which helps insulate the hot plate from the cold plate through the device.

Figure 7. Basic TEG design

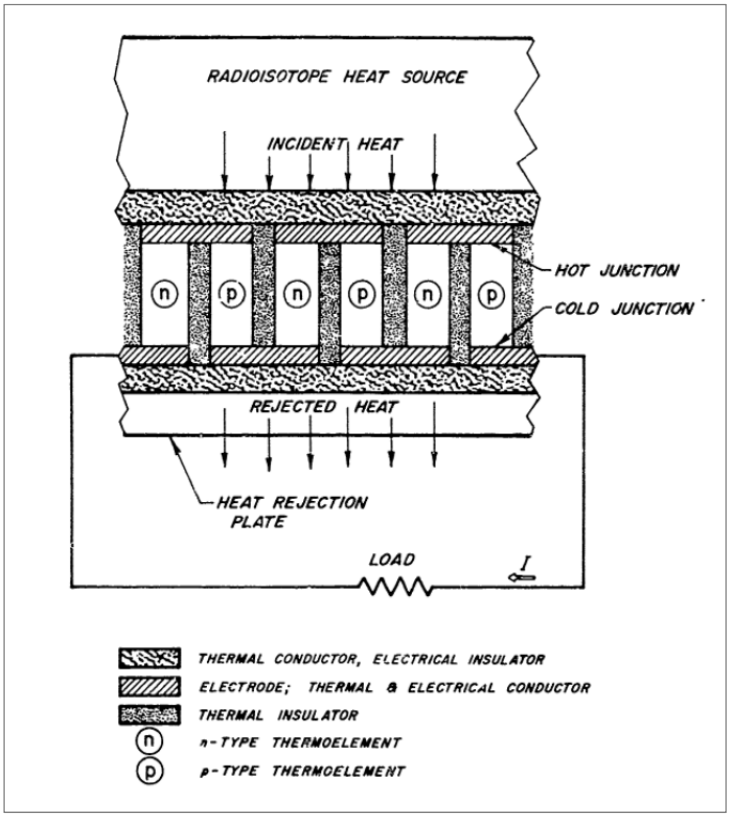

This figure describes a basic TEG design and is from "Radioisotope thermoelectric generators of the U.S. Navy," USN, Naval Power Unit, Port Hueneme, CA. Jul. 1978.

Unfortunately, TEGs are generally not very efficient, particularly with a small temperature difference (ΔT) across the device. Though theoretical efficiency for a given device can be complex to calculate, experimental results for a modern commercial TEG, obtained by O'Halloran and Rodriguez [15], showed a maximum efficiency of only 2.22% with an average ΔT = 68.1 °C. They later stated that other research has shown TEGs can potentially achieve an efficiency of 10% with a ΔT = 500 °C, but even this efficiency is a fair bit lower than modern PVs and would require remarkable engineering to maintain the required temperature difference.

Despite their lack of efficiency, TEGs are productive and reliable devices that have been used in radioisotope thermoelectric generators (RTGs) for some time. An RTG uses the heat of a decaying radio-active element to supply heat to a device that converts

that heat to electricity, as seen in Figure 8, normally either TEGs or TPVs. These devices have been employed for electric power production on missions that require an extended and reliable energy source in places where PVs cannot practically be employed, such as deep space and the deep sea [9], [14]. However, because TPVs are thinner and lighter than TEGs and do not require an additional system to maintain the temperature gradient across the device—which is not to say they do not require cooling, just that it is less complex and intensive—the use of TPVs in an RTG would potentially increases their efficiency and reduce their weight and complexity.

Figure 8. Basic RTG Design.

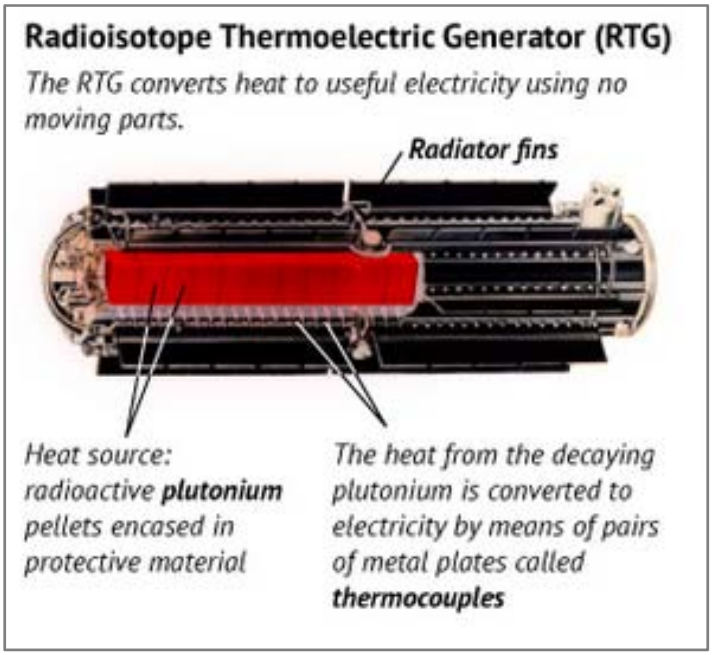

This figure shows a modern RTG that has been used in several NASA deep-space program power systems; it primarily consists of a radioactive heat source (Pu-238) and TEG elements to convert the emitted heat to electricity. The figure is from K. Tate. (2011, Nov. 21). Nuclear generators power NASA deep space probes (infographic). [Online]. Available: http://www.space.com/13702-nuclear-generators-rtg-power-nasa-planetary-probes-infographic.html

C. THERMO-PHOTOVOLTAICS

Thermo-photovoltaics (TPVs) operate in the same manner as PVs, such that all of the points and considerations discussed in Section II.A are as applicable to TPVs as PVs; however, TPVs are explicitly intended to operate in the infrared, vice visible, wavelength range of the EM spectrum. They utilize semiconductor materials that have a lower band gap, and are thus responsive to lower energy, longer wavelength photons.

The infrared range technically includes any wavelength between 0.7 and 1000 microns, but the practical range for infrared, terrestrially, is from 0.7 to 1.4 microns and 1.4 to 3 microns, which are considered the near-infrared (NIR) and short-wavelength infrared (SWIR), respectively. At the upper end of this range, at about 2.5 microns, our atmosphere is effectively opaque, which means that higher wavelengths are absorbed or attenuated by air over a relatively short distance. Thermo-photovoltaic cells do not generally operate over that entire range, as they are still limited by the band-gaps of the semiconductor materials of which they are constructed. Their intended applications have generally been as an internal component of a high heat producing system with a nominal temperature considerably higher than 300 K, such as an RTG or propane-gas engine, and with a peak wavelength in the IR range itself, near the band gap of the TPV material. Research into potential TPV application, such as that by Presby [16] and Davenport [5], suggests that employment of TPVs in systems that normally employ TEGs could result in considerable efficiency gains.

To appreciate why TPV cells have not historically been considered viable for use in a manner similar to PVs, it is useful to understand the concept of a black-body curve. A blackbody curve is the theoretical output, described as spectral energy density at a given wavelength throughout the EM spectrum, for a body at a given temperature. For example, our sun is generally considered to emit radiation similar to a 5800 K blackbody. Example curves for the radiation emitted by a blackbody at several different temperatures are given in Figure 9. The curves described are quite pronounced, and have a distinct peak wavelength (λ_{Max}), primarily dependent on the temperature (T) in Kelvin.

Figure 9. Blackbody Emission Curves at Various Temperatures.

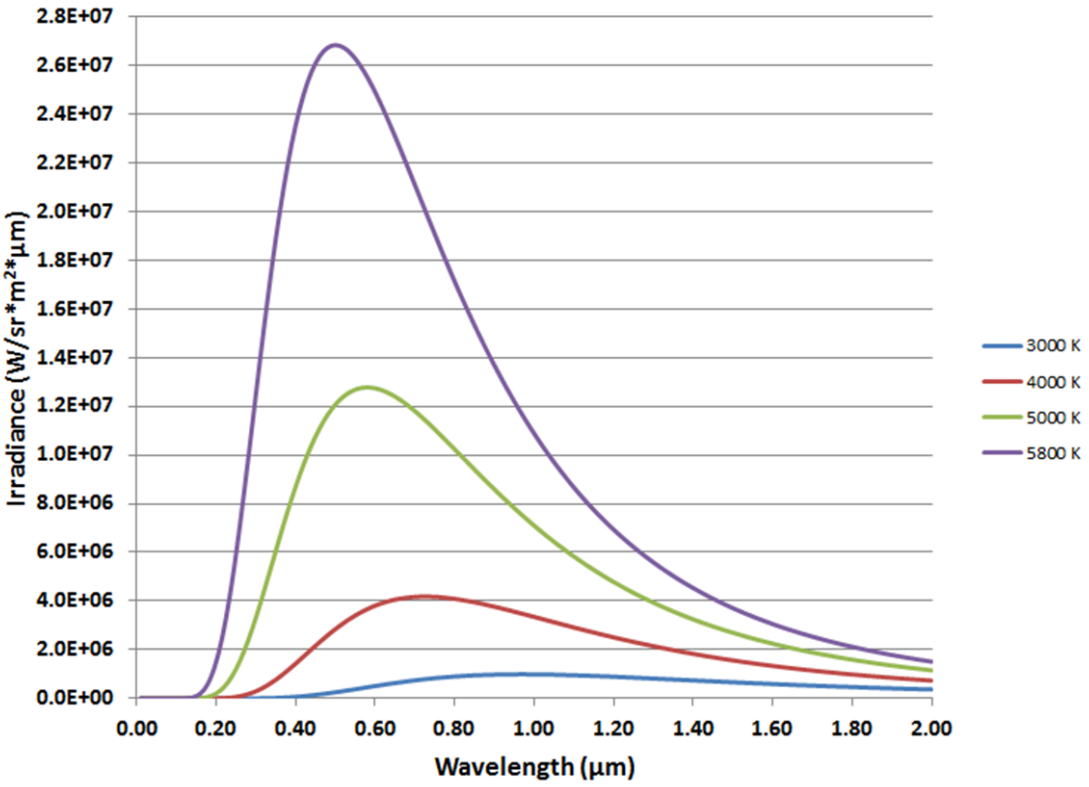

This figure shows the blackbody emission spectra curves at several temperatures over the EM wavelength range from 0 to 2 µm, and is from early work in this thesis involving the generation of data for a 1300K black body spectrum.

The peak temperature of a blackbody spectrum can be found using Wien's displacement law, where *b* is Wien's displacement constant (2.897E-3 mK):

$$\lambda_{Max} = \frac{b}{T} \tag{2}$$

The amount of radiation emitted above and below the peak wavelength drops off fairly sharply to either side, particularly at higher temperatures. Our sun, again, emitting radiation similar to a 5800 K black-body, has a peak wavelength near 500 nm, and the majority of the radiation it emits is in the range of 380–750 nm (or 0.3–0.7 microns), also known as the range of visible light. This means that the majority of the Sun's emitted

radiation has a much higher energy level than what would be ideal for most TPVs, which have a much lower optimal band gap. Determining the optimal band gap for a PV or TPV cell converting energy from a body emitting radiation at a specific temperature is relatively simple utilizing Planck's constant (h = 6.626E-34 J-s) and the speed of light (c = 2.998E8 m/s) to find the energy (E) of the photons at the peak wavelength for that body; finding the energy, in electron Volts (eV) relative to a wavelength in microns (μm), is even simpler:

$$E = \frac{hc}{\lambda}; E(eV) = \frac{1.24}{\lambda(\mu m)} \tag{3}$$

Whether for solar radiation or an enclosed RTG-like device, the optimal band gap for a semiconductor material to be used in a PV or TPV cell is one that is just below the peak wavelength for the emitting body. Longer wavelength photons in light incident on the cell will not have sufficient energy to excite an electron above the band gap of the material, and will either be lost or absorbed as heat, while shorter wavelength photons incident on the cell will have more than enough energy to excite an electron over the band gap of the material, but the additional energy will be lost as heat as well. However, there are still significant volumes of energy emitted by a blackbody-like radiator outside of the range used to determine an ideal band gap, and use or integration of PVs with TPVs could allow for harnessing that energy to improve overall PV cell efficiency.

Because TPV cells generally operate at a lower band gap, they typically output at a lower voltage but higher current. Aside from simple circuit design, placing cells in series and parallel, various techniques have been considered for optimization of TPV cells. One of these is the subdivision of a single cell into numerous close rows of smaller, narrower cells that are connected in series, below the level of the cell as a whole, in order to amplify the voltage output of the cell, though at the expense of the cell's current output. Another method has been the use of selective emitters, as suggested by Nefzaoui et al. [17], which are materials that emit radiation at specific wavelengths when heated or act as filters, only allowing the passage of specific wavelengths, while reflecting others

back to the emissive source. In theory, these materials could be designed such that they emit radiation specifically at the band gap of the TPV cell material in use.

IV. MODELING SOFTWARE AND ASSUMPTIONS

A. SILVACO ATLAS

SILVACO has been producing modeling software for semiconductor devices for over 30 years [18], and their ATLAS software has been used to model solar cells for quite a bit of that time. Its practicality of use for modeling potential solar cell technologies was evaluated independently at the Naval Postgraduate School (NPS) first by Michalapoulos [19] in 2002, later by Davenport [5], Presby [16], Canfield [20], and Utsler [21]. It is still in use for various modeling projects, both those relating to PV research and, more generally, to just about any electronic circuit component employing semiconductor materials. A selection of features and benefits purported by Silvaco for use of ATLAS, that are related to this effort, include [22]:

(1) Electrical, thermal and optical characterization of advanced semiconductor devices allows for device performance optimization

(2) Largest selection of silicon, III-V, II-VI, IV-IV, or polymer/organic technologies, including CMOS, bipolar, high voltage power device, VCSEL, TFT, optoelectronic, LASER, LED, CCD, sensor, fuse, NVM, ferro-electric, SOI, Fin-FET, HEMT, and HBT

(3) Parallel processing supported on multi-core, multiple processor SMP machines and distributed computing

(4) Addresses challenges of current technologies to help users reduce product development time

(5) Exploration of novel device technologies for next-generation devices

1. Overall Software Functionality

Silvaco ATLAS is one component of the Silvaco TCAD suite, and is used for the design and operating simulation of two or three dimensional models of semiconductor devices. The software employs a system similar to a finite element model to represent the physical properties of a device and to propagate the effects of various boundary conditions set for the device during a simulation [23]. The majority of initial physical characteristics are set by the design of the device and the properties of materials specified in the device model that are either drawn from databases built into the software, databases that are closely linked to the software—such as optical parameters drawn from the Sopra database—or that are specified by the user within the model itself [23].

When simulating the operation of a PV or TPV device, we are primarily concerned with how the modeling software propagates charge carrier concentration—specifically—electron and electron-hole migration, with the associated electric field potential—and how it propagates the absorption or transmission of EM radiation—to determine the potential photogeneration for a given device design. For electron and electron hole migration, Atlas employs the following equations, respectively, where n or p is the carrier concentration at any given node, q is the charge of the carrier, Ψ is the intrinsic potential, ϕ is the potential corresponding to the Fermi level of the material, k is Boltzmann's constant, and T is the temperature in kelvin [23].

$$n = n_{ie} \exp\left[\frac{q(\psi - \phi_n)}{kT_L}\right] \tag{4}$$

$$p = n_{ie} \exp\left[\frac{-q(\psi - \phi_p)}{kT_L}\right] \tag{5}$$

For absorption or transmission of EM radiation, ATLAS employs a sub-module called Luminous. This module performs ray-tracing and calculates the depth of propagation of EM waves for wavelengths tested in a given simulation based on the material's refractive index (n) and extinction coefficient (k). Though there are a variety of models that can be employed via the Luminous module, simple ray-tracing calculations

use the following formula to calculate reflection and transmission, where Θ_i represents the angle of incidence, Θ_r represents the angle of reflection, and Θ_t represents the angle of transmission [23].

$$\theta_r = \theta_i \tag{6}$$

$$n_1 \sin\theta_i = n_2 \sin\theta_t \tag{7}$$

Luminous calculates EM radiation absorption and photogeneration based on the following equations, where P represents the ray intensity factor, η_0 is the material's internal quantum efficiency, y is relative distance along the traced ray, h is Planck's constant, λ is the wavelength of the radiation, c is the speed of light, and α is the calculated absorption coefficient [23].

$$G = \eta_0 \frac{P\lambda}{hc} \alpha e^{-\alpha y} \tag{8}$$

$$\alpha = \frac{4\pi}{\lambda} k \tag{9}$$

These equations for charge carrier density, EM wave propagation, and photogeneration are examples of the calculations performed during an ATLAS simulation run to determine the state of charge carrier generation and transport throughout a device, as well as overarching electrical properties relating to boundary conditions set for a device, such as the voltage at a specific electrode. ATLAS then employs linear and non-linear solver routines to approximate these conditions throughout a device, and determine the properties which are being solved for in any given simulation, such as voltage or current output at a specified electrode.

2. Data Structures and Output

There are two primary data outputs from an ATLAS model run. The first is the actual semiconductor device model, called a structure (a .str file). This is essentially the finite element model of the device, with a two- or three-dimensional array of nodes representing the devices physical characteristics. The density of these nodes can be varied

based on the way the mesh—which is the network of nodes that overlays the material layers of the device—is specified, meaning that finer model resolution can be employed in areas of particular consideration for a given device. For example, the meshes specified for the PV, TPV, and tandem cell models have a higher density of nodes in the emitter layers, and at the P-N junctions, but a lower density of nodes in the areas of bulk substrate. The second main data file outputs from an ATLAS model run are log files (.log); these files store the solutions obtained by the ATLAS solver, which represent the resulting optical, electrical, or other properties calculated by the model under set conditions. For example, a light beam representing the AM0 spectrum, over the center of a PV cell's specified width (a variable in this statement), at a 90° angle of incidence, which can undergo reflection by elements within the electronic device, can be specified in the solver using a statement similar to the below, where the first term specifies the characteristic of the model being described—that this is a "beam"— the second term is an ordinal index for that characteristic (for reference by other statements and in case more than one of that element type is specified), and the remainder of the terms are specific to that element, as previously suggested.

```
beam num=1 x.origin=$cell_width/2 y.origin=$l_top-10
angle=90 AM0 back.refl
```

The solver can then be run with a statement specifying the use of this beam model, and telling ATLAS that you would like it to solve for the current generated in a PV cell by specific wavelengths of light in the AM0 spectrum, in order to generate a curve for the cell's spectral response. Numerous other characteristics can be specified in a similar manner, and can be incorporated as a component of the solver's calculated solutions. While a .str file will contain the entire model of a semiconductor device, the log file will contain only what is solved for and the relevant conditions for the cell, such as an array of values for generated current based on the incident wavelength of light.

Both types of data file can be viewed in the suite's companion application tonyplot, which will interpret either a .str file into a display of the device, relevant to the generated data you wish to view such as layers of different materials, a wireframe

representation of the model nodes, or calculated photo-generation under the conditions specified during the solver run. It will also generate x-y plots of the data in a .log file for analysis of device properties such as spectral response and current vs. voltage (IV) curves. Examples of each are provided in the Results section. While no other application would likely be viable for tonyplot's .str file plotting, its somewhat unwieldy interface means that its normal 2D data plotting capabilities leave much to be desired; however, tonyplot also functions for converting the Atlas .log files into normal data file formats such as comma-separated-value (.csv), which can be used in applications such as MATLAB and Microsoft Excel.

3. Using Deckbuild

The most widely used operating system, of those on which the ATLAS suite is designed to run, are the Microsoft Windows operating systems. Ironically, the normal Graphical User Interface (GUI) for semiconductor device modeling, designed to function with this software suite, does not work on Microsoft Windows. This is a known issue, and one which Silvaco seems to have no intention of changing. Thus, the normal interface for device modeling on a Microsoft operating system is a script-based interface called Deckbuild. While a script-based interface would seem far less intuitive than a GUI, the operation of the GUI itself is somewhat redundant as it is essentially used to generate the same commands that would be used in the script, in the background, in order to create the same device model you would with the script-based interface. While the lack of a GUI may seem frustrating at first, and may be particularly challenging for someone with little or no programming experience, it eventually allows for a no less, and potentially more, consistent model design and testing results, particularly when the user comes to understand both the base commands and that the remainder of the ATLAS application suite can be integrated into the analysis process through the Deckbuild script interface. This method can also better lend itself to integration with an overarching command-line interface that could be used to run multiple iterations of a script with varying parameters and thus varying models of the device based on those parameters. While this method was

not employed in this research, it has been in similar research [21] and has been found to be advantageous for the collection of highly granular data.

The majority of script commands and explanations are outlined in the Atlas User Manual [23], along with a great deal of detail on the different models employed by the solver, and their related calculations. While a thorough overview or examination of these is beyond the scope of this thesis, it is useful to have them readily available for the self-education of someone using the Atlas suite, such that they can correctly apply the models, solver instructions, and commands relevant to the semiconductor device modeling efforts they are conducting. However, it must be understood that—though there is likely overlap with other Silvaco software products—the numerous script commands and syntax variations used, while logical, are specific to the Atlas suite. Even with a basic background in electronics, semiconductor physics, programming, other similarly related fields, and even with examples provided with the software, these commands can take a great deal of time and practice to learn to employ correctly. For this reason, it may not be worthwhile to employ these modeling tools for a more limited effort, without a long-term gain for the user (e.g., a future career which heavily employs semiconductor device modeling), or without significant support by personnel more experienced with the software suite.

B. GAAS PV CELL

Gallium Arsenide (GaAs) PV cells are historically some of the most efficient available, and are commonly used in spacecraft applications. Though even single junction GaAs cells are considerably more efficient than Silicon (Si) cells—with even single junction single crystalline cells showing an efficiency of about 16%, as seen in Figure 6—GaAs is also a common base or substrate in multi-junction cells. One of the reasons for this is that GaAs, particularly in combination with Indium (In), Phosphorous (P) and some other impurities, has a tunable band gap.

While the potential for multilayer InGaAsP devices has certainly been considered and is being explored in modern research and design [21], the intent of this effort was to

determine the simple potential efficiency improvement of the incorporation of a PV cell with a TPV cell, which will be best achieved by eliminating extraneous variables such as variability of impurities, which could result in band gap variability as well. As a common, well-modeled PV semiconductor material, with a sharp spectral response termination at 0.9 μm, a simple, single-junction GaAs cell, with distinct N and P doping regions, should serve well for this purpose. A sample GaAs PV cell configuration is shown in Figure 10.

Figure 10. Sample GaAs PV Cell Plot

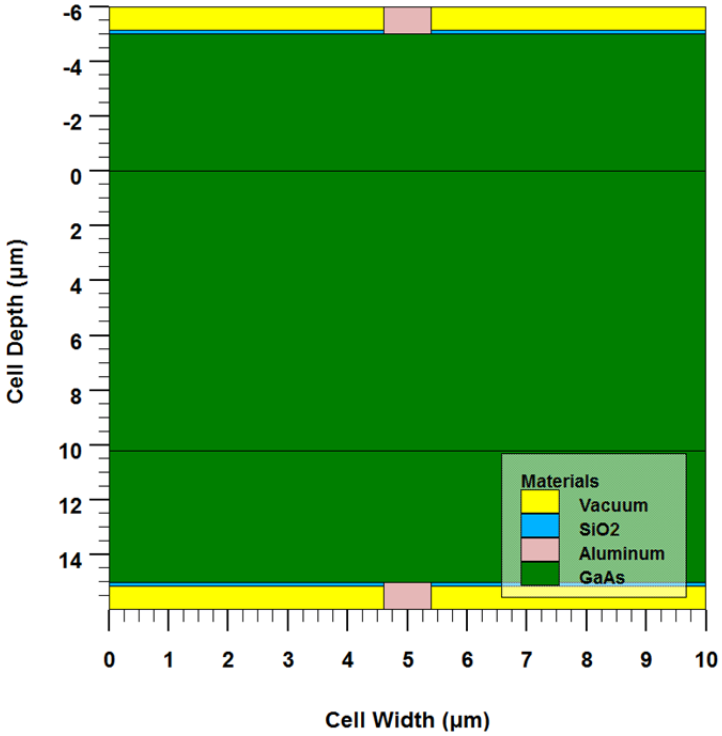

This plot describes the materials used in a sample tandem PV cell design, as well as the thickness (μm) and relative positioning for layers of each material. These thicknesses are not representative of any cell modeled used during this research; they are exaggerated for the sake of visibility, as normal layer proportions make it difficult to separately distinguish layers in a static image.

To this end, research was conducted to determine common parameters for a GaAs PV cell. Even with this restricted scope, it was found that there is still considerable

variability in the parameters employed in manufacturing a simple GaAs PV cell. The two most commonly varied parameters are substrate thickness, and doping profile. Having an expectation that the overall thickness of the GaAs top cell, in a tandem style configuration, would have a dominant effect on the efficiency of the lower cell, and knowing that the substrate layer of a PV cell is normally the thickest, it was decided to vary the substrate thickness of the cell across a relatively broad range (from 5–500 μm), to determine its effect on overall efficiency. The effects of doping profile can be equally pronounced, though to limit the problem space it was decided that two basic categories of doping profile, with unvaried constituent values, would be used for comparison: a low doping profile, and a high-doping profile, the values of which are provided in Table 3. Basic modeling efforts, prior to commencement of final experimental modeling, demonstrated that the inclusion of an ARC layer and a BSF layer produced model results more consistent with realistic values, so these were employed in final experimental modeling. Though both N on P and P on N methods have been used for GaAs PV cells, it was chosen to employ an N on P design with a P+ BSF, because this configuration appears to be more common.

Table 3. Doping Profiles for GaAs PV Cell.

	Low Doping profile (LD)	High Doping profile (HD)
Top (N) Layer	1.00 E17	1.50 E18
Substrate (P) Layer	1.00 E16	7.00 E17
BSF (P+) Layer	1.00 E17	8.00 E18

C. GASB TPV CELL

Contrary to the decision supporting the use of GaAs for the PV cell modeling, it was decided to use GaSb for TPV cell modeling because its coverage in research has not

been as thorough, but because it should serve equally well as an example of a TPV cell material as GaAs serves as an example of a PV cell material.

Because the majority of GaSb TPV cells found in research utilized a P on N design, this was chosen, with an N+ BSF, as the general construction for the TPV cell. A sample plot of a GaSb TPV cell is shown in Figure 11. A configuration of contacts and ARC similar to the PV cell were employed for testing of the single TPV cell.

Figure 11. Sample GaSb TPV Cell Plot (with Mesh Model Overlay)

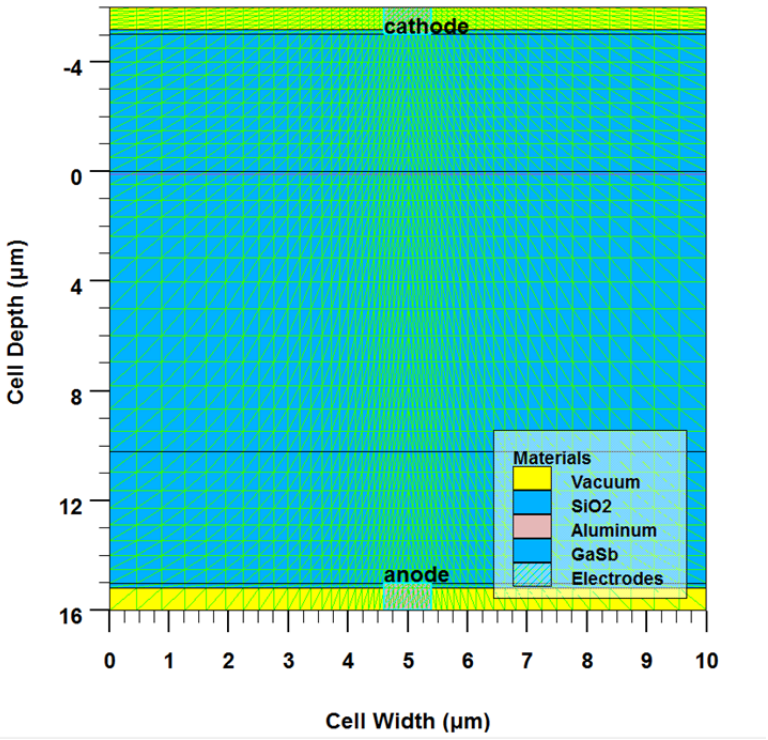

This plot describes the materials used in a sample tandem PV cell design, as well as the thickness (µm) and relative positioning for layers of each material. It also shows an overlay of the mesh used to model the nodes of the cell, as well as the highlighted anode and cathode contacts and a purple line representing the p-n junction. Again, the thicknesses shown are exaggerated for visibility and are not representative of any cell model used in this research.

Similar to the PV cell, two doping profiles were chosen for the TPV cell, one found experimentally to be sufficiently effective, relative to expected TPV efficiency

values—the Low Doping profile—and the other extracted from Davenport's research detailing the optimization of a GaSb TPV cell for a 1300 K blackbody [5]—the High Doping profile.

Table 4. Doping Profiles for GaSb TPV Cell.

	Low Doping profile (LD)	High Doping profile (HD)
Top (P) Layer	1.00 E17	9.80 E19
Substrate (N) Layer	3.50 E17	1.00 E20
BSF (N+) Layer	1.00 E18	1.00 E20

D. TANDEM GAAS-GASB PV-TPV CELL

The basic design for the tandem GaAs-GaSb PV-TPV cell is simply the PV cell, on top of the TPV cell, with the two electrically isolated from each other by a layer of "gap" material. A simple example model is shown in Figure 12, with the thickness of the layers exaggerated for visibility; in most of the modeling runs, the thickness of one layer relative to the others—as well as the contacts, ARC, and gap material—makes it difficult to visibly distinguish them from each other in a static image. Though tandem designs are not popularly employed in modern PV cell manufacturing, they were employed during the early years of PV cell development and were able to produce devices of considerably higher efficiency than other PV cells of the time in a manner similar to that of modern multi-junction PV cells, where the upper layer is intended to absorb photons at shorter wavelengths, successive lower layers are intended to absorb photons with longer wavelengths, and the material used at each layer possesses a band gap which best fits to the radiation which penetrates to its depth in the cell. The overall complexity and cost of manufacturing a tandem cell, along with the discovery of multi-junction implementation, was likely the driving factor in the reduction of interest in the design; however, modeling and simulation software allows for continued exploration of this design, with relatively

few concerns about cost, and the complexity of a modelled tandem design is arguably less than that of a multi-junction design, particularly in regard to degree of computation required by the model.

Figure 12. Sample Tandem PV-TPV Cell Plot

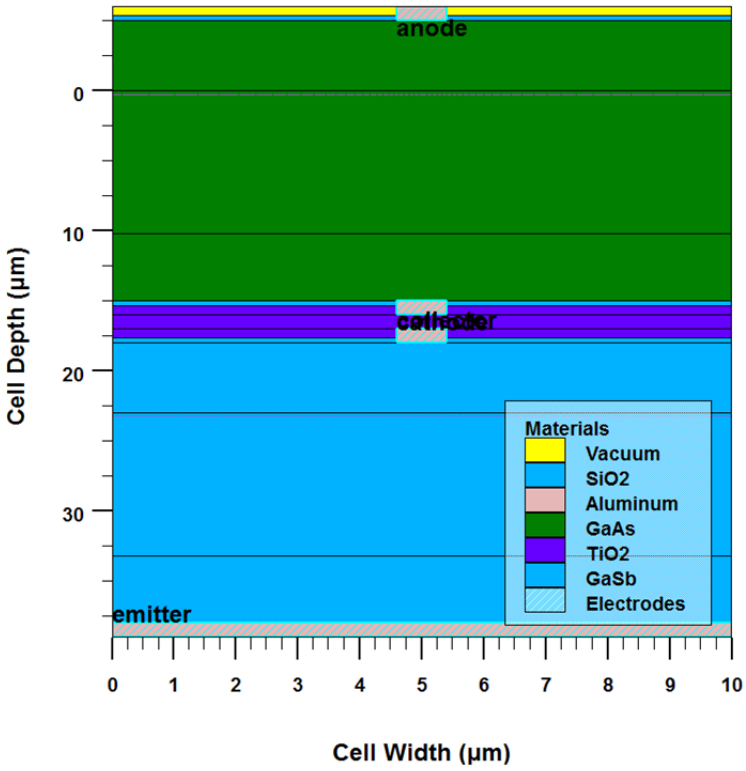

This plot describes the materials used in a sample tandem PV-TPV cell design, as well as the thickness and relative positioning for layers of each material. Once more, the thicknesses shown are exaggerated for visibility and are not representative of any cell model used in this research.

Considerations were made relative to the ordering of the N and P layers for the tandem cell overall, where, in a multi-junction cell, the ordering is required to be consistent to allow for the implementation of a tunnel junction between the overall cell junction layers, to allow the passing of current from one cell junction through to the other. However, research has shown the similarity of function between N on P and P on N implementations and both the electrical isolation of the cells from each other, in the

tandem model, and the ability to calculate potential overall values for a tandem or multi-junction cell, given these results, proved this to be an unnecessary consideration, which could have doubled the potential problem space for the tandem cell.

Other considerations for the design of the tandem cell model included the arrangement of electrical contacts between the cells, the thickness and type of gap material used, and the use of ARC between the cells. Given that upper electrical contacts are a major source of loss in an individual cell, due to the reflection of incident EM energy, it was decided that the contacts would be implemented at an appropriate thickness and width for a normal PV cell electrical contact, but that they would be positioned directly above and below each other to minimize this source of loss. Additionally, while a normal PV cell has thin, finger-like upper contacts to minimize reflected light, but a full surface back surface contact to maximize potential photon reflection back through the cell, it would not have been practical to employ a full surface contact on the upper of the tandem cells, as it would have blocked incident IR radiation from penetrating to the lower cell. Thus both the upper and lower contacts on the PV cell, as well as the upper contact on the TPV cell, are of a finger design, and only the bottom contact of the TPV cell is full surface.

The gap material used was TiO_2, which is both transparent and non-conductive. This allowed for the passage of IR and any remaining visible light energy through the top cell to the bottom, while preventing any potential passage of electrical current. In the majority of testing, the thickness of the gap layer was held at 1 μm, to maintain consistency of results relative to variation of the substrate thickness of the upper cell. However, in later tests of thinner upper cells, detailed in Chapter V, the gap layer thickness was significantly reduced to help eliminate its considerations as a potential source of energy loss between the upper and lower cells. Finally, ARC was employed between the cells in the majority of modeling runs, with its thickness adjusted to tune absorption for longer wavelengths of EM radiation for the lower cell. In the thin cell modeling runs, similar to the gap material, its thickness was adjusted on the upper cell and eliminated on the lower cell, to reduce its consideration as a potential source of loss.

V. RESULTS

A. GAAS UNDER AM1.5 AND AM0

Both LD and HD cell models were run over 5–500 µm substrate thickness to determine overall expected performance for a GaAs cell under AM1.5 and AM0 spectrums and compare to real-world performance values. Full electrical performance data for each run is detailed in Appendix A, and Figure 13 shows a comparison of results based on overall cell efficiency relative to substrate thickness.

Figure 13. Comparison of Low Doping and High Doping GaAs PV Cell Efficiencies Under AM1.5 and AM0 Spectrums

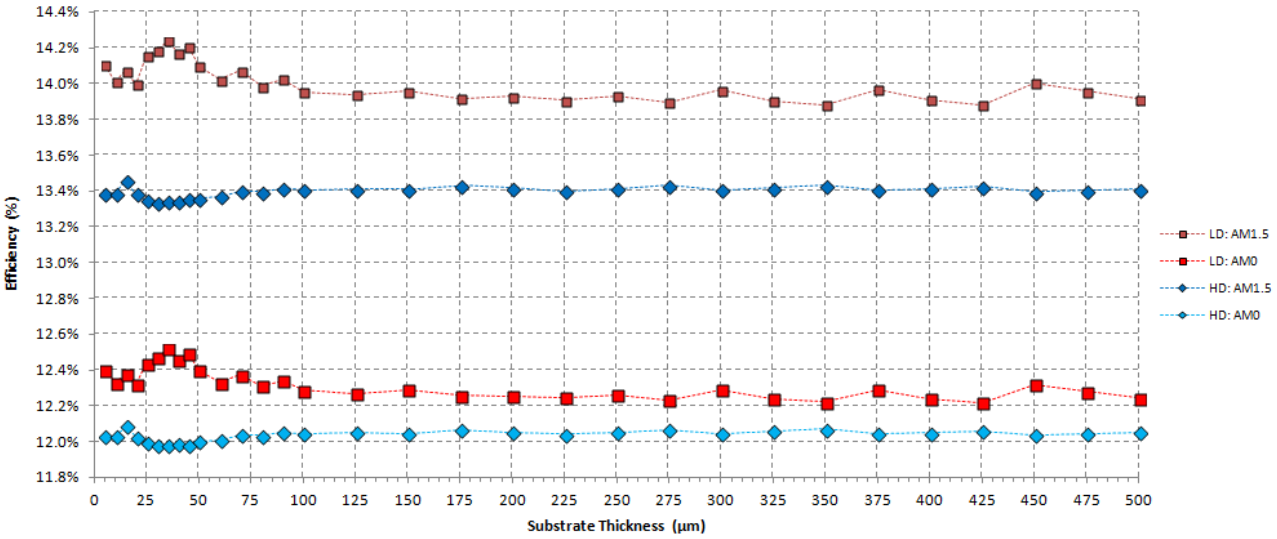

Highest performance, 14.24%, was shown by the LD profile cell under AM1.5 at a substrate thickness of 35 µm. Of interest is that both LD and HD profiles performed less efficiently under AM0 than under AM1.5—by approximately 1.5%—which is likely attributable to the bands of EM energy lost to the atmosphere under AM1.5 being outside of the spectral response range of this GaAs cell. Unfortunately, for spacecraft power systems our primary interest is efficiency under the AM0 spectrum, for which the highest

result, 12.52%, was again shown by the LD profile at a thickness of 35 µm. A plot of the cell model, the cell's spectral response curve, and the cell's IV and power curves are shown in Figures 14, 15, and 16, respectively. Though both cells showed respectable performance for a single junction mono-crystalline PV cell, under both AM1.5 and AM0, they did not show performance comparable to modern single-junction GaAs cells—approximately 18–29% [11]. It is believed that the simplicity of the PV cell model design is the likely source of this difference in performance. While it was intended to down-select to the higher performing doping profile for use in modeling a tandem design, the overall similarity among efficiencies for each profile, and a sufficient allowance of time, led to the testing of both doping profiles in the tandem design.

Figure 14. AM0 Optimal GaAs PV Cell Model

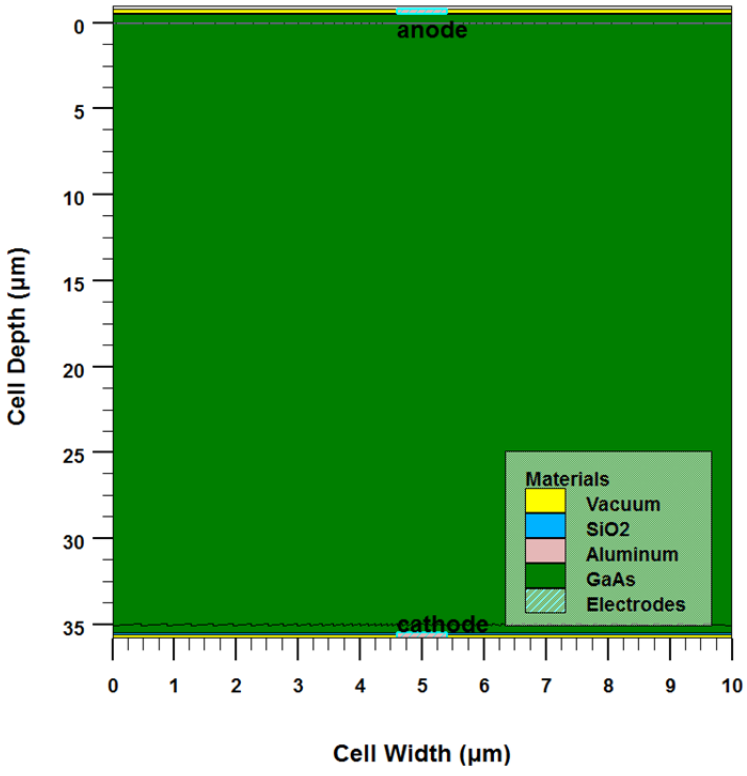

Figure 15. AM0 Optimal GaAs PV Cell Spectral Response

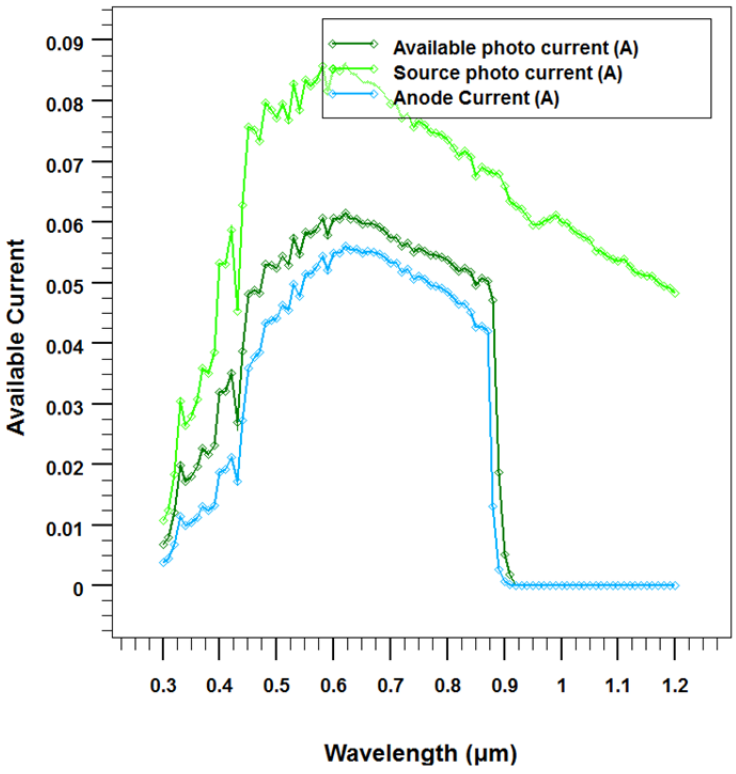

Figure 16. AM0 Optimal GaAs PV Cell IV and Power Curves

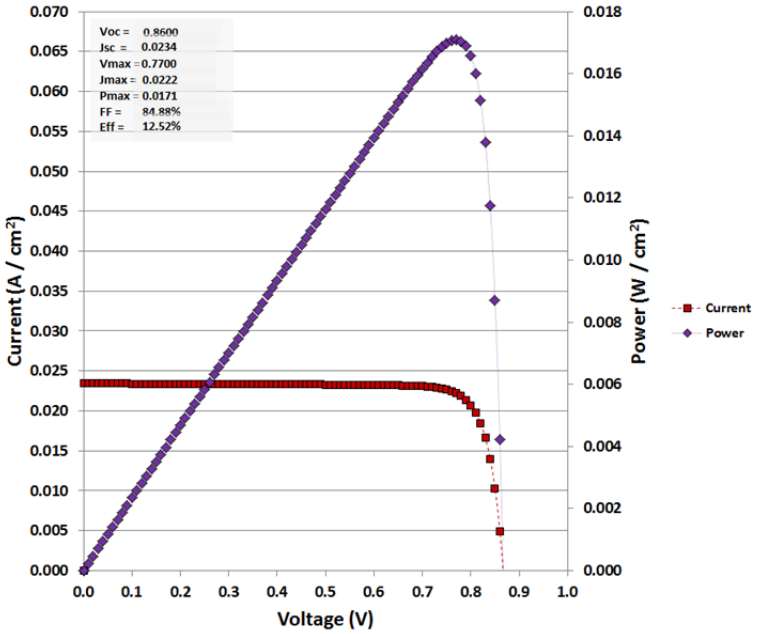

B. GASB UNDER AM1.5 AND AM0

Both LD and HD cell models were run over 5–500 µm substrate thickness to determine overall expected performance for a GaSb cell under AM1.5 and AM0 spectrums and compare to real-world performance values. Full electrical performance data for each run is detailed in Appendix A, and Figure 17 shows a comparison of results based on overall cell efficiency relative to substrate thickness.

Figure 17. Comparison of Low Doping and High Doping GaSb PV Cell Efficiencies Under AM1.5 and AM0 Spectrums

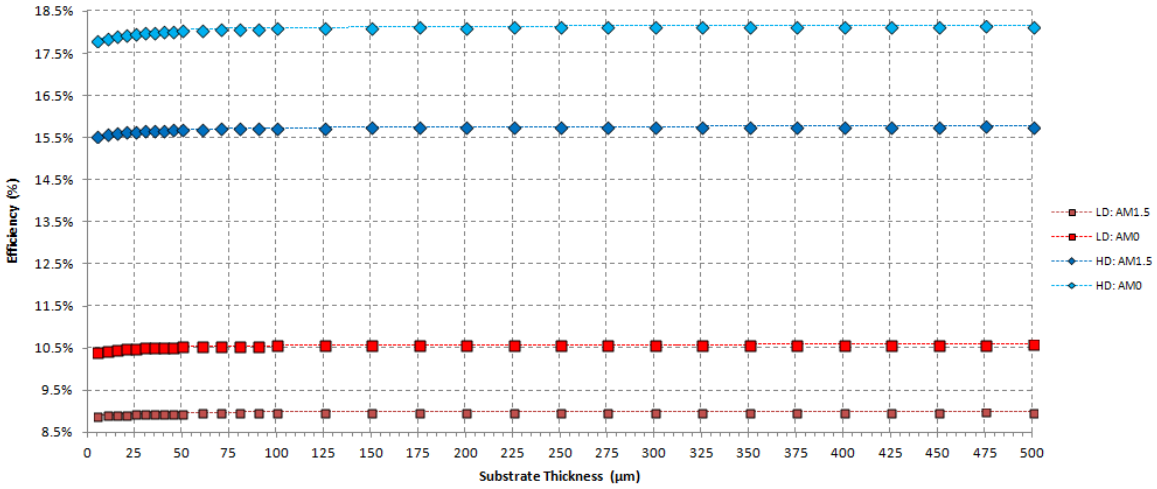

The GaSb TPV cell design showed increasing efficiency with substrate thickness, well past the 500 µm range. Though this makes it difficult to determine overall highest performance, based on substrate thickness, it can be seen that the HD profile, overall, performed considerably better than the LD profile—by 6.5% and 7.5% under AM1.5 and AM0 respectively. Due to this drastic difference in efficiency, and for the opportunity to restrict the problem space to a reasonable size, the LD profile was down-selected for use in the tandem design, in favor of the HD profile.

It can also be seen that there is little variation in efficiency based on substrate thickness within an individual doping profile under a given spectrum, the greatest being within the HD profile under AM0, where a 5 µm substrate thickness shows an efficiency

of 17.82% and a 500 µm substrate thickness shows an efficiency of 18.16%—a difference of only 0.34%. For this reason, it was chosen to fix the substrate thickness of the TPV cell in the tandem design to a thickness somewhere near the "knee" of the curve, at the lowest thickness where the increase in efficiency, relative to substrate thickness, begins to level off. Though somewhat arbitrary, this, again, allowed for some restriction of the problem space for the tandem design; the chosen thickness was at 50 µm, which showed a single-cell efficiency of 18.04%. The cell model, spectral response, and IV and power curves for this cell are shown in Figures 18, 19, and 20, respectively.

Figure 18. AM0 Optimal GaSb TPV Cell Model

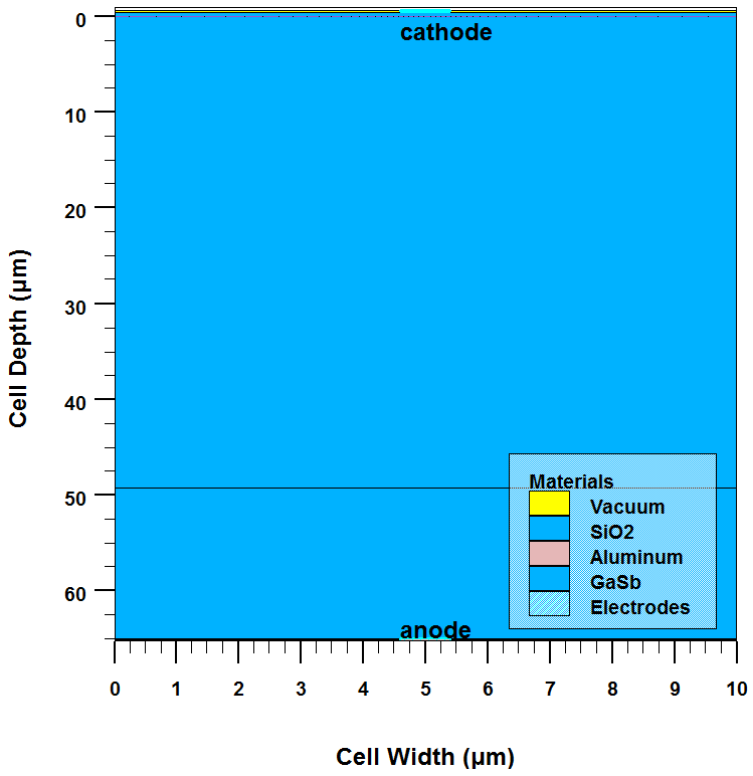

Figure 19. AM0 Optimal GaSb TPV Cell Spectral Response

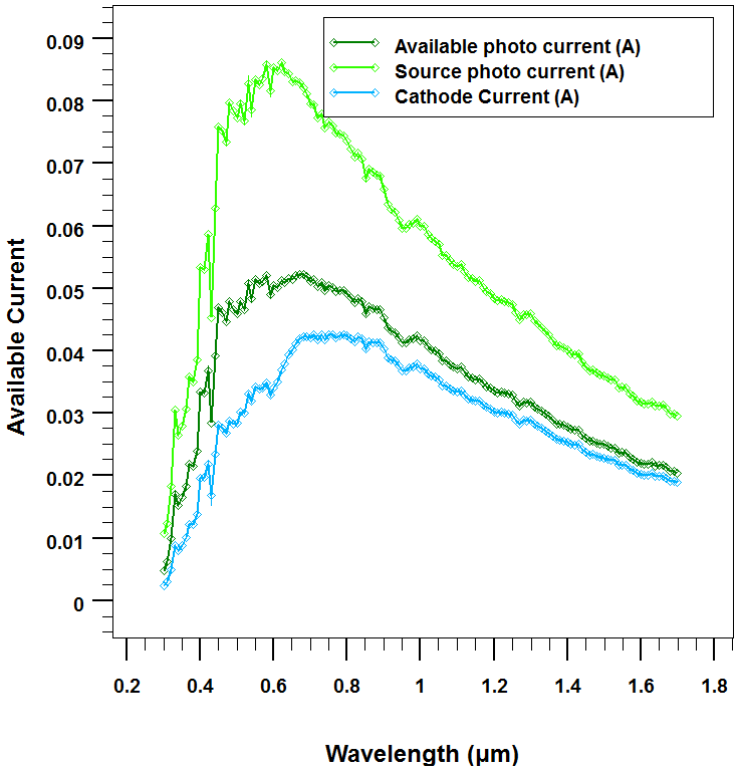

Figure 20. AM0 Optimal GaSb TPV Cell IV and Power Curves

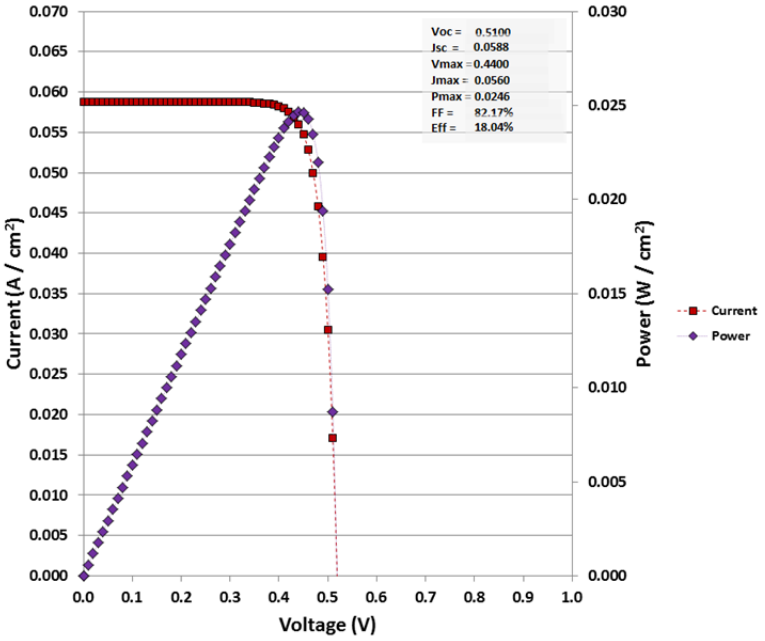

Another important consideration is the relative performance of the GaSb cell to the GaAs cell. Contrary to the decreased performance of the GaAs cell between AM1.5 and AM0, the GaSb cell showed an increase in performance between AM1.5 and AM0 of about 2.5%. Again, this can likely be attributed to the differences in spectral distribution due to atmospheric absorption, but, in this case, those areas of the EM spectrum absorbed by the atmosphere are within the spectral response range of GaSb, where they were not with GaAs. Also, though the LD profile, at no point, performed better than the GaAs cell, under either spectrum, the HD profile performed better under both AM1.5 and AM0 than the peak performance of the GaAs cell. Compared to the 12.52% efficient GaAs performance under AM0, the chosen thickness of HD GaSb, at 50 μm, showed an efficiency increase of 5.53%—an improvement of 44%. Tough it was important to examine the modeled performance of single-cell GaSb, for comparison to its performance in a tandem design, because GaSb cells have not commonly been considered as a PV material, by themselves, it is difficult to relate these results to anything found in the literature.

C. GAAS-GASB TANDEM CELL UNDER AM0

Once the expected performance of the individual cell models was established, the models were combined to determine a single, tandem cell, with the GaAs PV cell on top, the GaSb TPV cell on the bottom, and a layer of TiO_2 gap material between to electrically isolate the cells from one another. Again, while the HD profile and a set substrate thickness of 50 μm were chosen for the GaSb TPV cell, the substrate thickness of the GaAs PV cell was varied to determine overall impact on the efficiency of the TPV cell, and in search of a near optimal cell thickness, based on overall PV-TPV efficiency. Tests for these cell models were initially run under the AM0 spectrum only.

Performance of both the Upper Cell (GaAs, PV), abbreviated as “U” in Figures 21 and 22, and the Lower Cell (GaSb, TPV), abbreviated as “L” in Figures 21 and 22, were independently recorded over substrate thicknesses originally varying between 5 and 500 μm, as with the GaAs and GaSb single-cell models. These results were then used to mathematically calculate the potential performance for either a Tandem or Dual-Junction

design. Modeling runs for upper cell substrate thickness less than 5 microns, considered a thin cell design for the purposes of this research, were later run, and the overall efficiency results obtained in the same way as for the thicker substrates

Figure 21 shows the overall results for these calculations when substrate thickness is varied from less than 1 μm to 500 μm. Over the entire range of upper cell substrate thickness, the energy absorbed by the upper cell significantly reduced the efficiency of the lower cell; however, over the majority of the range, the lower cell's efficiency was never less than 1.86%. Given the original GaSb TPV cell efficiency was calculated at 18.04%, this suggest that approximately 10.3% of the incident electromagnetic radiation, a significant portion, penetrates to the depth of the TPV cell and is available for conversion to electrical energy. As can be seen in Figure 21, the lower cell efficiency values for both LD and HD profiles of the upper cell overlap over the majority of the range, suggesting that differences in upper cell doping profile do not have an overall significant impact on energy available to the lower cell. The performance of the upper cell was similar to the results obtained during the single GaAs PV cell modeling, with the highest performance being 13.50% by the LD profile at a substrate thickness of 2 μm.

Unfortunately, the conjunction of these two disparate power elements resulted in a significant overall decrease in efficiency over the majority of the range of upper cell substrate thickness—from approximately 5 to 500 μm. With the Tandem results, the calculations are based on use of power sources of different voltage and current ratings in either a parallel or series circuit, whichever could produce the greater power output. With the Dual-Junction results, the calculations are based only on the potential result of output from power sources of different voltage or current ratings in a series circuit. In a parallel circuit, the overall output is restricted by the lowest voltage rating of the given elements, and the current ratings are added. With a series circuit, the overall output is restricted by the lowest current rating of the given elements, and the voltage ratings are added. With the Tandem results, the overall voltage was significantly restricted by the lower cell, and with the Dual-Junction results, the overall current was significantly restricted by the

lower cell. Thus in each configuration, the overall Tandem cell was, on average 5.3% less efficient than the upper cell efficiency alone, an overall loss of over 30% in most cases.

However, this trend reverses for upper cell substrate thicknesses of less than 5 μm, as can be surmised from the significant changes in data on the far left range limits of Figure 21, and as is shown in detail on Figure 22, which describes the overall Tandem and Dual Junction efficiency results for LD and HD profiles. Overall efficiency results for the thinner top cell substrates increase to matching, and even exceeding, the results for the upper cell alone. It is expected that as the upper cell thins it becomes effectively transparent to greater and greater quantities of the incident EM radiation. Though this leads to decreasing efficiency for the upper cell, due largely to decreased current production, it means that increasing quantities of this energy pass through to the lower cell, which, in turn, results in an increase in efficiency based on increased current production. These shifts can both be seen in Figure 22 and can be perused in greater detail via the data provided in Appendix A. As the upper cell current decreases and the lower cell current increases, they eventually come to a point where the current for both cells is matched. This is the optimal configuration for power production in a Dual-Junction cell design, and it is at this point in both the LD and HD profiles where we find their respective highest efficiency ratings. The higher of the two, 15.08%, is once again exhibited by the LD profile and is at a substrate thickness of 0.164 μm. The cell model, spectral response curves, and IV and power curve for this cell, based on Dual-Junction calculations are shown in figures 23, 24, and 25, respectively. It should be noted that the Tandem and Dual-Junction results were seen to strictly overlap, for both LD and HD profiles, except in the case of the thinnest substrate thicknesses tested, which were near the apparent failure point for the upper cell.

Figure 21. Upper Cell (GaAs, PV), Lower Cell (GaSb, TPV), and Overall Tandem Design Efficiency for LD and HD Profiles.

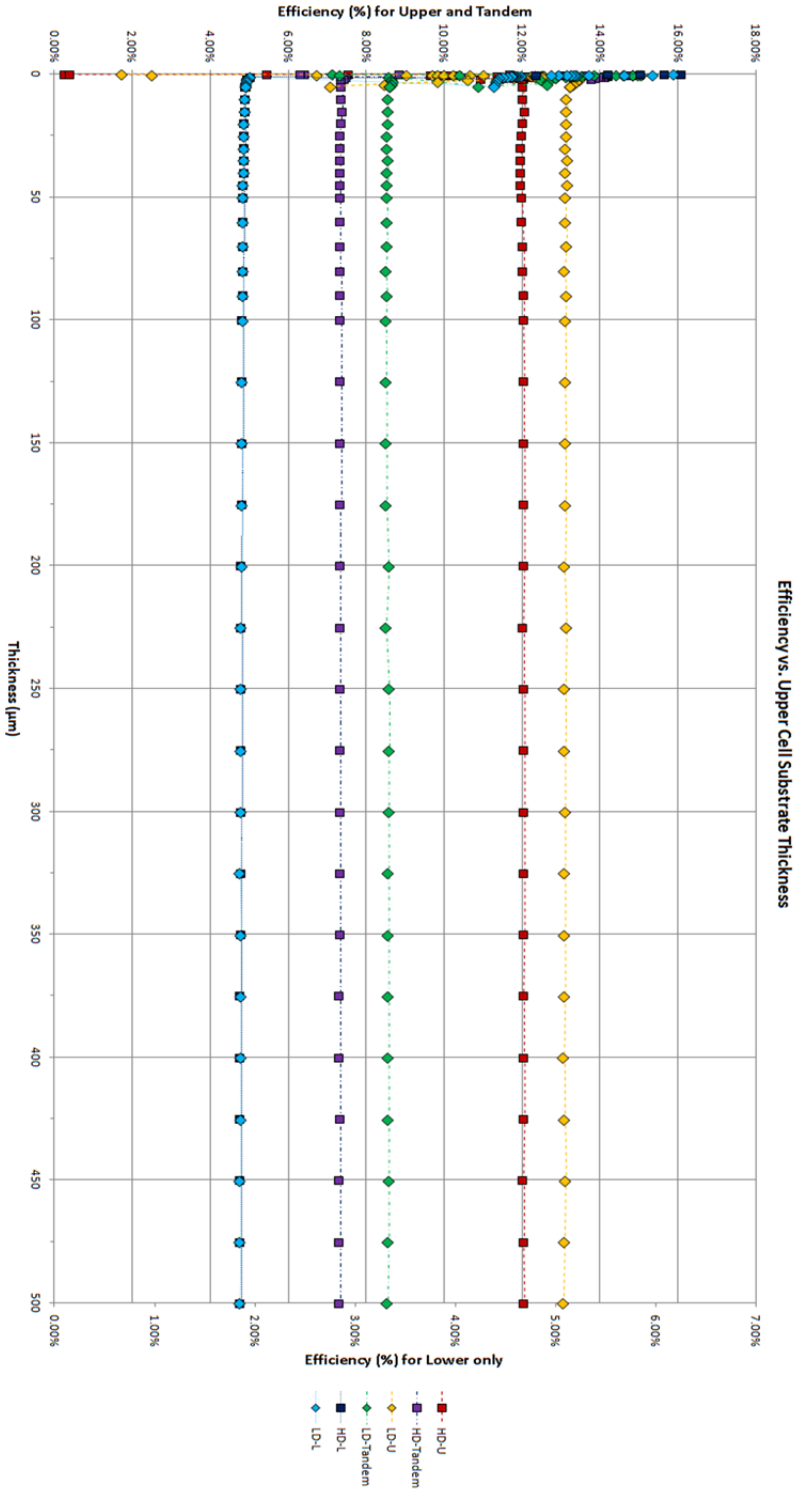

Figure 22. Tandem and Dual-Junction Efficiency for LD and HD Profiles (Thin Upper Cell)

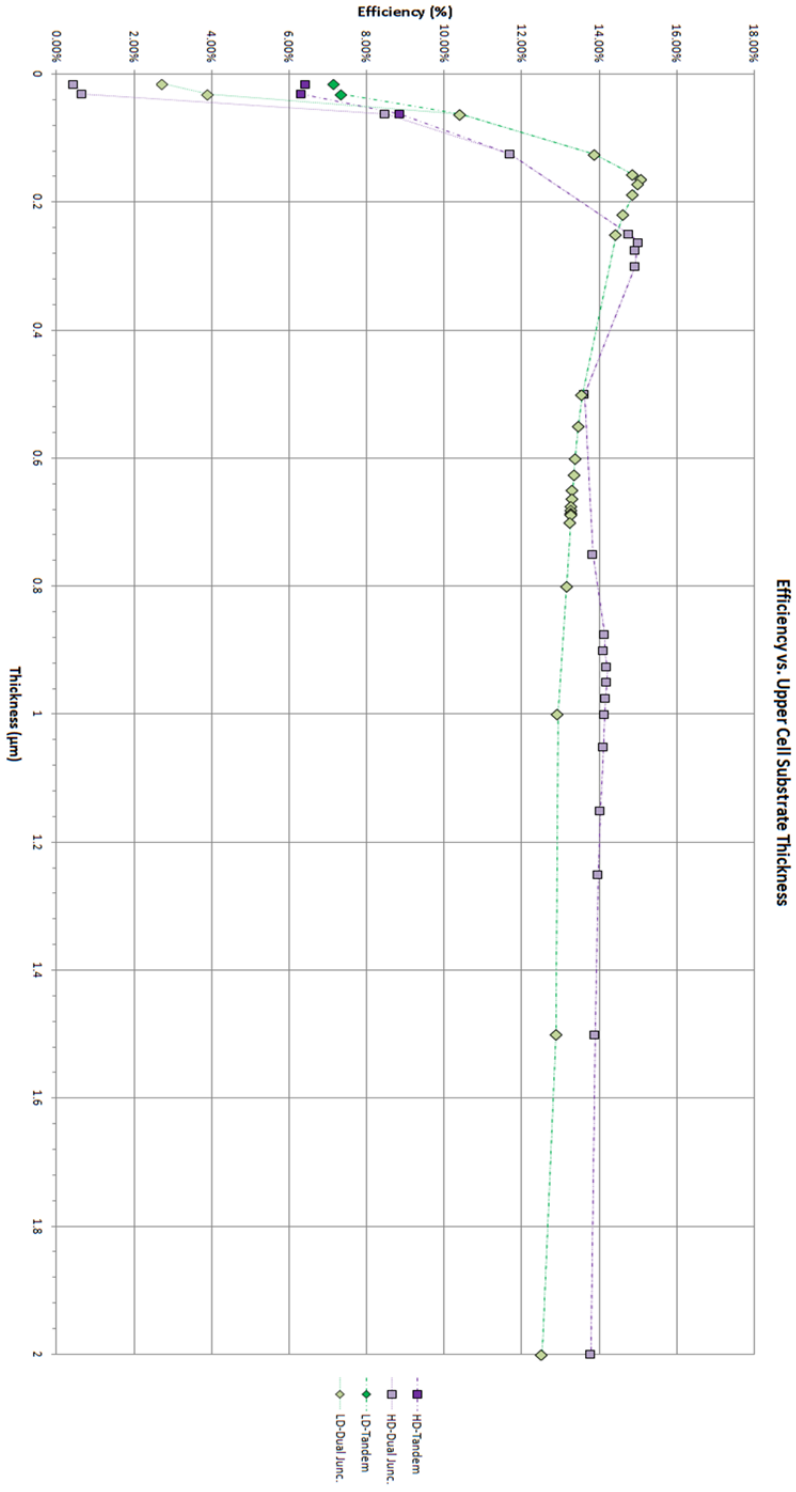

Figure 23. Optimal GaAs-GaSb PV-TPV Cell Model

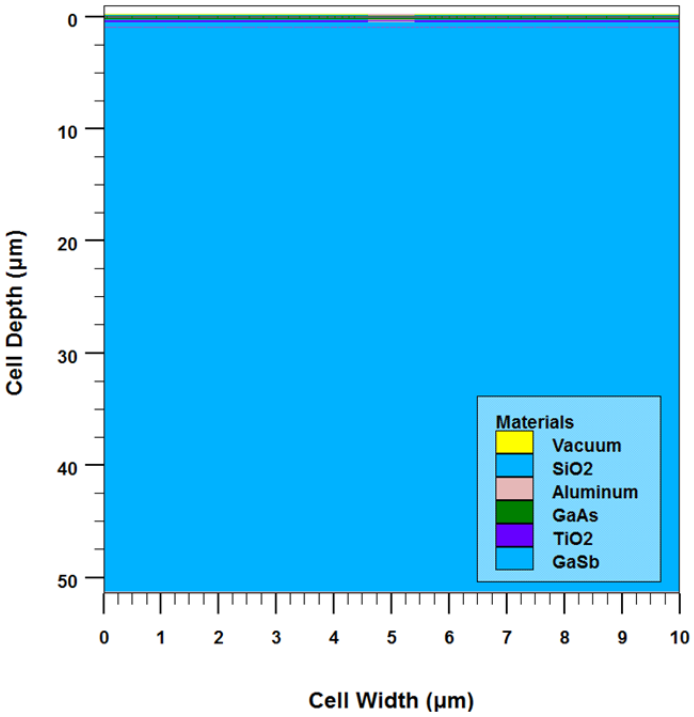

Figure 24. Optimal GaAs-GaSb PV-TPV Cell Spectral Response

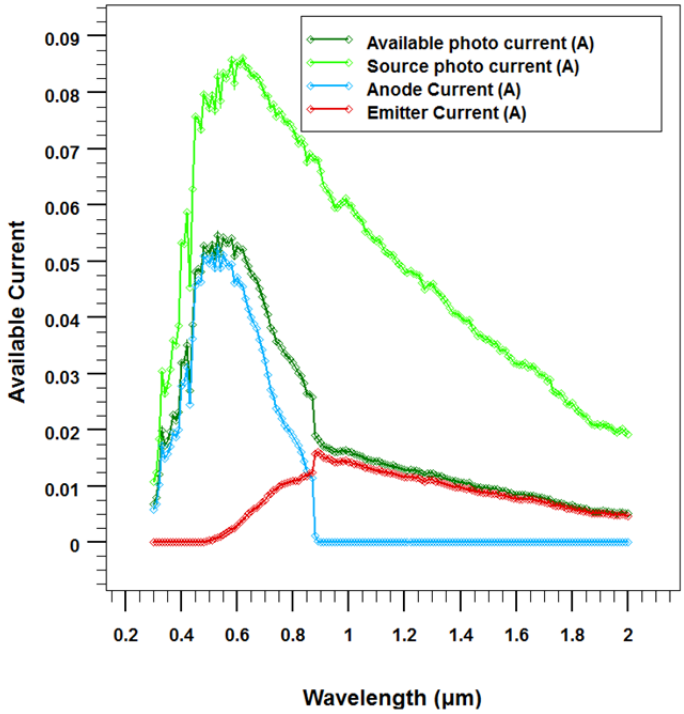

Figure 25. Optimal GaAs-GaSb PV-TPV Cell IV and Power Curves (Dual-Junction)

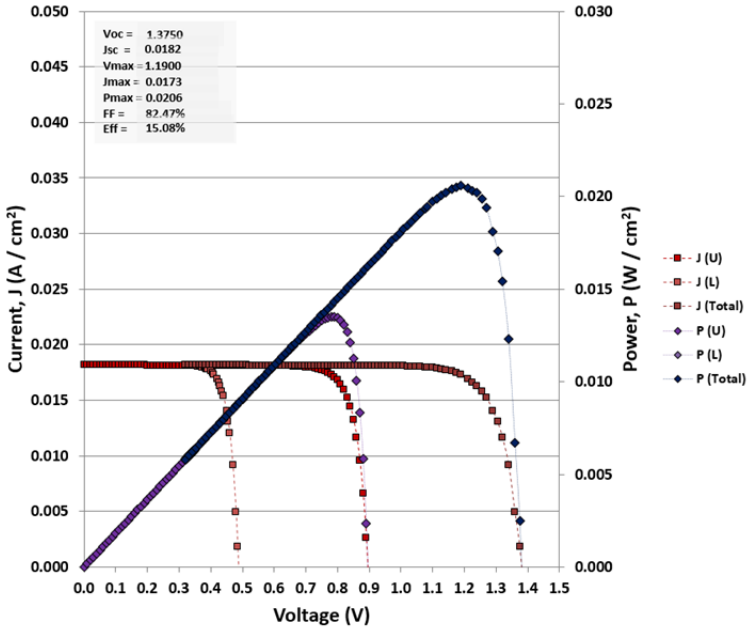

Of note in Figure 23 is that the relative thickness of the upper cell layers to the lower cell make it very difficult to discern in the cell model. Similar disparity can be seen in the multi-junction cell example diagram in Figure 4, where the base and substrate layers of the design are considerably thicker than those of the upper, emitter, layers. It is expected that, as an example, this figure is actually not to scale, and the disparity would be considerably more extreme in a true design, which would be much more similar in scale to Figure 23.

Also of note, in Figure 24, is the overlap in spectral response curves for the upper cell—GaAs, listed as anode current—and lower cell—GaSb, listed as emitter current. While the spectral response of the upper cell cuts off sharply at about 0.9 µm, as expected of GaAs, it also decreases more rapidly approaching this point than is seen in Figure 15. Conversely, the lower cell shows very little spectral response in the 0.3 to 0.6 µm range, but its spectral response then increases relatively rapidly, as the upper cell spectral response decreases, to the point where the upper cell ceases to respond, and the lower cell

recovers what it can of the remaining EM radiation. As was suggested earlier, the decreased spectral response of the upper cell is likely indicative of the lesser current production as the cell's thickness is insufficient to interact with longer wavelengths of radiation, which then simply passes through to the lower cell, resulting in its increased spectral response.

Two changes that occurred between the thin cell designs and the remainder of the test range must be noted. First, in the majority of the test range, both the thickness of the electrodes and of the gap between the upper and lower cells was held at 1 μm. For the thin upper cell tests, both the gap and electrode thicknesses where reduced to 0.1 μm. The combined decrease in both gap and electrode thickness equated to a total thickness reduction, between the upper and lower cells, of 2.7 μm. Second, for the majority of the test range, ARC was applied to both the upper and lower cells, with the upper ARC thickness being optimized for $\lambda = 0.6$ μm and the lower cell ARC being optimized for $\lambda = 1.0$ μm. For the thin cell tests, there was no ARC applied to the lower cell, and the thickness of ARC for the upper cell was optimized for $\lambda = 0.5$ μm. Though it is difficult to quantify the overall impact of these changes, they were made based on a minor overall improvement in cell performance seen during various model test runs. It is expected that the overall decrease in gap thickness, relative to the thickness in upper cell substrate, may have contributed to the majority of this improvement.

D. GAAS-GASB TANDEM CELL UNDER 2000 K BLACKBODY SPECTRUM

Though the focus of this research has been examination of potential performance improvements for a PV cell under AM0 by the integration of TPV technology, the conjunction of PV and TPV technology could be seen as having the potential to act as a hybrid power element capable of producing power relatively efficiently under AM0 or by utilizing a lower temperature blackbody spectrum such as would be emitted by an RTG. To examine this possibility, the cell design optimized for AM0 was simulated under an approximate 2000k blackbody spectrum—similar to what would be emitted by an RTG—to determine the potential improvements to a TPV design by the integration of PV

technology. This design was then varied in a manner similar to that used for rough optimization of the tandem cell under AM0 to determine a range of potential performance for a GaAs-GaSb PV-TPV tandem cell employed in an RTG.

As calculated by Wien's Displacement law, a 2000 K blackbody produces a spectrum with a peak wavelength at 1.4485 μm, which is slightly higher in energy than the E_g wavelength of GaSb, at 1.7 μm. This is a fairly optimal temperature for the GaSb TPV cell in the tandem design. However, it is well below the E_g wavelength for GaAs, so the amount of energy proportionally available to the GaAs PV cell will be considerably less than was available under AM0. This is almost the reverse of the AM0 case, where the E_g wavelength of GaAs (0.87 μm) was slightly below the dominant wavelength of the AM0 spectrum (0.499 μm), allowing it to absorb the majority of the incident photonic radiation, but still allowing a considerable portion of the longer wavelength radiation to pass through for absorption by the GaSb TPV cell. The expected results of this situation are that the upper PV cell should be able to absorb whatever is available in the smaller wavelength portion of the spectrum, but the majority of the radiation should pass through to the lower TPV cell. As can be seen in Figure 26, the modeled spectral response of one of these cells shows this is exactly what would occur.

Figure 26. GaAs-GaSb PV-TPV Tandem Cell Spectral Response Under 2000 K Blackbody Spectrum

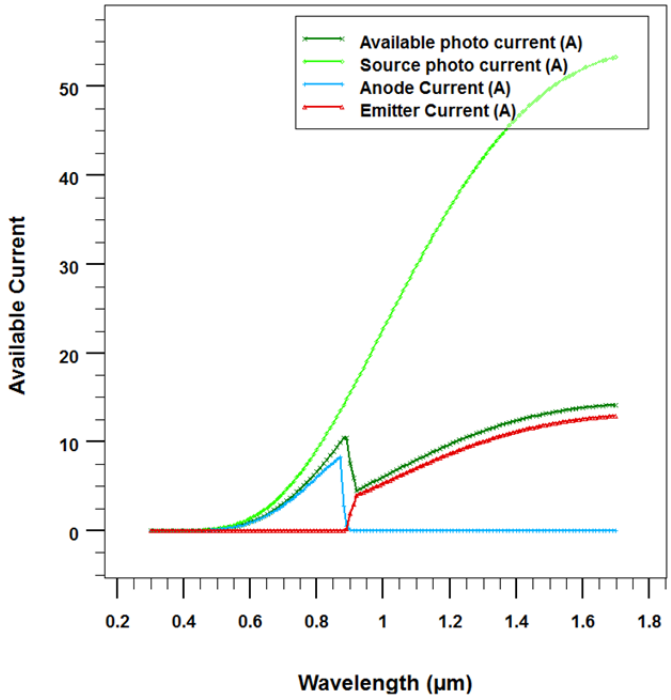

Unfortunately, as the data at the end of Appendix A indicate, and as is shown in Figure 27, the amount of current available from the upper cell, and thus its efficiency, is far below that for the lower cell, resulting in a considerable overall reduction in efficiency in a dual-junction implementation of this design. A tandem implementation shows an overall marginal improvement—an average increase of approximately 0.8%—over the performance of the lower cell alone. In the AM0 case, the current output of the upper and lower cells was close enough that minor adjustments in thickness allowed for a balance in the performance of the upper and lower cells, based on output of electrical current, which led to a considerable overall improvement in efficiency using dual-junction calculations. In this case, the difference in current output is so large that the performance of the lower cell would have to be severely degraded in order to obtain a similar match, which would result in a considerable overall loss in efficiency. While the tandem design does show improvement, the overall output increase of approximately 3% may not be worth the added cost and complexity of the design.

Figure 27. Upper Cell (GaAs, PV), Lower Cell (GaSb, TPV) and Overall Tandem and Dual-Junction Efficiency Under 2000 K Blackbody Spectrum

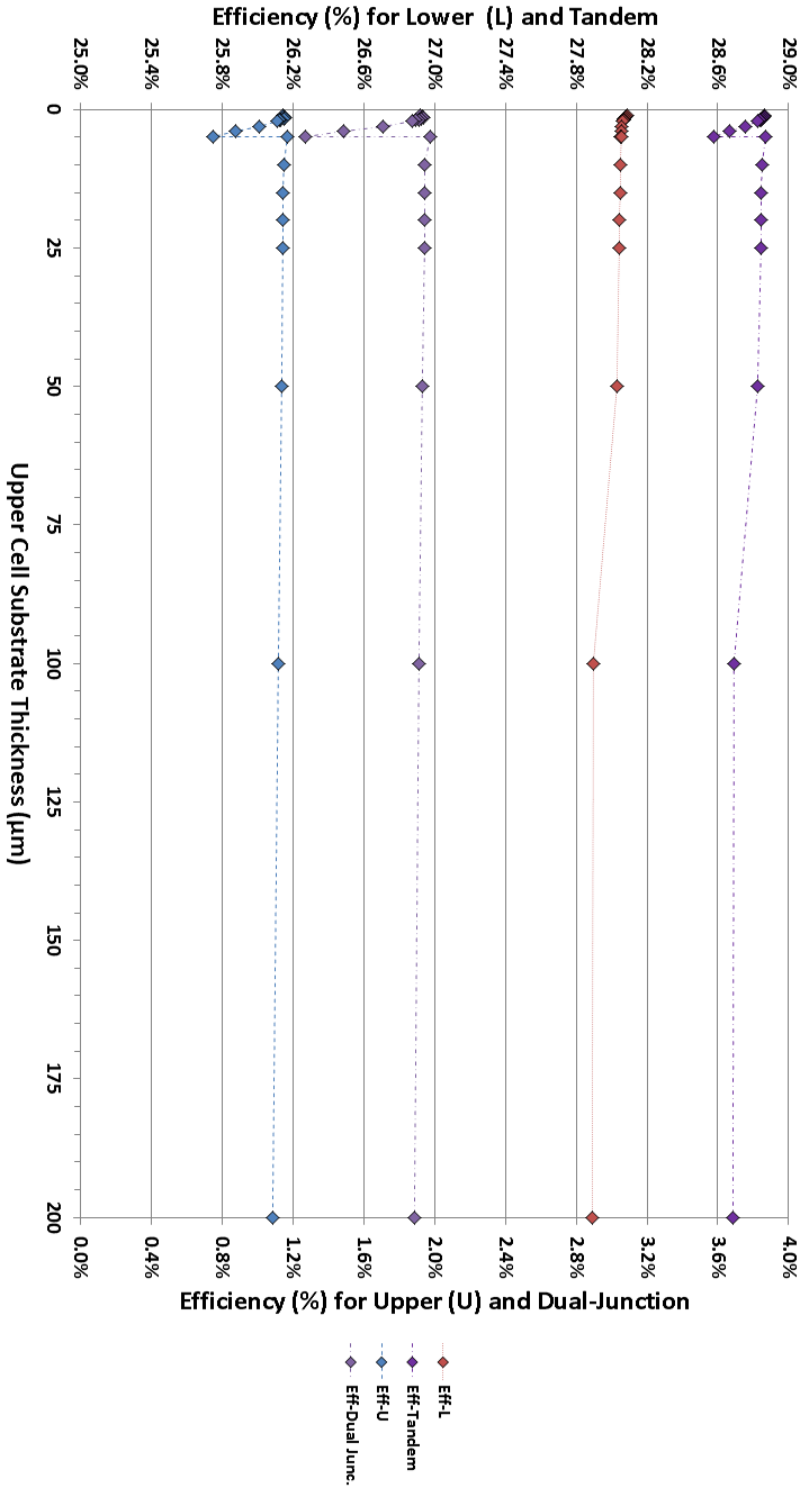

THIS PAGE INTENTIONALLY LEFT BLANK

VI. CONCLUSIONS AND FUTURE WORK

A. OVERALL PV-TPV PERFORMANCE

While the overall performance of the thicker upper cell designs was discouraging, even though indicative of potential efficiency gains, the overall performance of the thin upper cell designs was decidedly encouraging, showing great promise for potential efficiency gains. Given the overall highest efficiency of both the single cell GaAs PV design and the overall highest efficiency of the GaAs-GaSb PV-TPV design, utilizing dual-junction calculations—12.52% and 15.08% respectively—we see an increase in efficiency of 2.56%, which equates to a 20.4% increase in power output.

These results are comparable to those found by Andreev, et al. in their examination of solar cells based on GaSb, where actual manufactured cells utilizing GaSb were examined "behind a filter based on the GaInP/GaAs heterostructure" of a potential upper cell in a tandem design [24]. Their results showed a potential efficiency for the lower cell to be between 4.5% and 6.5% at solar concentrations of 50 to 750 suns depending on the material used for the upper cell and its doping profile [24]. The same study showed tests of a GaSb cell "without a wide-gap cell" covering it to have photocurrent density nearly 2.1 times greater than when covered [24]. The range of lower cell efficiency results obtained with thin cell models in this study—between 4.4% and 6.26%—compares favorably with these results. However, the overall expected efficiency and photocurrent density for a single GaSb cell in [24] suggest a single cell efficiency of no greater than 13.15%, which is quite different from the maximum GaSb single cell efficiency of well over 18% found in this study. Though this similarity in tandem design results is, again, promising, the suggested difference in overall GaSb cell efficiency warrants further investigation.

It is important to note that the base efficiency of the GaAs PV cell used in these models, while comparable to early GaAs PV cell designs, is not comparable to modern GaAs PV cell designs. Modern GaAs cell efficiencies are considerably higher, especially

for thin film cells which exhibit cell efficiencies in excess of 28% [11]. The manufacturer cited for producing thin-film GaAs cells at these efficiencies is Alta Devices [11]. Alta Devices employs metalorganic chemical vapor deposition (MOCVD) to manufacture these thin film cells [25]. This technology has the potential to manufacture devices at thicknesses approaching those of the thin upper cell model designs near which the optimal PV-TPV model efficiency was seen in this research [25]. The data in this research suggest that use of a TPV cell in conjunction with a modern, higher efficiency PV cell design such as this has the potential to result in a PV-TPV cell with efficiencies between 30% and 34%.

The 2000 K blackbody emitter results require some additional consideration in conjunction with the AM0 results. While the overall performance change for the modeled tandem cell design under this spectrum showed little improvement, it is important to consider these results relative to both the band gaps of the materials utilized and the chosen emitter spectrum. The AM0 spectrum was utilized for the majority of the modeling tests because it represents the normal spectrum available for PV power production in the space environment. The 2000 K blackbody spectrum was chosen because it represents a sufficiently close approximation to the spectrum emitted within an RTG. Neither of these spectrums was chosen to match the ideal potential power output for a PV-TPV design utilizing GaAs and GaSb. This is normally the case with renewable energy sources, where there is an existing source of energy, and a power production system is designed to draw from that, not the other way around. If it were possible to shift this design philosophy, such that a power source was designed to emit EM radiation at a wavelength that produced ideal results for a given cell design, then an emitter with a wavelength closer to 1.3 μm, which would have considerably greater overlap with the spectral response range of GaAs, could produce much greater results. This wavelength corresponds to about 2230 K, which is not much higher than the emitter temperature considered, thus, with the correct blend of radioactive materials in an RTG, this temperature may be possible to achieve.

B. DUAL-JUNCTION VS. TANDEM PERFORMANCE

Calculations were performed, given the separate electrical properties determined for the upper and lower cells, which would represent the cell's performance in either a dual-junction or tandem design. Because the design of this cell was not directly in line with a true dual-junction cell model, the calculated values cannot be seen to be as realistic as those that would be produced by a more true dual-junction PV-TPV model, however, they are sufficiently accurate, given the determined electrical properties of each cell, to be representative of the values that could be expected from such a model, and they offer the benefit of being able to independently examine the electrical properties of distinct layers in a dual or multi-junction design, with the modeling software utilized.

Contrary to their comparison in real-world PV cell design and manufacturing, where the two are quite different, distinguishing between these two potential configurations, based on the model utilized, is somewhat arbitrary. In this case, with the calculations for a dual-junction design, the two cells are treated as though they must be in series (as would be the case with a real-world design involving a tunnel junction), which means that the voltage output of the two cells is the sum of that from each individual cell, while the current output is restricted to the lesser of the two. With the calculations for a tandem design, which this model more closely approximates, the cells could potentially be configured in series or in parallel, where the series configuration results would directly match those for a dual-junction design, but the parallel results would be based on the lower of the two voltages between the cells, but the current output would be the sum of the two cells. Thus, while the parallel configuration for a tandem design could potentially have optimal results quite different from those of a dual-junction design, the optimal results for a series configuration are shown to be nearly identical, based on the results of this research. Data listed in Appendix A suggest further similarity among these results, for the models utilized, where the efficiency results for the thin cell models tested were nearly identical for both tandem and dual-junction calculations.

Only for the thicker substrate designs, where the lower cell efficiency was significantly reduced, are there substantial differences among the tandem and dual-

junction calculation results. In these cases, the Tandem designs prove more efficient—by between 1.21% for the least difference in results with the HD profile and 3.11% for the greatest difference in results for the LD profile. However, the overall lower efficiency of these designs is not likely to warrant consideration of these differences.

C. PV-TPV OPTIMIZATION

Basic optimization methods were utilized to find a rough peak of performance for a dual junction or tandem PV/TPV solar cell based on the developed model. The simple method utilized was to determine the cells maximum power output and efficiency over a range of values, plot a curve of these values based on top / PV cell thickness to determine a relative peak, perform a finer grained range of calculations in the vicinity of that peak, and repeat until there was little or no variance in the highest value determined.

Other optimization methods have been used in the past to find a greater or even absolute theoretical peak of performance for various research explorations, including for the parameters of PV and TPV cells. Future research utilizing techniques such as genetic algorithms or simulated annealing, in conjunction with the developed Deckbuild scripts, could produce considerably more optimal results than those found during the course of this research. In past NPS theses, MATLAB has been used in conjunction with Deckbuild to apply similar techniques to explore various optimization problems [19], [21]. The flexibility and effectiveness of such methods could allow for variation of a considerably greater number of both PV and TPV cell parameters, such as doping and thickness of individual layers, and could also be used to determine the variation of optimality across a range of environmental characteristics.

D. TEMPERATURE AND RADIATION EFFECTS ON A TANDEM PV-TPV CELL

The space environment is considerably more extreme in temperature than what was represented in the models used for this research (an unvarying temperature of 300 K), and it is known that temperature variation can have a great deal of impact on PV cell performance. Various statistical data taken from real PV cells at varying temperatures has

shown a trend that temperature increases of one °C generally correlate to a voltage decrease of about 2 mV and an amperage increase of about 0.6 mA, normally resulting in an overall slight loss in efficiency with increases in temperature. While space itself is often considered to be very cold, any object in space that is consistently exposed to solar radiation, particularly those that are dark in color, such as PV panels, heats up very quickly before reaching a fairly high equilibrium temperature, normally 100 °C or higher. Though the correlated 0.2 V loss for this may not seem overly significant, it is important to recall that the V_{oc} for the upper cell in this study was just under 1.0 V—thus suggesting a potential voltage reduction of over 20%—and the V_{oc} for the lower cell was just under 0.5 V—thus suggesting a potential voltage reduction of over 40%. An additional complication might be that the shading of the upper cell could reduce the resulting temperature increase in the lower cell, which would also be nearer the backside of the panel and thus cooler, resulting in lower voltage losses, but that the increased heat and lesser though still increased temperature would result in substantial gains in current production. The temperature impacts to a tandem cell design in a space environment are potentially quite complex, and warrant careful consideration when attempting to optimize such a cell for this environment.

Also, the degree of radiation present in the space environment is considerably higher and more complex than was represented in the models used for this research—which is to say, none. As was expressed in Section II.B., high energy particles and photons can have relatively extreme negative impacts on electrical or electronic components. While the simplicity of a PV cell, relative to other electronic components, generally minimizes the appearance of these effects, they do still occur with sufficient frequency to be of concern, and the related overall degradation of cell performance due to these effects is considerably more evident in the space environment than it is terrestrially. Exploration of the effects of various types of radiation on a PV-TPV tandem cell would allow for better understanding of the chance of these impacts causing a critical device failure, and would also provide some appreciation for the expected degradation of cell performance over time, one of the primary considerations for designing the power budget for a long-life system such as most spacecraft.

Though it is likely not the only application to do so, SILVACO Atlas does provide the capability to explore either or both of these concerns, and the scripts developed during this research could be employed for this purpose with fairly minimal adaptation.

E. TEG INTEGRATION

One of the early concepts behind this thesis was the potential integration of various types of direct energy conversion devices, to include thermo-electric generators. While, by themselves, they are fairly inefficient, without a high temperature gradient, both previous research and this thesis have shown that the proper balance of various energy generation techniques can potentially lead to a similar or greater overall efficiency than use of a single technique alone.

Though time did not allow for investigation of this type, it is possible that the integration of a TEG layer, in a similar manner to the TPV layer integrated with the PV layer in this thesis, could result in additional energy production, given that the "hot foot" of the TEG is a PV/TPV array facing the sun and the "cold foot" of the TEG is the shadowed side of the array directed at the vacuum of space—normally used for spacecraft cooling—or an alternative, even terrestrial, cooling system.

APPENDIX A. DATA

SILVACO ATLAS Modelling Stats for GaAs solar cell (N on P on BSF-P+)(AM1.5)

Divs*:	10	Points:	4399	Triangles:	8528			Low Doping						
N-t	N-d	P-t	P-d	BSF-t	BSF-d	ARC*	Lambda-0	Jsc	Voc	Pmax	Vmax	Imax	FF	Eff
0.5	1.00E+17	5	1.00E+16	0.5	1.00E+17	SiO2	0.6000	1.9756E-02	8.6165E-01	1.4104E-02	7.6000E-01	1.8557E-02	82.85%	14.10%
0.5	1.00E+17	10	1.00E+16	0.5	1.00E+17	SiO2	0.6000	1.9679E-02	8.5951E-01	1.4010E-02	7.6000E-01	1.8435E-02	82.83%	14.01%
0.5	1.00E+17	15	1.00E+16	0.5	1.00E+17	SiO2	0.6000	1.9670E-02	8.6058E-01	1.4073E-02	7.5999E-01	1.8517E-02	83.13%	14.07%
0.5	1.00E+17	20	1.00E+16	0.5	1.00E+17	SiO2	0.6000	1.9672E-02	8.5923E-01	1.3997E-02	7.6000E-01	1.8417E-02	82.81%	14.00%
0.5	1.00E+17	25	1.00E+16	0.5	1.00E+17	SiO2	0.6000	1.9672E-02	8.6051E-01	1.4155E-02	7.6000E-01	1.8625E-02	83.62%	14.15%
0.5	1.00E+17	30	1.00E+16	0.5	1.00E+17	SiO2	0.6000	1.9671E-02	8.6097E-01	1.4189E-02	7.5999E-01	1.8670E-02	83.78%	14.19%
0.5	1.00E+17	35	1.00E+16	0.5	1.00E+17	SiO2	0.6000	1.9674E-02	8.6159E-01	1.4240E-02	7.6000E-01	1.8737E-02	84.01%	14.24%
0.5	1.00E+17	40	1.00E+16	0.5	1.00E+17	SiO2	0.6000	1.9672E-02	8.6109E-01	1.4170E-02	7.5999E-01	1.8646E-02	83.66%	14.17%
0.5	1.00E+17	45	1.00E+16	0.5	1.00E+17	SiO2	0.6000	1.9674E-02	8.6149E-01	1.4208E-02	7.5999E-01	1.8695E-02	83.83%	14.21%
0.5	1.00E+17	50	1.00E+16	0.5	1.00E+17	SiO2	0.6000	1.9671E-02	8.6063E-01	1.4100E-02	7.5999E-01	1.8553E-02	83.28%	14.10%
0.5	1.00E+17	60	1.00E+16	0.5	1.00E+17	SiO2	0.6000	1.9670E-02	8.6008E-01	1.4023E-02	7.5999E-01	1.8452E-02	82.89%	14.02%
0.5	1.00E+17	70	1.00E+16	0.5	1.00E+17	SiO2	0.6000	1.9674E-02	8.6047E-01	1.4072E-02	7.6000E-01	1.8516E-02	83.12%	14.07%
0.5	1.00E+17	80	1.00E+16	0.5	1.00E+17	SiO2	0.6000	1.9672E-02	8.5971E-01	1.3985E-02	7.5999E-01	1.8401E-02	82.69%	13.98%
0.5	1.00E+17	90	1.00E+16	0.5	1.00E+17	SiO2	0.6000	1.9674E-02	8.6012E-01	1.4026E-02	7.6000E-01	1.8455E-02	82.88%	14.03%
0.5	1.00E+17	100	1.00E+16	0.5	1.00E+17	SiO2	0.6000	1.9671E-02	8.5932E-01	1.3952E-02	7.5984E-01	1.8362E-02	82.54%	13.95%
0.5	1.00E+17	125	1.00E+16	0.5	1.00E+17	SiO2	0.6000	1.9669E-02	8.5909E-01	1.3938E-02	7.5000E-01	1.8585E-02	82.49%	13.94%
0.5	1.00E+17	150	1.00E+16	0.5	1.00E+17	SiO2	0.6000	1.9671E-02	8.5914E-01	1.3959E-02	7.5000E-01	1.8612E-02	82.59%	13.96%
0.5	1.00E+17	175	1.00E+16	0.5	1.00E+17	SiO2	0.6000	1.9674E-02	8.5896E-01	1.3919E-02	7.5000E-01	1.8559E-02	82.37%	13.92%
0.5	1.00E+17	200	1.00E+16	0.5	1.00E+17	SiO2	0.6000	1.9669E-02	8.5886E-01	1.3928E-02	7.5000E-01	1.8570E-02	82.45%	13.93%
0.5	1.00E+17	225	1.00E+16	0.5	1.00E+17	SiO2	0.6000	1.9675E-02	8.5883E-01	1.3907E-02	7.4999E-01	1.8543E-02	82.31%	13.91%
0.5	1.00E+17	250	1.00E+16	0.5	1.00E+17	SiO2	0.6000	1.9672E-02	8.5884E-01	1.3932E-02	7.5000E-01	1.8576E-02	82.46%	13.93%
0.5	1.00E+17	275	1.00E+16	0.5	1.00E+17	SiO2	0.6000	1.9674E-02	8.5864E-01	1.3895E-02	7.5000E-01	1.8526E-02	82.25%	13.89%
0.5	1.00E+17	300	1.00E+16	0.5	1.00E+17	SiO2	0.6000	1.9671E-02	8.5910E-01	1.3965E-02	7.5000E-01	1.8619E-02	82.63%	13.96%
0.5	1.00E+17	325	1.00E+16	0.5	1.00E+17	SiO2	0.6000	1.9667E-02	8.5865E-01	1.3905E-02	7.5000E-01	1.8540E-02	82.34%	13.90%
0.5	1.00E+17	350	1.00E+16	0.5	1.00E+17	SiO2	0.6000	1.9674E-02	8.5856E-01	1.3884E-02	7.5000E-01	1.8512E-02	82.19%	13.88%
0.5	1.00E+17	375	1.00E+16	0.5	1.00E+17	SiO2	0.6000	1.9671E-02	8.5916E-01	1.8625E-02	7.5000E-01	1.8625E-02	82.65%	13.97%
0.5	1.00E+17	400	1.00E+16	0.5	1.00E+17	SiO2	0.6000	1.9663E-02	8.5871E-01	1.3911E-02	7.5000E-01	1.8548E-02	82.39%	13.91%
0.5	1.00E+17	425	1.00E+16	0.5	1.00E+17	SiO2	0.6000	1.9672E-02	8.5850E-01	1.3882E-02	7.5000E-01	1.8510E-02	82.20%	13.88%
0.5	1.00E+17	450	1.00E+16	0.5	1.00E+17	SiO2	0.6000	1.9672E-02	8.5955E-01	1.4006E-02	7.5951E-01	1.8441E-02	82.83%	14.01%
0.5	1.00E+17	475	1.00E+16	0.5	1.00E+17	SiO2	0.6000	1.9671E-02	8.5910E-01	1.3959E-02	7.5000E-01	1.8612E-02	82.60%	13.96%
0.5	1.00E+17	500	1.00E+16	0.5	1.00E+17	SiO2	0.6000	1.9671E-02	8.5874E-01	1.3915E-02	7.5000E-01	1.8553E-02	82.37%	13.91%

*Divisions: used as a measure of model complexity, a setting for the number of vertical and horizontal divisions for each region in the model (in the single cell models there are about 5 X-axis, and 10 Y-axis divisions, each subdivided by the "divs" number).

**ARC: thickness of ARC is dependent on Lambda-0 (optimal wavelength)and ARC refractive index --> arc_depth = Lambda-0 / (4*arc_refractive_index)

SILVACO ATLAS Modelling Stats for GaAs solar cell (N on P on BSF-P+)(AM0)

Divs*:	10	Points:	4399	Triangles:	8528			Low Doping						
N-t	N-d	P-t	P-d	BSF-t	BSF-d	ARC*	Lambda-0	Jsc	Voc	Pmax	Vmax	Imax	FF	Eff
0.5	1.00E+17	5	1.00E+16	0.5	1.00E+17	SiO2	0.6000	2.3510E-02	8.6683E-01	1.6939E-02	7.6000E-01	2.2883E-02	83.12%	12.40%
0.5	1.00E+17	10	1.00E+16	0.5	1.00E+17	SiO2	0.6000	2.3429E-02	8.6441E-01	1.6842E-02	7.5999E-01	2.2160E-02	83.16%	12.33%
0.5	1.00E+17	15	1.00E+16	0.5	1.00E+17	SiO2	0.6000	2.3422E-02	8.6539E-01	1.6907E-02	7.7000E-01	2.1957E-02	83.41%	12.38%
0.5	1.00E+17	20	1.00E+16	0.5	1.00E+17	SiO2	0.6000	2.3422E-02	8.6418E-01	1.6829E-02	7.6000E-01	2.2143E-02	83.14%	12.32%
0.5	1.00E+17	25	1.00E+16	0.5	1.00E+17	SiO2	0.6000	2.3422E-02	8.6528E-01	1.6991E-02	7.6992E-01	2.2069E-02	83.84%	12.44%
0.5	1.00E+17	30	1.00E+16	0.5	1.00E+17	SiO2	0.6000	2.3422E-02	8.6577E-01	1.7037E-02	7.7000E-01	2.2125E-02	84.02%	12.47%
0.5	1.00E+17	35	1.00E+16	0.5	1.00E+17	SiO2	0.6000	2.3425E-02	8.6645E-01	1.7100E-02	7.7000E-01	2.2074E-02	84.25%	12.52%
0.5	1.00E+17	40	1.00E+16	0.5	1.00E+17	SiO2	0.6000	2.3423E-02	8.6592E-01	1.7018E-02	7.7000E-01	2.2102E-02	83.91%	12.46%
0.5	1.00E+17	45	1.00E+16	0.5	1.00E+17	SiO2	0.6000	2.3424E-02	8.6635E-01	1.7063E-02	7.6999E-01	2.2159E-02	84.08%	12.49%
0.5	1.00E+17	50	1.00E+16	0.5	1.00E+17	SiO2	0.6000	2.3422E-02	8.6543E-01	1.6935E-02	7.7000E-01	2.1994E-02	83.55%	12.40%
0.5	1.00E+17	60	1.00E+16	0.5	1.00E+17	SiO2	0.6000	2.3404E-02	8.6483E-01	1.6842E-02	7.5999E-01	2.2161E-02	83.21%	12.33%
0.5	1.00E+17	70	1.00E+16	0.5	1.00E+17	SiO2	0.6000	2.3425E-02	8.6527E-01	1.6902E-02	7.5999E-01	2.2240E-02	83.39%	12.37%
0.5	1.00E+17	80	1.00E+16	0.5	1.00E+17	SiO2	0.6000	2.3422E-02	8.6455E-01	1.6815E-02	7.5999E-01	2.2126E-02	83.04%	12.31%
0.5	1.00E+17	90	1.00E+16	0.5	1.00E+17	SiO2	0.6000	2.3425E-02	8.6490E-01	1.6856E-02	7.5999E-01	2.2179E-02	83.20%	12.34%
0.5	1.00E+17	100	1.00E+16	0.5	1.00E+17	SiO2	0.6000	2.3422E-02	8.6426E-01	1.6783E-02	7.6000E-01	2.2083E-02	82.91%	12.29%
0.5	1.00E+17	125	1.00E+16	0.5	1.00E+17	SiO2	0.6000	2.3406E-02	8.6407E-01	1.6755E-02	7.6000E-01	2.2047E-02	82.85%	12.27%
0.5	1.00E+17	150	1.00E+16	0.5	1.00E+17	SiO2	0.6000	2.3422E-02	8.6412E-01	1.6786E-02	7.5999E-01	2.2087E-02	82.93%	12.29%
0.5	1.00E+17	175	1.00E+16	0.5	1.00E+17	SiO2	0.6000	2.3425E-02	8.6399E-01	1.6743E-02	7.6000E-01	2.2030E-02	82.73%	12.26%
0.5	1.00E+17	200	1.00E+16	0.5	1.00E+17	SiO2	0.6000	2.3410E-02	8.6390E-01	1.6741E-02	7.6000E-01	2.2028E-02	82.78%	12.26%
0.5	1.00E+17	225	1.00E+16	0.5	1.00E+17	SiO2	0.6000	2.3426E-02	8.6390E-01	1.6728E-02	7.6000E-01	2.2010E-02	82.66%	12.25%
0.5	1.00E+17	250	1.00E+16	0.5	1.00E+17	SiO2	0.6000	2.3422E-02	8.6391E-01	1.6750E-02	7.5999E-01	2.2040E-02	82.78%	12.26%
0.5	1.00E+17	275	1.00E+16	0.5	1.00E+17	SiO2	0.6000	2.3425E-02	8.6376E-01	1.6710E-02	7.6000E-01	2.1986E-02	82.59%	12.23%
0.5	1.00E+17	300	1.00E+16	0.5	1.00E+17	SiO2	0.6000	2.3422E-02	8.6411E-01	1.6787E-02	7.6000E-01	2.2188E-02	82.94%	12.29%
0.5	1.00E+17	325	1.00E+16	0.5	1.00E+17	SiO2	0.6000	2.3423E-02	8.6378E-01	1.6722E-02	7.6000E-01	2.2003E-02	82.65%	12.24%
0.5	1.00E+17	350	1.00E+16	0.5	1.00E+17	SiO2	0.6000	2.3425E-02	8.6370E-01	1.6695E-02	7.5999E-01	2.1967E-02	82.51%	12.22%
0.5	1.00E+17	375	1.00E+16	0.5	1.00E+17	SiO2	0.6000	2.3422E-02	8.6416E-01	1.6789E-02	7.5999E-01	2.2091E-02	82.95%	12.29%
0.5	1.00E+17	400	1.00E+16	0.5	1.00E+17	SiO2	0.6000	2.3412E-02	8.6382E-01	1.6721E-02	7.6000E-01	2.2001E-02	82.68%	12.24%
0.5	1.00E+17	425	1.00E+16	0.5	1.00E+17	SiO2	0.6000	2.3424E-02	8.6366E-01	1.6690E-02	7.5997E-01	2.1961E-02	82.50%	12.22%
0.5	1.00E+17	450	1.00E+16	0.5	1.00E+17	SiO2	0.6000	2.3423E-02	8.6446E-01	1.6830E-02	7.6000E-01	2.2145E-02	83.12%	12.32%
0.5	1.00E+17	475	1.00E+16	0.5	1.00E+17	SiO2	0.6000	2.3422E-02	8.6412E-01	1.6774E-02	7.5999E-01	2.2072E-02	82.88%	12.28%
0.5	1.00E+17	500	1.00E+16	0.5	1.00E+17	SiO2	0.6000	2.3421E-02	8.6385E-01	1.6722E-02	7.6000E-01	2.2003E-02	82.65%	12.24%

*Divisions: used as a measure of model complexity, a setting for the number of vertical and horizontal divisions for each region in the model (in the single cell models there are about 5 X-axis, and 10 Y-axis divisions, each subdivided by the "divs" number).

**ARC: thickness of ARC is dependent on Lambda-0 (optimal wavelength)and ARC refractive index --> arc_depth = Lambda-0 / (4*arc_refractive_index)

SILVACO ATLAS Modelling Stats for GaAs solar cell (N on P on BSF-P+)(AM1.5)

Divs*:	10	Points:	4399	Triangles:	8528			High Doping (Davenport, 2004)						
N-t	N-d	P-t	P-d	BSF-t	BSF-d	ARC**	Lambda-0	Jsc	Voc	Pmax	Vmax	Imax	FF	Eff
0.2	1.50E+18	5	7.00E+17	0.5	8.00E+18	SiO2	0.6000	1.6476E-02	9.4821E-01	1.3383E-02	8.5000E-01	1.5745E-02	85.67%	13.38%
0.2	1.50E+18	10	7.00E+17	0.5	8.00E+18	SiO2	0.6000	1.6483E-02	9.4822E-01	1.3390E-02	8.5000E-01	1.5753E-02	85.67%	13.39%
0.2	1.50E+18	15	7.00E+17	0.5	8.00E+18	SiO2	0.6000	1.6481E-02	9.4922E-01	1.3455E-02	8.5993E-01	1.5647E-02	86.01%	13.46%
0.2	1.50E+18	20	7.00E+17	0.5	8.00E+18	SiO2	0.6000	1.6481E-02	9.4821E-01	1.3387E-02	8.4999E-01	1.5749E-02	85.66%	13.39%
0.2	1.50E+18	25	7.00E+17	0.5	8.00E+18	SiO2	0.6000	1.6490E-02	9.4751E-01	1.3350E-02	8.5000E-01	1.5705E-02	85.44%	13.35%
0.2	1.50E+18	30	7.00E+17	0.5	8.00E+18	SiO2	0.6000	1.6486E-02	9.4714E-01	1.3333E-02	8.4999E-01	1.5686E-02	85.39%	13.33%
0.2	1.50E+18	35	7.00E+17	0.5	8.00E+18	SiO2	0.6000	1.6497E-02	9.4707E-01	1.3341E-02	8.5000E-01	1.5695E-02	85.39%	13.34%
0.2	1.50E+18	40	7.00E+17	0.5	8.00E+18	SiO2	0.6000	1.6486E-02	9.4707E-01	1.3342E-02	8.5000E-01	1.5697E-02	85.45%	13.34%
0.2	1.50E+18	45	7.00E+17	0.5	8.00E+18	SiO2	0.6000	1.6492E-02	9.4724E-01	1.3357E-02	8.5000E-01	1.5714E-02	85.50%	13.36%
0.2	1.50E+18	50	7.00E+17	0.5	8.00E+18	SiO2	0.6000	1.6483E-02	9.4730E-01	1.3359E-02	8.4999E-01	1.5717E-02	85.56%	13.36%
0.2	1.50E+18	60	7.00E+17	0.5	8.00E+18	SiO2	0.6000	1.6478E-02	9.4753E-01	1.3371E-02	8.4999E-01	1.5730E-02	85.64%	13.37%
0.2	1.50E+18	70	7.00E+17	0.5	8.00E+18	SiO2	0.6000	1.6491E-02	9.4795E-01	1.3398E-02	8.5000E-01	1.5762E-02	85.70%	13.40%
0.2	1.50E+18	80	7.00E+17	0.5	8.00E+18	SiO2	0.6000	1.6480E-02	9.4803E-01	1.3395E-02	8.5000E-01	1.5759E-02	85.74%	13.39%
0.2	1.50E+18	90	7.00E+17	0.5	8.00E+18	SiO2	0.6000	1.6494E-02	9.4837E-01	1.3416E-02	8.5000E-01	1.5793E-02	85.77%	13.42%
0.2	1.50E+18	100	7.00E+17	0.5	8.00E+18	SiO2	0.6000	1.6482E-02	9.4828E-01	1.3406E-02	8.5000E-01	1.5772E-02	85.77%	13.41%
0.2	1.50E+18	125	7.00E+17	0.5	8.00E+18	SiO2	0.6000	1.6482E-02	9.4845E-01	1.3410E-02	8.5000E-01	1.5777E-02	85.79%	13.41%
0.2	1.50E+18	150	7.00E+17	0.5	8.00E+18	SiO2	0.6000	1.6483E-02	9.4845E-01	1.3409E-02	8.5000E-01	1.5775E-02	85.77%	13.41%
0.2	1.50E+18	175	7.00E+17	0.5	8.00E+18	SiO2	0.6000	1.6495E-02	9.4886E-01	1.3431E-02	8.5000E-01	1.5801E-02	85.82%	13.43%
0.2	1.50E+18	200	7.00E+17	0.5	8.00E+18	SiO2	0.6000	1.6485E-02	9.4865E-01	1.3416E-02	8.5000E-01	1.5784E-02	85.79%	13.42%
0.2	1.50E+18	225	7.00E+17	0.5	8.00E+18	SiO2	0.6000	1.6486E-02	9.4837E-01	1.3401E-02	8.5000E-01	1.5766E-02	85.71%	13.40%
0.2	1.50E+18	250	7.00E+17	0.5	8.00E+18	SiO2	0.6000	1.6486E-02	9.4865E-01	1.3415E-02	8.5000E-01	1.5782E-02	85.78%	13.41%
0.2	1.50E+18	275	7.00E+17	0.5	8.00E+18	SiO2	0.6000	1.6495E-02	9.4891E-01	1.3431E-02	8.5000E-01	1.5802E-02	85.81%	13.43%
0.2	1.50E+18	300	7.00E+17	0.5	8.00E+18	SiO2	0.6000	1.6487E-02	9.4851E-01	1.3408E-02	8.4999E-01	1.5774E-02	85.74%	13.41%
0.2	1.50E+18	325	7.00E+17	0.5	8.00E+18	SiO2	0.6000	1.6488E-02	9.4873E-01	1.3419E-02	8.5000E-01	1.5787E-02	85.78%	13.42%
0.2	1.50E+18	350	7.00E+17	0.5	8.00E+18	SiO2	0.6000	1.6497E-02	9.4894E-01	1.3433E-02	8.4999E-01	1.5803E-02	85.81%	13.43%
0.2	1.50E+18	375	7.00E+17	0.5	8.00E+18	SiO2	0.6000	1.6487E-02	9.4846E-01	1.3405E-02	8.5000E-01	1.5771E-02	85.72%	13.41%
0.2	1.50E+18	400	7.00E+17	0.5	8.00E+18	SiO2	0.6000	1.6486E-02	9.4864E-01	1.3413E-02	8.5000E-01	1.5780E-02	85.76%	13.41%
0.2	1.50E+18	425	7.00E+17	0.5	8.00E+18	SiO2	0.6000	1.6493E-02	9.4882E-01	1.3425E-02	8.4999E-01	1.5794E-02	85.79%	13.42%
0.2	1.50E+18	450	7.00E+17	0.5	8.00E+18	SiO2	0.6000	1.6488E-02	9.4830E-01	1.3395E-02	8.5000E-01	1.5759E-02	85.67%	13.40%
0.2	1.50E+18	475	7.00E+17	0.5	8.00E+18	SiO2	0.6000	1.6488E-02	9.4845E-01	1.3404E-02	8.4999E-01	1.5770E-02	85.72%	13.40%
0.2	1.50E+18	500	7.00E+17	0.5	8.00E+18	SiO2	0.6000	1.6487E-02	9.4860E-01	1.3411E-02	8.5000E-01	1.5778E-02	85.75%	13.41%

*Divisions: used as a measure of model complexity, a setting for the number of vertical and horizontal divisions for each region in the model (in the single cell models there are about 5 X-axis, and 10 Y-axis divisions, each subdivided by the "divs" number).

**ARC: thickness of ARC is dependent on Lambda-0 (optimal wavelength)and ARC refractive index --> arc_depth = Lambda-0 / (4*arc_refractive_index)

SILVACO ATLAS Modelling Stats for GaAs solar cell (N on P on BSF-P+)(AM0)

Divs*:	10	Points:	4399	Triangles:	8528			High Doping (Davenport, 2004)						
N-t	N-d	P-t	P-d	BSF-t	BSF-d	ARC*	Lambda-0	Jsc	Voc	Pmax	Vmax	Imax	FF	Eff
0.2	1.50E+18	5	7.00E+17	0.5	8.00E+18	SiO2	0.6000	2.0081E-02	9.5338E-01	1.6434E-02	8.6000E-01	1.9110E-02	85.84%	12.03%
0.2	1.50E+18	10	7.00E+17	0.5	8.00E+18	SiO2	0.6000	2.0081E-02	9.5338E-01	1.6435E-02	8.6000E-01	1.9110E-02	85.84%	12.03%
0.2	1.50E+18	15	7.00E+17	0.5	8.00E+18	SiO2	0.6000	2.0072E-02	9.5413E-01	1.6508E-02	8.5999E-01	1.9196E-02	86.20%	12.09%
0.2	1.50E+18	20	7.00E+17	0.5	8.00E+18	SiO2	0.6000	2.0075E-02	9.5337E-01	1.6429E-02	8.6000E-01	1.9103E-02	85.84%	12.03%
0.2	1.50E+18	25	7.00E+17	0.5	8.00E+18	SiO2	0.6000	2.0089E-02	9.5283E-01	1.6384E-02	8.5997E-01	1.9052E-02	85.60%	11.99%
0.2	1.50E+18	30	7.00E+17	0.5	8.00E+18	SiO2	0.6000	2.0084E-02	9.5253E-01	1.6362E-02	8.5995E-01	1.9027E-02	85.53%	11.98%
0.2	1.50E+18	35	7.00E+17	0.5	8.00E+18	SiO2	0.6000	2.0090E-02	9.5246E-01	1.6366E-02	8.5999E-01	1.9030E-02	85.53%	11.98%
0.2	1.50E+18	40	7.00E+17	0.5	8.00E+18	SiO2	0.6000	2.0084E-02	9.5245E-01	1.6372E-02	8.5996E-01	1.9038E-02	85.59%	11.99%
0.2	1.50E+18	45	7.00E+17	0.5	8.00E+18	SiO2	0.6000	2.0061E-02	9.5254E-01	1.6365E-02	8.6000E-01	1.9029E-02	85.64%	11.98%
0.2	1.50E+18	50	7.00E+17	0.5	8.00E+18	SiO2	0.6000	2.0080E-02	9.5262E-01	1.6393E-02	8.6000E-01	1.9062E-02	85.70%	12.00%
0.2	1.50E+18	60	7.00E+17	0.5	8.00E+18	SiO2	0.6000	2.0073E-02	9.5280E-01	1.6406E-02	8.6000E-01	1.9077E-02	85.78%	12.01%
0.2	1.50E+18	70	7.00E+17	0.5	8.00E+18	SiO2	0.6000	2.0090E-02	9.5312E-01	1.6441E-02	8.5999E-01	1.9117E-02	85.86%	12.04%
0.2	1.50E+18	80	7.00E+17	0.5	8.00E+18	SiO2	0.6000	2.0077E-02	9.5318E-01	1.6438E-02	8.6000E-01	1.9114E-02	85.90%	12.03%
0.2	1.50E+18	90	7.00E+17	0.5	8.00E+18	SiO2	0.6000	2.0093E-02	9.5345E-01	1.6464E-02	8.6000E-01	1.9145E-02	85.94%	12.05%
0.2	1.50E+18	100	7.00E+17	0.5	8.00E+18	SiO2	0.6000	2.0080E-02	9.5339E-01	1.6453E-02	8.6000E-01	1.9131E-02	85.94%	12.04%
0.2	1.50E+18	125	7.00E+17	0.5	8.00E+18	SiO2	0.6000	2.0082E-02	9.5353E-01	1.6460E-02	8.6000E-01	1.9140E-02	85.96%	12.05%
0.2	1.50E+18	150	7.00E+17	0.5	8.00E+18	SiO2	0.6000	2.0081E-02	9.5352E-01	1.6456E-02	8.6000E-01	1.9135E-02	85.94%	12.05%
0.2	1.50E+18	175	7.00E+17	0.5	8.00E+18	SiO2	0.6000	2.0094E-02	9.5384E-01	1.6485E-02	8.6000E-01	1.9168E-02	86.01%	12.07%
0.2	1.50E+18	200	7.00E+17	0.5	8.00E+18	SiO2	0.6000	2.0075E-02	9.5367E-01	1.6460E-02	8.6000E-01	1.9139E-02	85.97%	12.05%
0.2	1.50E+18	225	7.00E+17	0.5	8.00E+18	SiO2	0.6000	2.0084E-02	9.5346E-01	1.6447E-02	8.6000E-01	1.9125E-02	85.89%	12.04%
0.2	1.50E+18	250	7.00E+17	0.5	8.00E+18	SiO2	0.6000	2.0086E-02	9.5368E-01	1.6466E-02	8.6000E-01	1.9147E-02	85.96%	12.05%
0.2	1.50E+18	275	7.00E+17	0.5	8.00E+18	SiO2	0.6000	2.0094E-02	9.5388E-01	1.6485E-02	8.6000E-01	1.9168E-02	86.00%	12.07%
0.2	1.50E+18	300	7.00E+17	0.5	8.00E+18	SiO2	0.6000	2.0085E-02	9.5357E-01	1.6456E-02	8.6000E-01	1.9134E-02	85.92%	12.05%
0.2	1.50E+18	325	7.00E+17	0.5	8.00E+18	SiO2	0.6000	2.0089E-02	9.5375E-01	1.6471E-02	8.5999E-01	1.9153E-02	85.97%	12.06%
0.2	1.50E+18	350	7.00E+17	0.5	8.00E+18	SiO2	0.6000	2.0096E-02	9.5391E-01	1.6486E-02	8.6000E-01	1.9170E-02	86.00%	12.07%
0.2	1.50E+18	375	7.00E+17	0.5	8.00E+18	SiO2	0.6000	2.0086E-02	9.5354E-01	1.6452E-02	8.6000E-01	1.9130E-02	85.90%	12.04%
0.2	1.50E+18	400	7.00E+17	0.5	8.00E+18	SiO2	0.6000	2.0078E-02	9.5367E-01	1.6457E-02	8.5999E-01	1.9136E-02	85.95%	12.05%
0.2	1.50E+18	425	7.00E+17	0.5	8.00E+18	SiO2	0.6000	2.0084E-02	9.5381E-01	1.6470E-02	8.6000E-01	1.9151E-02	85.98%	12.06%
0.2	1.50E+18	450	7.00E+17	0.5	8.00E+18	SiO2	0.6000	2.0087E-02	9.5341E-01	1.6440E-02	8.6000E-01	1.9116E-02	85.84%	12.04%
0.2	1.50E+18	475	7.00E+17	0.5	8.00E+18	SiO2	0.6000	2.0086E-02	9.5353E-01	1.6451E-02	8.6000E-01	1.9129E-02	85.89%	12.04%
0.2	1.50E+18	500	7.00E+17	0.5	8.00E+18	SiO2	0.6000	2.0086E-02	9.5365E-01	1.6460E-02	8.5998E-01	1.9140E-02	85.93%	12.05%

*Divisions: used as a measure of model complexity, a setting for the number of vertical and horizontal divisions for each region in the model (in the single cell models there are about 5 X-axis, and 10 Y-axis divisions, each subdivided by the "divs" number).

**ARC: thickness of ARC is dependent on Lambda-0 (optimal wavelength)and ARC refractive index --> arc_depth = Lambda-0 / (4*arc_refractive_index)

SILVACO ATLAS Modelling Stats for GaSb solar cell (P on N on BSF-N+)(AM1.5)

Divs*:	10	Points:	4346	Triangles:	8424			Low Doping						
P-t	P-d	N-t	N-d	BSF-t	BSF-d	ARC*	Lambda-0	Jsc	Voc	Pmax	Vmax	Imax	FF	Eff
0.5	1.00E+17	5	3.50E+17	0.5	1.00E+18	SiO2	0.6000	3.6966E-02	3.2791E-01	8.8920E-03	2.7000E-01	3.2933E-02	73.36%	8.89%
0.5	1.00E+17	10	3.50E+17	0.5	1.00E+18	SiO2	0.6000	3.7013E-02	3.2810E-01	8.9103E-03	2.7000E-01	3.3001E-02	73.37%	8.91%
0.5	1.00E+17	15	3.50E+17	0.5	1.00E+18	SiO2	0.6000	3.7047E-02	3.2825E-01	8.9237E-03	2.7000E-01	3.3051E-02	73.38%	8.92%
0.5	1.00E+17	20	3.50E+17	0.5	1.00E+18	SiO2	0.6000	3.7071E-02	3.2835E-01	8.9334E-03	2.7000E-01	3.3087E-02	73.39%	8.93%
0.5	1.00E+17	25	3.50E+17	0.5	1.00E+18	SiO2	0.6000	3.7090E-02	3.2843E-01	8.9408E-03	2.7000E-01	3.3115E-02	73.40%	8.94%
0.5	1.00E+17	30	3.50E+17	0.5	1.00E+18	SiO2	0.6000	3.7103E-02	3.2849E-01	8.9461E-03	2.7000E-01	3.3134E-02	73.40%	8.95%
0.5	1.00E+17	35	3.50E+17	0.5	1.00E+18	SiO2	0.6000	3.7115E-02	3.2854E-01	8.9509E-03	2.7000E-01	3.3152E-02	73.41%	8.95%
0.5	1.00E+17	40	3.50E+17	0.5	1.00E+18	SiO2	0.6000	3.7125E-02	3.2858E-01	8.9548E-03	2.7000E-01	3.3166E-02	73.41%	8.95%
0.5	1.00E+17	45	3.50E+17	0.5	1.00E+18	SiO2	0.6000	3.7131E-02	3.2862E-01	8.9576E-03	2.7000E-01	3.3176E-02	73.41%	8.96%
0.5	1.00E+17	50	3.50E+17	0.5	1.00E+18	SiO2	0.6000	3.7140E-02	3.2865E-01	8.9608E-03	2.7000E-01	3.3188E-02	73.41%	8.96%
0.5	1.00E+17	60	3.50E+17	0.5	1.00E+18	SiO2	0.6000	3.7149E-02	3.2870E-01	8.9648E-03	2.7000E-01	3.3203E-02	73.42%	8.96%
0.5	1.00E+17	70	3.50E+17	0.5	1.00E+18	SiO2	0.6000	3.7161E-02	3.2874E-01	8.9691E-03	2.7000E-01	3.3219E-02	73.42%	8.97%
0.5	1.00E+17	80	3.50E+17	0.5	1.00E+18	SiO2	0.6000	3.7167E-02	3.2877E-01	8.9717E-03	2.7000E-01	3.3229E-02	73.42%	8.97%
0.5	1.00E+17	90	3.50E+17	0.5	1.00E+18	SiO2	0.6000	3.7174E-02	3.2880E-01	8.9742E-03	2.7000E-01	3.3238E-02	73.42%	8.97%
0.5	1.00E+17	100	3.50E+17	0.5	1.00E+18	SiO2	0.6000	3.7175E-02	3.2881E-01	8.9750E-03	2.7000E-01	3.3241E-02	73.42%	8.97%
0.5	1.00E+17	125	3.50E+17	0.5	1.00E+18	SiO2	0.6000	3.7186E-02	3.2885E-01	8.9792E-03	2.7000E-01	3.3256E-02	73.43%	8.98%
0.5	1.00E+17	150	3.50E+17	0.5	1.00E+18	SiO2	0.6000	3.7195E-02	3.2888E-01	8.9823E-03	2.7000E-01	3.3268E-02	73.43%	8.98%
0.5	1.00E+17	175	3.50E+17	0.5	1.00E+18	SiO2	0.6000	3.7201E-02	3.2890E-01	8.9842E-03	2.7000E-01	3.3275E-02	73.43%	8.98%
0.5	1.00E+17	200	3.50E+17	0.5	1.00E+18	SiO2	0.6000	3.7202E-02	3.2892E-01	8.9851E-03	2.7000E-01	3.3278E-02	73.43%	8.99%
0.5	1.00E+17	225	3.50E+17	0.5	1.00E+18	SiO2	0.6000	3.7208E-02	3.2893E-01	8.9869E-03	2.7000E-01	3.3285E-02	73.43%	8.99%
0.5	1.00E+17	250	3.50E+17	0.5	1.00E+18	SiO2	0.6000	3.7201E-02	3.2899E-01	8.9855E-03	2.7000E-01	3.3280E-02	73.43%	8.99%
0.5	1.00E+17	275	3.50E+17	0.5	1.00E+18	SiO2	0.6000	3.7213E-02	3.2895E-01	8.9887E-03	2.7000E-01	3.3291E-02	73.43%	8.99%
0.5	1.00E+17	300	3.50E+17	0.5	1.00E+18	SiO2	0.6000	3.7214E-02	3.2896E-01	8.9893E-03	2.7000E-01	3.3294E-02	73.43%	8.99%
0.5	1.00E+17	325	3.50E+17	0.5	1.00E+18	SiO2	0.6000	3.7215E-02	3.2897E-01	8.9896E-03	2.7000E-01	3.3295E-02	73.43%	8.99%
0.5	1.00E+17	350	3.50E+17	0.5	1.00E+18	SiO2	0.6000	3.7217E-02	3.2897E-01	8.9905E-03	2.7000E-01	3.3298E-02	73.43%	8.99%
0.5	1.00E+17	375	3.50E+17	0.5	1.00E+18	SiO2	0.6000	3.7218E-02	3.2898E-01	8.9908E-03	2.7000E-01	3.3299E-02	73.43%	8.99%
0.5	1.00E+17	400	3.50E+17	0.5	1.00E+18	SiO2	0.6000	3.7215E-02	3.2898E-01	8.9901E-03	2.7000E-01	3.3297E-02	73.43%	8.99%
0.5	1.00E+17	425	3.50E+17	0.5	1.00E+18	SiO2	0.6000	3.7218E-02	3.2898E-01	8.9910E-03	2.7000E-01	3.3300E-02	73.43%	8.99%
0.5	1.00E+17	450	3.50E+17	0.5	1.00E+18	SiO2	0.6000	3.7221E-02	3.2899E-01	8.9918E-03	2.7000E-01	3.3303E-02	73.43%	8.99%
0.5	1.00E+17	475	3.50E+17	0.5	1.00E+18	SiO2	0.6000	3.7222E-02	3.2899E-01	8.9921E-03	2.7000E-01	3.3304E-02	73.43%	8.99%
0.5	1.00E+17	500	3.50E+17	0.5	1.00E+18	SiO2	0.6000	3.7218E-02	3.2899E-01	8.9910E-03	2.7000E-01	3.3300E-02	73.43%	8.99%

*Divisions: used as a measure of model complexity, a setting for the number of vertical and horizontal divisions for each region in the model (in the single cell models there are about 5 X-axis, and 10 Y-axis divisions, each subdivided by the "divs" number).

**ARC: thickness of ARC is dependent on Lambda-0 (optimal wavelength)and ARC refractive index --> arc_depth = Lambda-0 / (4*arc_refractive_index)

SILVACO ATLAS Modelling Stats for GaSb solar cell (P on N on BSF-N+)(AM0)

Divs*:	10	Points:	4346	Triangles:	8424			Low Doping						
P-t	P-d	N-t	N-d	BSF-t	BSF-d	ARC*	Lambda-0	Jsc	Voc	Pmax	Vmax	Imax	FF	Eff
0.5	1.00E+17	5	3.50E+17	0.5	1.00E+18	SiO2	0.6000	5.6652E-02	3.3910E-01	1.4197E-02	2.8000E-01	5.0704E-02	73.90%	10.39%
0.5	1.00E+17	10	3.50E+17	0.5	1.00E+18	SiO2	0.6000	5.6834E-02	3.3936E-01	1.4257E-02	2.8000E-01	5.0917E-02	73.92%	10.44%
0.5	1.00E+17	15	3.50E+17	0.5	1.00E+18	SiO2	0.6000	5.6921E-02	3.3953E-01	1.4288E-02	2.8000E-01	5.1028E-02	73.93%	10.46%
0.5	1.00E+17	20	3.50E+17	0.5	1.00E+18	SiO2	0.6000	5.6984E-02	3.3965E-01	1.4310E-02	2.8000E-01	5.1107E-02	73.94%	10.48%
0.5	1.00E+17	25	3.50E+17	0.5	1.00E+18	SiO2	0.6000	5.7039E-02	3.3975E-01	1.4329E-02	2.7999E-01	5.1177E-02	73.94%	10.49%
0.5	1.00E+17	30	3.50E+17	0.5	1.00E+18	SiO2	0.6000	5.7073E-02	3.3982E-01	1.4341E-02	2.7998E-01	5.1222E-02	73.95%	10.50%
0.5	1.00E+17	35	3.50E+17	0.5	1.00E+18	SiO2	0.6000	5.7107E-02	3.3988E-01	1.4353E-02	2.7999E-01	5.1265E-02	73.95%	10.51%
0.5	1.00E+17	40	3.50E+17	0.5	1.00E+18	SiO2	0.6000	5.7130E-02	3.3993E-01	1.4361E-02	2.8000E-01	5.1291E-02	73.95%	10.51%
0.5	1.00E+17	45	3.50E+17	0.5	1.00E+18	SiO2	0.6000	5.7152E-02	3.3998E-01	1.4370E-02	2.8000E-01	5.1320E-02	73.95%	10.52%
0.5	1.00E+17	50	3.50E+17	0.5	1.00E+18	SiO2	0.6000	5.7169E-02	3.4001E-01	1.4376E-02	2.8000E-01	5.1341E-02	73.96%	10.52%
0.5	1.00E+17	60	3.50E+17	0.5	1.00E+18	SiO2	0.6000	5.7197E-02	3.4005E-01	1.4386E-02	2.8000E-01	5.1378E-02	73.96%	10.53%
0.5	1.00E+17	70	3.50E+17	0.5	1.00E+18	SiO2	0.6000	5.7224E-02	3.4008E-01	1.4395E-02	2.8000E-01	5.1410E-02	73.97%	10.54%
0.5	1.00E+17	80	3.50E+17	0.5	1.00E+18	SiO2	0.6000	5.7243E-02	3.4010E-01	1.4402E-02	2.7999E-01	5.1436E-02	73.97%	10.54%
0.5	1.00E+17	90	3.50E+17	0.5	1.00E+18	SiO2	0.6000	5.7258E-02	3.4012E-01	1.4407E-02	2.7999E-01	5.1454E-02	73.98%	10.55%
0.5	1.00E+17	100	3.50E+17	0.5	1.00E+18	SiO2	0.6000	5.7269E-02	3.4014E-01	1.4411E-02	2.8000E-01	5.1467E-02	73.98%	10.55%
0.5	1.00E+17	125	3.50E+17	0.5	1.00E+18	SiO2	0.6000	5.7290E-02	3.4017E-01	1.4418E-02	2.7999E-01	5.1495E-02	73.98%	10.56%
0.5	1.00E+17	150	3.50E+17	0.5	1.00E+18	SiO2	0.6000	5.7311E-02	3.4019E-01	1.4426E-02	2.8000E-01	5.1520E-02	73.99%	10.56%
0.5	1.00E+17	175	3.50E+17	0.5	1.00E+18	SiO2	0.6000	5.7324E-02	3.4021E-01	1.4430E-02	2.7999E-01	5.1537E-02	73.99%	10.56%
0.5	1.00E+17	200	3.50E+17	0.5	1.00E+18	SiO2	0.6000	5.7333E-02	3.4022E-01	1.4433E-02	2.8000E-01	5.1546E-02	73.99%	10.57%
0.5	1.00E+17	225	3.50E+17	0.5	1.00E+18	SiO2	0.6000	5.7342E-02	3.4023E-01	1.4436E-02	2.8000E-01	5.1557E-02	73.99%	10.57%
0.5	1.00E+17	250	3.50E+17	0.5	1.00E+18	SiO2	0.6000	5.7341E-02	3.4024E-01	1.4436E-02	2.7999E-01	5.1559E-02	73.99%	10.57%
0.5	1.00E+17	275	3.50E+17	0.5	1.00E+18	SiO2	0.6000	5.7354E-02	3.4025E-01	1.4440E-02	2.8000E-01	5.1571E-02	74.00%	10.57%
0.5	1.00E+17	300	3.50E+17	0.5	1.00E+18	SiO2	0.6000	5.7358E-02	3.4026E-01	1.4442E-02	2.8000E-01	5.1577E-02	74.00%	10.57%
0.5	1.00E+17	325	3.50E+17	0.5	1.00E+18	SiO2	0.6000	5.7362E-02	3.4026E-01	1.4443E-02	2.8000E-01	5.1582E-02	74.00%	10.57%
0.5	1.00E+17	350	3.50E+17	0.5	1.00E+18	SiO2	0.6000	5.7366E-02	3.4026E-01	1.4444E-02	2.8000E-01	5.1586E-02	74.00%	10.57%
0.5	1.00E+17	375	3.50E+17	0.5	1.00E+18	SiO2	0.6000	5.7369E-02	3.4027E-01	1.4445E-02	2.8000E-01	5.1590E-02	74.00%	10.57%
0.5	1.00E+17	400	3.50E+17	0.5	1.00E+18	SiO2	0.6000	5.7371E-02	3.4027E-01	1.4446E-02	2.8000E-01	5.1592E-02	74.00%	10.58%
0.5	1.00E+17	425	3.50E+17	0.5	1.00E+18	SiO2	0.6000	5.7373E-02	3.4027E-01	1.4446E-02	2.7999E-01	5.1596E-02	74.00%	10.58%
0.5	1.00E+17	450	3.50E+17	0.5	1.00E+18	SiO2	0.6000	5.7375E-02	3.4028E-01	1.4447E-02	2.8000E-01	5.1597E-02	74.00%	10.58%
0.5	1.00E+17	475	3.50E+17	0.5	1.00E+18	SiO2	0.6000	5.7377E-02	3.4028E-01	1.4448E-02	2.8000E-01	5.1600E-02	74.00%	10.58%
0.5	1.00E+17	500	3.50E+17	0.5	1.00E+18	SiO2	0.6000	5.7379E-02	3.4028E-01	1.4448E-02	2.8000E-01	5.1601E-02	73.99%	10.58%

*Divisions: used as a measure of model complexity, a setting for the number of vertical and horizontal divisions for each region in the model (in the single cell models there are about 5 X-axis, and 10 Y-axis divisions, each subdivided by the "divs" number).

**ARC: thickness of ARC is dependent on Lambda-0 (optimal wavelength)and ARC refractive index --> arc_depth = Lambda-0 / (4*arc_refractive_index)

SILVACO ATLAS Modelling Stats for GaSb solar cell (P on N on BSF-N+)(AM1.5)

Divs*:	10	Points:	4346	Triangles:	8424			High Doping (Davenport, 2004)						
P-t	P-d	N-t	N-d	BSF-t	BSF-d	ARC*	Lambda-0	Jsc	Voc	Pmax	Vmax	Imax	FF	Eff
0.37	9.80E+19	5	1.00E+20	15	1.00E+20	SiO2	0.6000	3.8148E-02	5.0560E-01	1.5536E-02	4.3000E-01	3.6131E-02	80.55%	15.54%
0.37	9.80E+19	10	1.00E+20	15	1.00E+20	SiO2	0.6000	3.8217E-02	5.0607E-01	1.5579E-02	4.3000E-01	3.6231E-02	80.55%	15.58%
0.37	9.80E+19	15	1.00E+20	15	1.00E+20	SiO2	0.6000	3.8256E-02	5.0639E-01	1.5605E-02	4.3000E-01	3.6291E-02	80.55%	15.61%
0.37	9.80E+19	20	1.00E+20	15	1.00E+20	SiO2	0.6000	3.8283E-02	5.0667E-01	1.5625E-02	4.3000E-01	3.6337E-02	80.55%	15.62%
0.37	9.80E+19	25	1.00E+20	15	1.00E+20	SiO2	0.6000	3.8315E-02	5.0689E-01	1.5644E-02	4.3000E-01	3.6383E-02	80.55%	15.64%
0.37	9.80E+19	30	1.00E+20	15	1.00E+20	SiO2	0.6000	3.8332E-02	5.0706E-01	1.5656E-02	4.3000E-01	3.6410E-02	80.55%	15.66%
0.37	9.80E+19	35	1.00E+20	15	1.00E+20	SiO2	0.6000	3.8353E-02	5.0720E-01	1.5669E-02	4.3000E-01	3.6440E-02	80.55%	15.67%
0.37	9.80E+19	40	1.00E+20	15	1.00E+20	SiO2	0.6000	3.8366E-02	5.0732E-01	1.5678E-02	4.3000E-01	3.6460E-02	80.55%	15.68%
0.37	9.80E+19	45	1.00E+20	15	1.00E+20	SiO2	0.6000	3.8378E-02	5.0741E-01	1.5685E-02	4.3000E-01	3.6477E-02	80.55%	15.69%
0.37	9.80E+19	50	1.00E+20	15	1.00E+20	SiO2	0.6000	3.8387E-02	5.0750E-01	1.5692E-02	4.3000E-01	3.6492E-02	80.55%	15.69%
0.37	9.80E+19	60	1.00E+20	15	1.00E+20	SiO2	0.6000	3.8403E-02	5.0763E-01	1.5702E-02	4.3000E-01	3.6516E-02	80.54%	15.70%
0.37	9.80E+19	70	1.00E+20	15	1.00E+20	SiO2	0.6000	3.8415E-02	5.0774E-01	1.5710E-02	4.3000E-01	3.6534E-02	80.54%	15.71%
0.37	9.80E+19	80	1.00E+20	15	1.00E+20	SiO2	0.6000	3.8424E-02	5.0783E-01	1.5716E-02	4.3000E-01	3.6549E-02	80.54%	15.72%
0.37	9.80E+19	90	1.00E+20	15	1.00E+20	SiO2	0.6000	3.8425E-02	5.0789E-01	1.5718E-02	4.3000E-01	3.6554E-02	80.54%	15.72%
0.37	9.80E+19	100	1.00E+20	15	1.00E+20	SiO2	0.6000	3.8439E-02	5.0795E-01	1.5725E-02	4.3000E-01	3.6571E-02	80.54%	15.73%
0.37	9.80E+19	125	1.00E+20	15	1.00E+20	SiO2	0.6000	3.8445E-02	5.0806E-01	1.5731E-02	4.3000E-01	3.6584E-02	80.54%	15.73%
0.37	9.80E+19	150	1.00E+20	15	1.00E+20	SiO2	0.6000	3.8460E-02	5.0815E-01	1.5739E-02	4.3000E-01	3.6603E-02	80.54%	15.74%
0.37	9.80E+19	175	1.00E+20	15	1.00E+20	SiO2	0.6000	3.8468E-02	5.0825E-01	1.5746E-02	4.3000E-01	3.6618E-02	80.53%	15.75%
0.37	9.80E+19	200	1.00E+20	15	1.00E+20	SiO2	0.6000	3.8468E-02	5.0825E-01	1.5746E-02	4.3000E-01	3.6618E-02	80.53%	15.75%
0.37	9.80E+19	225	1.00E+20	15	1.00E+20	SiO2	0.6000	3.8476E-02	5.0829E-01	1.5750E-02	4.3000E-01	3.6627E-02	80.53%	15.75%
0.37	9.80E+19	250	1.00E+20	15	1.00E+20	SiO2	0.6000	3.8479E-02	5.0832E-01	1.5752E-02	4.3000E-01	3.6632E-02	80.53%	15.75%
0.37	9.80E+19	275	1.00E+20	15	1.00E+20	SiO2	0.6000	3.8479E-02	5.0834E-01	1.5752E-02	4.3000E-01	3.6634E-02	80.53%	15.75%
0.37	9.80E+19	300	1.00E+20	15	1.00E+20	SiO2	0.6000	3.8484E-02	5.0837E-01	1.5755E-02	4.3000E-01	3.6640E-02	80.53%	15.76%
0.37	9.80E+19	325	1.00E+20	15	1.00E+20	SiO2	0.6000	3.8486E-02	5.0839E-01	1.5757E-02	4.3000E-01	3.6643E-02	80.53%	15.76%
0.37	9.80E+19	350	1.00E+20	15	1.00E+20	SiO2	0.6000	3.8488E-02	5.0840E-01	1.5758E-02	4.3000E-01	3.6646E-02	80.53%	15.76%
0.37	9.80E+19	375	1.00E+20	15	1.00E+20	SiO2	0.6000	3.8483E-02	5.0841E-01	1.5756E-02	4.3000E-01	3.6642E-02	80.53%	15.76%
0.37	9.80E+19	400	1.00E+20	15	1.00E+20	SiO2	0.6000	3.8491E-02	5.0843E-01	1.5760E-02	4.3000E-01	3.6650E-02	80.53%	15.76%
0.37	9.80E+19	425	1.00E+20	15	1.00E+20	SiO2	0.6000	3.8492E-02	5.0844E-01	1.5760E-02	4.3000E-01	3.6652E-02	80.53%	15.76%
0.37	9.80E+19	450	1.00E+20	15	1.00E+20	SiO2	0.6000	3.8493E-02	5.0845E-01	1.5761E-02	4.3000E-01	3.6653E-02	80.53%	15.76%
0.37	9.80E+19	475	1.00E+20	15	1.00E+20	SiO2	0.6000	3.8494E-02	5.0846E-01	1.5762E-02	4.3000E-01	3.6655E-02	80.53%	15.76%
0.37	9.80E+19	500	1.00E+20	15	1.00E+20	SiO2	0.6000	3.8489E-02	5.0846E-01	1.5760E-02	4.3000E-01	3.6651E-02	80.53%	15.76%

*Divisions: used as a measure of model complexity, a setting for the number of vertical and horizontal divisions for each region in the model (in the single cell models there are about 5 X-axis, and 10 Y-axis divisions, each subdivided by the "divs" number).

**ARC: thickness of ARC is dependent on Lambda-0 (optimal wavelength)and ARC refractive index --> arc_depth = Lambda-0 / (4*arc_refractive_index)

SILVACO ATLAS Modelling Stats for GaSb solar cell (P on N on BSF-N+)(AM0)

Divs*:	10	Points:	4346	Triangles:	8424			High Doping (Davenport, 2004)						
P-t	P-d	N-t	N-d	BSF-t	BSF-d	ARC*	Lambda-0	Jsc	Voc	Pmax	Vmax	Imax	FF	Eff
0.37	9.80E+19	5	1.00E+20	15	1.00E+20	SiO2	0.6000	5.8293E-02	5.1661E-01	2.4343E-02	4.4000E-01	5.5324E-02	80.83%	17.82%
0.37	9.80E+19	10	1.00E+20	15	1.00E+20	SiO2	0.6000	5.8439E-02	5.1713E-01	2.4427E-02	4.4000E-01	5.5516E-02	80.83%	17.88%
0.37	9.80E+19	15	1.00E+20	15	1.00E+20	SiO2	0.6000	5.8531E-02	5.1747E-01	2.4481E-02	4.4000E-01	5.5638E-02	80.83%	17.92%
0.37	9.80E+19	20	1.00E+20	15	1.00E+20	SiO2	0.6000	5.8610E-02	5.1778E-01	2.4528E-02	4.4000E-01	5.5744E-02	80.82%	17.96%
0.37	9.80E+19	25	1.00E+20	15	1.00E+20	SiO2	0.6000	5.8657E-02	5.1801E-01	2.4557E-02	4.4000E-01	5.5812E-02	80.82%	17.98%
0.37	9.80E+19	30	1.00E+20	15	1.00E+20	SiO2	0.6000	5.8704E-02	5.1819E-01	2.4585E-02	4.4000E-01	5.5874E-02	80.82%	18.00%
0.37	9.80E+19	35	1.00E+20	15	1.00E+20	SiO2	0.6000	5.8759E-02	5.1835E-01	2.4615E-02	4.4000E-01	5.5942E-02	80.82%	18.02%
0.37	9.80E+19	40	1.00E+20	15	1.00E+20	SiO2	0.6000	5.8790E-02	5.1848E-01	2.4633E-02	4.4000E-01	5.5984E-02	80.81%	18.03%
0.37	9.80E+19	45	1.00E+20	15	1.00E+20	SiO2	0.6000	5.8817E-02	5.1858E-01	2.4648E-02	4.4000E-01	5.6019E-02	80.81%	18.04%
0.37	9.80E+19	50	1.00E+20	15	1.00E+20	SiO2	0.6000	5.8839E-02	5.1868E-01	2.4662E-02	4.4000E-01	5.6049E-02	80.81%	18.05%
0.37	9.80E+19	60	1.00E+20	15	1.00E+20	SiO2	0.6000	5.8876E-02	5.1882E-01	2.4683E-02	4.4000E-01	5.6098E-02	80.81%	18.07%
0.37	9.80E+19	70	1.00E+20	15	1.00E+20	SiO2	0.6000	5.8904E-02	5.1894E-01	2.4699E-02	4.4000E-01	5.6135E-02	80.80%	18.08%
0.37	9.80E+19	80	1.00E+20	15	1.00E+20	SiO2	0.6000	5.8926E-02	5.1903E-01	2.4713E-02	4.4000E-01	5.6165E-02	80.80%	18.09%
0.37	9.80E+19	90	1.00E+20	15	1.00E+20	SiO2	0.6000	5.8928E-02	5.1910E-01	2.4716E-02	4.4000E-01	5.6173E-02	80.80%	18.09%
0.37	9.80E+19	100	1.00E+20	15	1.00E+20	SiO2	0.6000	5.8960E-02	5.1917E-01	2.4733E-02	4.4000E-01	5.6210E-02	80.80%	18.11%
0.37	9.80E+19	125	1.00E+20	15	1.00E+20	SiO2	0.6000	5.8989E-02	5.1930E-01	2.4750E-02	4.4000E-01	5.6249E-02	80.79%	18.12%
0.37	9.80E+19	150	1.00E+20	15	1.00E+20	SiO2	0.6000	5.9010E-02	5.1938E-01	2.4762E-02	4.4000E-01	5.6277E-02	80.79%	18.13%
0.37	9.80E+19	175	1.00E+20	15	1.00E+20	SiO2	0.6000	5.9026E-02	5.1945E-01	2.4771E-02	4.4000E-01	5.6297E-02	80.79%	18.13%
0.37	9.80E+19	200	1.00E+20	15	1.00E+20	SiO2	0.6000	5.9018E-02	5.1949E-01	2.4769E-02	4.4000E-01	5.6294E-02	80.79%	18.13%
0.37	9.80E+19	225	1.00E+20	15	1.00E+20	SiO2	0.6000	5.9047E-02	5.1954E-01	2.4783E-02	4.4000E-01	5.6326E-02	80.79%	18.14%
0.37	9.80E+19	250	1.00E+20	15	1.00E+20	SiO2	0.6000	5.9055E-02	5.1957E-01	2.4788E-02	4.4000E-01	5.6300E-02	80.79%	18.15%
0.37	9.80E+19	275	1.00E+20	15	1.00E+20	SiO2	0.6000	5.9061E-02	5.1960E-01	2.4792E-02	4.4000E-01	5.6344E-02	80.79%	18.15%
0.37	9.80E+19	300	1.00E+20	15	1.00E+20	SiO2	0.6000	5.9067E-02	5.1962E-01	2.4795E-02	4.4000E-01	5.6352E-02	80.78%	18.15%
0.37	9.80E+19	325	1.00E+20	15	1.00E+20	SiO2	0.6000	5.9071E-02	5.1964E-01	2.4798E-02	4.4000E-01	5.6358E-02	80.78%	18.15%
0.37	9.80E+19	350	1.00E+20	15	1.00E+20	SiO2	0.6000	5.9075E-02	5.1966E-01	2.4800E-02	4.4000E-01	5.6363E-02	80.78%	18.16%
0.37	9.80E+19	375	1.00E+20	15	1.00E+20	SiO2	0.6000	5.9062E-02	5.1967E-01	2.4795E-02	4.4000E-01	5.6351E-02	80.78%	18.15%
0.37	9.80E+19	400	1.00E+20	15	1.00E+20	SiO2	0.6000	5.9082E-02	5.1969E-01	2.4804E-02	4.4000E-01	5.6372E-02	80.78%	18.16%
0.37	9.80E+19	425	1.00E+20	15	1.00E+20	SiO2	0.6000	5.9085E-02	5.1970E-01	2.4805E-02	4.4000E-01	5.6376E-02	80.78%	18.16%
0.37	9.80E+19	450	1.00E+20	15	1.00E+20	SiO2	0.6000	5.9087E-02	5.1971E-01	2.4807E-02	4.4000E-01	5.6379E-02	80.78%	18.16%
0.37	9.80E+19	475	1.00E+20	15	1.00E+20	SiO2	0.6000	5.9089E-02	5.1972E-01	2.4808E-02	4.4000E-01	5.6382E-02	80.78%	18.16%
0.37	9.80E+19	500	1.00E+20	15	1.00E+20	SiO2	0.6000	5.9070E-02	5.1972E-01	2.4800E-02	4.4000E-01	5.6364E-02	80.78%	18.16%

*Divisions: used as a measure of model complexity, a setting for the number of vertical and horizontal divisions for each region in the model (in the single cell models there are about 5 X-axis, and 10 Y-axis divisions, each subdivided by the "divs" number).

**ARC: thickness of ARC is dependent on Lambda-0 (optimal wavelength)and ARC refractive index --> arc_depth = Lambda-0 / (4*arc_refractive_index)

SILVACO ATLAS Modelling Stats for Tandem GaAs (N-P-P+) GaSb (P-N-N+) solar cell (AM0)

Divs*: 10 Pointz: 4346 Triangles: 8424 Low Doping

P-In 0.1366

									Upper Cell (GaAs)								Lower Cell (GaSb)								Upper Cell							LowerCell							Combined Results						
																																					Dual Junction					Tandem		
N-t	N-d	P-t	P-d	BSF-t	BSF-d	ARC*	L-0	Gap-t	P-t	P-d	N-t	N-d	BSF-t	BSF-d	ARC*	L-0	Jsc	Voc	Pmax	Vmax	Imax	FF	Eff-u	Jsc	Voc	Pmax	Vmax	Imax	FF	Eff-l	V-t	I-t	P-t	Eff-t	W/m^2	P-t	Eff-t	W/m^2
0.00781	1.00E+17	0.01563	1.00E+16	0.00781	1.00E+17	SiO2	0.5000	0.10	0.37	9.00E+19	50	1.00E+20	0.37	1.00E+20	TiO2	0.00	3.6679E-03	0.5375E-01	2.4111E-03	7.6000E-01	3.1725E-03	77.01%	1.77%	2.1415E-02	4.9206E-01	8.4467E-03	4.2000E-01	2.0111E-02	80.16%	6.18%	1.1900E+00	3.1725E-03	3.7434E-03	2.74%	37.44	9.7792E-03	7.16%	100.50
0.01563	1.00E+17	0.03125	1.00E+16	0.01563	1.00E+17	SiO2	0.5000	0.10	0.37	9.00E+19	50	1.00E+20	0.37	1.00E+20	TiO2	0.00	6.4732E-03	0.6189E-01	3.4659E-03	7.7000E-01	4.5012E-03	62.12%	2.54%	2.0755E-02	4.9134E-01	8.1695E-03	4.2000E-01	1.9451E-02	80.11%	5.98%	1.1900E+00	4.5012E-03	5.3564E-03	3.92%	53.56	1.0060E-02	7.36%	116.35
0.03125	1.00E+17	0.0625	1.00E+16	0.03125	1.00E+17	SiO2	0.5000	0.10	0.37	9.00E+19	50	1.00E+20	0.37	1.00E+20	TiO2	0.00	1.2478E-02	0.8524E-01	9.2574E-03	7.8000E-01	1.1868E-02	83.81%	6.78%	1.9840E-02	4.9035E-01	7.7852E-03	4.2000E-01	1.8534E-02	80.02%	5.70%	1.2000E+00	1.1868E-02	1.4242E-02	10.43%	142.42	1.4242E-02	10.43%	170.43
0.0625	1.00E+17	0.125	1.00E+16	0.0625	1.00E+17	SiO2	0.5000	0.10	0.37	9.00E+19	50	1.00E+20	0.37	1.00E+20	TiO2	0.00	1.6610E-02	0.9234E-01	1.2300E-02	7.8000E-01	1.5673E-02	83.43%	9.06%	1.8632E-02	4.8866E-01	7.2992E-03	4.1999E-01	1.7380E-02	79.95%	5.34%	1.2099E+00	1.5673E-02	1.8963E-02	13.88%	189.63	1.8963E-02	13.88%	196.00
0.07813	1.00E+17	0.15625	1.00E+16	0.07813	1.00E+17	SiO2	0.5000	0.10	0.37	9.00E+19	50	1.00E+20	0.37	1.00E+20	TiO2	0.00	1.7402E-02	0.9456E-01	1.3216E-02	7.8000E-01	1.7071E-02	83.16%	9.75%	1.8235E-02	4.8800E-01	7.1235E-03	4.1999E-01	1.7254E-02	79.94%	5.23%	1.2100E+00	1.7071E-02	2.0315E-02	14.87%	203.15	2.0315E-02	14.87%	204.49
0.08203	1.00E+17	0.16406	1.00E+16	0.08203	1.00E+17	SiO2	0.5000	0.10	0.37	9.00E+19	50	1.00E+20	0.37	1.00E+20	TiO2	0.00	1.7417E-02	0.9473E-01	1.3309E-02	7.7995E-01	1.7208E-02	83.08%	9.83%	1.8197E-02	4.8774E-01	7.0673E-03	4.1999E-01	1.6831E-02	79.54%	5.20%	1.2100E+00	1.7208E-02	2.0457E-02	15.00%	204.57	2.0457E-02	15.00%	204.57
0.01594	1.00E+17	0.17188	1.00E+16	0.08594	1.00E+17	SiO2	0.5000	0.10	0.37	9.00E+19	50	1.00E+20	0.37	1.00E+20	TiO2	0.00	1.8431E-02	0.9487E-01	1.3467E-02	7.8000E-01	1.7560E-02	83.02%	10.03%	1.8114E-02	4.8776E-01	7.0637E-03	4.1999E-01	1.7229E-02	79.95%	5.17%	1.1900E+00	1.7229E-02	2.0502E-02	15.01%	205.02	2.0502E-02	15.01%	207.51
0.09375	1.00E+17	0.1875	1.00E+16	0.09375	1.00E+17	SiO2	0.5000	0.10	0.37	9.00E+19	50	1.00E+20	0.37	1.00E+20	TiO2	0.00	1.8907E-02	0.9498E-01	1.4030E-02	7.8000E-01	1.7981E-02	82.91%	10.27%	1.7964E-02	4.8759E-01	7.0003E-03	4.1999E-01	1.7074E-02	79.95%	5.12%	1.1900E+00	1.7074E-02	2.0319E-02	14.87%	203.18	2.0319E-02	14.87%	210.21
0.10938	1.00E+17	0.21875	1.00E+16	0.10938	1.00E+17	SiO2	0.5000	0.10	0.37	9.00E+19	50	1.00E+20	0.37	1.00E+20	TiO2	0.00	1.9722E-02	0.9508E-01	1.4621E-02	7.7995E-01	1.8746E-02	82.80%	10.70%	1.7691E-02	4.8700E-01	6.8899E-03	4.1999E-01	1.6805E-02	79.96%	5.04%	1.1900E+00	1.6805E-02	1.9997E-02	14.64%	199.97	1.9997E-02	14.64%	215.11
0.125	1.00E+17	0.25	1.00E+16	0.125	1.00E+17	SiO2	0.5000	0.10	0.37	9.00E+19	50	1.00E+20	0.37	1.00E+20	TiO2	0.00	2.0379E-02	0.9504E-01	1.5002E-02	7.7995E-01	1.9236E-02	82.68%	11.04%	1.7464E-02	4.8672E-01	6.7969E-03	4.1999E-01	1.6578E-02	79.97%	4.98%	1.1900E+00	1.6578E-02	1.9727E-02	14.44%	197.27	1.9727E-02	14.44%	219.79
0.25	1.00E+17	0.5	1.00E+16	0.25	1.00E+17	SiO2	0.5000	0.10	0.37	9.00E+19	50	1.00E+20	0.37	1.00E+20	TiO2	0.00	2.2665E-02	0.9407E-01	1.6776E-02	7.8000E-01	2.1508E-02	82.79%	12.28%	1.6458E-02	4.8511E-01	6.3846E-03	4.1999E-01	1.5972E-02	79.97%	4.67%	1.1900E+00	1.5972E-02	1.8931E-02	13.97%	189.31	1.8931E-02	13.97%	231.61
0.275	1.00E+17	0.55	1.00E+16	0.275	1.00E+17	SiO2	0.5000	0.10	0.37	9.00E+19	50	1.00E+20	0.37	1.00E+20	TiO2	0.00	2.2914E-02	0.9377E-01	1.7009E-02	7.8000E-01	2.1806E-02	83.05%	12.45%	1.6350E-02	4.8494E-01	6.3403E-03	4.1999E-01	1.5846E-02	79.97%	4.64%	1.1900E+00	1.5846E-02	1.8402E-02	13.47%	184.02	1.8402E-02	13.47%	233.49
0.3	1.00E+17	0.6	1.00E+16	0.3	1.00E+17	SiO2	0.5000	0.10	0.37	9.00E+19	50	1.00E+20	0.37	1.00E+20	TiO2	0.00	2.3110E-02	0.9298E-01	1.7118E-02	7.8000E-01	2.1946E-02	82.94%	12.53%	1.6258E-02	4.8479E-01	6.3025E-03	4.1999E-01	1.5372E-02	79.96%	4.61%	1.1900E+00	1.5372E-02	1.8293E-02	13.39%	182.93	1.8293E-02	13.39%	234.21
0.3125	1.00E+17	0.625	1.00E+16	0.3125	1.00E+17	SiO2	0.5000	0.10	0.37	9.00E+19	50	1.00E+20	0.37	1.00E+20	TiO2	0.00	2.3196E-02	0.9252E-01	1.7128E-02	7.7995E-01	2.1972E-02	82.78%	12.55%	1.6217E-02	4.8473E-01	6.2840E-03	4.1999E-01	1.5332E-02	79.97%	4.60%	1.1900E+00	1.5332E-02	1.8244E-02	13.36%	182.44	1.8244E-02	13.36%	234.24
0.325	1.00E+17	0.65	1.00E+16	0.325	1.00E+17	SiO2	0.5000	0.10	0.37	9.00E+19	50	1.00E+20	0.37	1.00E+20	TiO2	0.00	2.3270E-02	0.9213E-01	1.7158E-02	7.8000E-01	2.1997E-02	82.65%	12.56%	1.6160E-02	4.8467E-01	6.2705E-03	4.1999E-01	1.5294E-02	79.96%	4.59%	1.1900E+00	1.5294E-02	1.8200E-02	13.32%	182.00	1.8200E-02	13.32%	234.28
0.33125	1.00E+17	0.6625	1.00E+16	0.33125	1.00E+17	SiO2	0.5000	0.10	0.37	9.00E+19	50	1.00E+20	0.37	1.00E+20	TiO2	0.00	2.3304E-02	0.9190E-01	1.7173E-02	7.7995E-01	2.2017E-02	82.61%	12.57%	1.6162E-02	4.8464E-01	6.2632E-03	4.1999E-01	1.5276E-02	79.96%	4.59%	1.1900E+00	1.5276E-02	1.8179E-02	13.31%	181.79	1.8179E-02	13.31%	234.36
0.3375	1.00E+17	0.675	1.00E+16	0.3375	1.00E+17	SiO2	0.5000	0.10	0.37	9.00E+19	50	1.00E+20	0.37	1.00E+20	TiO2	0.00	2.3334E-02	0.9166E-01	1.7193E-02	7.8000E-01	2.2042E-02	82.61%	12.59%	1.6145E-02	4.8461E-01	6.2562E-03	4.1999E-01	1.5259E-02	79.96%	4.58%	1.1900E+00	1.5259E-02	1.8158E-02	13.29%	181.58	1.8158E-02	13.29%	234.49
0.34063	1.00E+17	0.68125	1.00E+16	0.34063	1.00E+17	SiO2	0.5000	0.10	0.37	9.00E+19	50	1.00E+20	0.37	1.00E+20	TiO2	0.00	2.3351E-02	0.9111E-01	1.7205E-02	7.8000E-01	2.2057E-02	82.62%	12.59%	1.6127E-02	4.8599E-01	6.2529E-03	4.1999E-01	1.5251E-02	79.96%	4.58%	1.1900E+00	1.5251E-02	1.8149E-02	13.29%	181.49	1.8149E-02	13.29%	234.59
0.34219	1.00E+17	0.64438	1.00E+16	0.34219	1.00E+17	SiO2	0.5000	0.10	0.37	9.00E+19	50	1.00E+20	0.37	1.00E+20	TiO2	0.00	2.3359E-02	0.9171E-01	1.7211E-02	7.7995E-01	2.2066E-02	82.62%	12.60%	1.6122E-02	4.8459E-01	6.2511E-03	4.1999E-01	1.5247E-02	79.96%	4.58%	1.1900E+00	1.5247E-02	1.8143E-02	13.28%	181.43	1.8143E-02	13.28%	234.62
0.343	1.00E+17	0.686	1.00E+16	0.343	1.00E+17	SiO2	0.5000	0.10	0.37	9.00E+19	50	1.00E+20	0.37	1.00E+20	TiO2	0.00	2.2956E-02	0.9124E-01	1.6599E-02	7.8000E-01	2.1644E-02	82.60%	12.37%	1.6120E-02	4.8459E-01	6.2502E-03	4.1999E-01	1.5244E-02	79.96%	4.58%	1.1900E+00	1.5244E-02	1.8141E-02	13.28%	181.41	1.8141E-02	13.28%	231.49
0.34375	1.00E+17	0.6875	1.00E+16	0.34375	1.00E+17	SiO2	0.5000	0.10	0.37	9.00E+19	50	1.00E+20	0.37	1.00E+20	TiO2	0.00	2.2954E-02	0.9125E-01	1.6602E-02	7.8000E-01	2.1649E-02	82.60%	12.37%	1.6122E-02	4.8459E-01	6.2495E-03	4.1999E-01	1.5242E-02	79.96%	4.58%	1.1900E+00	1.5242E-02	1.8129E-02	13.28%	181.29	1.8129E-02	13.28%	231.51
0.35	1.00E+17	0.7	1.00E+16	0.35	1.00E+17	SiO2	0.5000	0.10	0.37	9.00E+19	50	1.00E+20	0.37	1.00E+20	TiO2	0.00	2.2982E-02	0.9108E-01	1.6692E-02	7.8000E-01	2.1703E-02	82.55%	12.39%	1.6112E-02	4.8456E-01	6.2431E-03	4.1999E-01	1.5227E-02	79.96%	4.57%	1.1900E+00	1.5227E-02	1.8120E-02	13.27%	181.20	1.8120E-02	13.27%	231.72
0.4	1.00E+17	0.8	1.00E+16	0.4	1.00E+17	SiO2	0.5000	0.10	0.37	9.00E+19	50	1.00E+20	0.37	1.00E+20	TiO2	0.00	2.3116E-02	0.9031E-01	1.7176E-02	7.7995E-01	2.2021E-02	83.42%	12.57%	1.6004E-02	4.8388E-01	6.1967E-03	4.1999E-01	1.5119E-02	79.96%	4.54%	1.1900E+00	1.5119E-02	1.7991E-02	13.17%	179.91	1.7991E-02	13.17%	233.75
0.5	1.00E+17	1	1.00E+16	0.5	1.00E+17	SiO2	0.5000	0.10	0.37	9.00E+19	50	1.00E+20	0.37	1.00E+20	TiO2	0.00	2.3167E-02	0.8956E-01	1.6945E-02	7.7000E-01	2.2006E-02	82.59%	12.40%	1.5860E-02	4.8416E-01	6.1263E-03	4.1999E-01	1.4974E-02	79.95%	4.49%	1.1900E+00	1.4974E-02	1.7669E-02	12.93%	176.69	1.7669E-02	12.93%	230.04
0.75	1.00E+17	1.5	1.00E+16	0.75	1.00E+17	SiO2	0.5000	0.10	0.37	9.00E+19	50	1.00E+20	0.37	1.00E+20	TiO2	0.00	2.3623E-02	0.8192E-01	1.6143E-02	7.7999E-01	2.0697E-02	84.66%	11.02%	1.5697E-02	4.8390E-01	6.0725E-03	4.1999E-01	1.4811E-02	79.95%	4.45%	1.1900E+00	1.4811E-02	1.7625E-02	12.90%	176.25	1.7625E-02	12.90%	222.16
1	1.00E+17	2	1.00E+16	1	1.00E+17	SiO2	0.5000	0.10	0.37	9.00E+19	50	1.00E+20	0.37	1.00E+20	TiO2	0.00	2.0616E-02	0.6570E-01	1.4552E-02	7.4999E-01	1.9403E-02	81.53%	10.65%	1.5638E-02	4.8380E-01	6.0483E-03	4.1999E-01	1.4752E-02	79.95%	4.43%	1.1900E+00	1.4752E-02	1.7112E-02	12.53%	171.12	1.7112E-02	12.53%	206.00
1.5	1.00E+17	3	1.00E+16	1.5	1.00E+17	SiO2	0.5000	0.10	0.37	9.00E+19	50	1.00E+20	0.37	1.00E+20	TiO2	0.00	1.9211E-02	0.6906E-01	1.3478E-02	7.7000E-01	1.7504E-02	85.16%	9.87%	1.5594E-02	4.8373E-01	6.0304E-03	4.1999E-01	1.4701E-02	79.94%	4.41%	1.1900E+00	1.4701E-02	1.7354E-02	12.71%	173.54	1.7354E-02	12.71%	195.09
2	1.00E+17	4	1.00E+16	2	1.00E+17	SiO2	0.5000	0.10	0.37	9.00E+19	50	1.00E+20	0.37	1.00E+20	TiO2	0.00	1.5635E-02	0.6473E-01	1.1632E-02	7.7000E-01	1.5106E-02	86.03%	8.52%	1.5572E-02	4.8370E-01	6.0214E-03	4.1999E-01	1.4684E-02	79.94%	4.41%	1.1900E+00	1.4684E-02	1.7330E-02	12.69%	173.30	1.7330E-02	12.69%	176.53
2.5	1.00E+17	5	1.00E+16	2.5	1.00E+17	SiO2	0.5000	0.10	0.37	9.00E+19	50	1.00E+20	0.37	1.00E+20	TiO2	0.00	1.3157E-02	0.5954E-01	9.7226E-03	7.7000E-01	1.2427E-02	85.97%	7.12%	1.5555E-02	4.8367E-01	6.0142E-03	4.1999E-01	1.4669E-02	79.94%	4.40%	1.1900E+00	1.2427E-02	1.4900E-02	10.91%	149.00	1.4900E-02	10.91%	157.37
0.5	1.00E+17	1	1.00E+16	0.5	1.00E+17	SiO2	0.6000	0.50	0.37	9.00E+19	50	1.00E+20	15	1.00E+20	SiO2	1.00	2.4603E-02	0.8932E-01	1.8188E-02	7.8000E-01	2.3318E-02	83.13%	13.31%	7.2842E-03	4.6432E-01	2.6840E-03	3.9000E-01	6.8020E-03	79.33%	1.96%	1.1700E+00	6.8020E-03	0.0519E-03	0.89%	80.52	1.1771E-02	0.62%	200.72
0.5	1.00E+17	2	1.00E+16	0.5	1.00E+17	SiO2	0.6000	0.50	0.37	9.00E+19	50	1.00E+20	15	1.00E+20	SiO2	1.00	2.5156E-02	0.8007E-01	1.8444E-02	7.7999E-01	2.3646E-02	73.31%	13.50%	7.1850E-03	4.6397E-01	2.6445E-03	3.9000E-01	6.7000E-03	79.33%	1.94%	1.1700E+00	6.7000E-03	7.9335E-03	5.81%	79.34	1.1867E-02	0.69%	210.88
0.5	1.00E+17	3	1.00E+16	0.5	1.00E+17	SiO2	0.6000	0.50	0.37	9.00E+19	50	1.00E+20	15	1.00E+20	SiO2	1.00	2.5100E-02	0.7420E-01	1.8261E-02	7.7000E-01	2.3845E-02	83.40%	13.44%	7.1507E-03	4.6385E-01	2.6311E-03	3.9000E-01	6.7465E-03	79.33%	1.93%	1.1600E+00	6.7465E-03	7.8259E-03	5.73%	78.26	1.1931E-02	0.73%	209.92
0.5	1.00E+17	4	1.00E+16	0.5	1.00E+17	SiO2	0.6000	0.50	0.37	9.00E+19	50	1.00E+20	15	1.00E+20	SiO2	1.00	2.5109E-02	0.7124E-01	1.8229E-02	7.6999E-01	2.3618E-02	83.37%	13.35%	7.1058E-03	4.6379E-01	2.6253E-03	3.9000E-01	6.7316E-03	79.33%	1.92%	1.1600E+00	6.7316E-03	7.8085E-03	5.72%	78.09	1.1914E-02	0.68%	201.65
0.5	1.00E+17	5	1.00E+16	0.5	1.00E+17	SiO2	0.6000	0.50	0.37	9.00E+19	50	1.00E+20	15	1.00E+20	SiO2	1.00	2.5049E-02	0.6966E-01	1.8144E-02	7.7000E-01	2.3563E-02	83.31%	13.28%	7.1267E-03	4.6376E-01	2.6219E-03	3.9000E-01	6.7225E-03	79.33%	1.92%	1.1600E+00	6.7225E-03	7.7981E-03	5.71%	77.98	1.1911E-02	0.65%	207.65
0.5	1.00E+17	5	1.00E+16	0.5	1.00E+17	SiO2	0.6000	1.00	0.37	9.00E+19	50	1.00E+20	15	1.00E+20	SiO2	1.00	2.5002E-02	0.6963E-01	1.8115E-02	7.7000E-01	2.3524E-02	83.33%	13.26%	7.1252E-03	4.6376E-01	2.6212E-03	3.9000E-01	6.7219E-03	79.33%	1.92%	1.1600E+00	6.7219E-03	7.7963E-03	5.71%	77.96	1.1794E-02	0.64%	207.26
0.5	1.00E+17	10	1.00E+16	0.5	1.00E+17	SiO2	0.6000	1.00	0.37	9.00E+19	50	1.00E+20	15	1.00E+20	SiO2	1.00	2.4915E-02	0.6691E-01	1.7989E-02	7.6996E-01	2.3364E-02	83.29%	13.17%	7.1055E-03	4.6369E-01	2.6125E-03	3.9000E-01	6.7014E-03	79.32%	1.91%	1.1600E+00	6.7014E-03	7.7733E-03	5.69%	77.73	1.1725E-02	0.58%	206.03
0.5	1.00E+17	15	1.00E+16	0.5	1.00E+17	SiO2	0.6000	1.00	0.37	9.00E+19	50	1.00E+20	15	1.00E+20	SiO2	1.00	2.4906E-02	0.6680E-01	1.8002E-02	7.7000E-01	2.3379E-02	83.29%	13.18%	7.0020E-03	4.6361E-01	2.6047E-03	3.9000E-01	6.6788E-03	79.32%	1.91%	1.1600E+00	6.6788E-03	7.7474E-03	5.67%	77.47	1.1722E-02	0.58%	206.06
0.5	1.00E+17	20	1.00E+16	0.5	1.00E+17	SiO2	0.6000	1.00	0.37	9.00E+19	50	1.00E+20	15	1.00E+20	SiO2	1.00	2.4885E-02	0.6682E-01	1.7991E-02	7.7000E-01	2.3365E-02	83.40%	13.17%	7.0708E-03	4.6357E-01	2.6000E-03	3.9000E-01	6.6667E-03	79.32%	1.90%	1.1600E+00	6.6667E-03	7.7333E-03	5.66%	77.33	1.1712E-02	0.57%	205.91
0.5	1.00E+17	25	1.00E+16	0.5	1.00E+17	SiO2	0.6000	1.00	0.37	9.00E+19	50	1.00E+20	15	1.00E+20	SiO2	1.00	2.4904E-02	0.6681E-01	1.7989E-02	7.6997E-01	2.3363E-02	83.33%	13.17%	7.0695E-03	4.6356E-01	2.5995E-03	3.9000E-01	6.6653E-03	79.32%	1.90%	1.1600E+00	6.6653E-03	7.7316E-03	5.66%	77.32	1.1711E-02	0.57%	205.88
0.5	1.00E+17	30	1.00E+16	0.5	1.00E+17	SiO2	0.6000	1.00	0.37	9.00E+19	50	1.00E+20	15	1.00E+20	SiO2	1.00	2.4905E-02	0.6671E-01	1.7963E-02	7.6999E-01	2.3329E-02	83.22%	13.15%	7.0618E-03	4.6354E-01	2.5965E-03	3.9000E-01	6.6577E-03	79.32%	1.90%	1.1600E+00	6.6577E-03	7.7228E-03	5.65%	77.23	1.1695E-02	0.56%	205.60
0.5	1.00E+17	35	1.00E+16	0.5	1.00E+17	SiO2	0.6000	1.00	0.37	9.00E+19	50	1.00E+20	15	1.00E+20	SiO2	1.00	2.4904E-02	0.6691E-01	1.8008E-02	7.7000E-01	2.3387E-02	83.41%	13.18%	7.0496E-03	4.6349E-01	2.5917E-03	3.9000E-01	6.6455E-03	79.32%	1.90%	1.1600E+00	6.6455E-03	7.7087E-03	5.64%	77.09	1.1713E-02	0.57%	206.00
0.5	1.00E+17	40	1.00E+16	0.5	1.00E+17	SiO2	0.6000	1.00	0.37	9.00E+19	50	1.00E+20	15	1.00E+20	SiO2	1.00	2.4905E-02	0.6671E-01	1.7960E-02	7.7000E-01	2.3325E-02	83.21%	13.15%	7.0500E-03	4.6349E-01	2.5919E-03	3.9000E-01	6.6458E-03	79.32%	1.90%	1.1600E+00	6.6458E-03	7.7091E-03	5.64%	77.09	1.1698E-02	0.56%	205.52
0.5	1.00E+17	45	1.00E+16	0.5	1.00E+17	SiO2	0.6000	1.00	0.37	9.00E+19	50	1.00E+20	15	1.00E+20	SiO2	1.00	2.4904E-02	0.6692E-01	1.8005E-02	7.7000E-01	2.3384E-02	83.40%	13.18%	7.0394E-03	4.6346E-01	2.5877E-03	3.9000E-01	6.6352E-03	79.32%	1.89%	1.1600E+00	6.6352E-03	7.6969E-03	5.63%	76.97	1.1707E-02	0.57%	205.93
0.5	1.00E+17	50	1.00E+16	0.5	1.00E+17	SiO2	0.6000	1.00	0.37	9.00E+19	50	1.00E+20	15	1.00E+20	SiO2	1.00	2.4905E-02	0.6666E-01	1.7950E-02	7.7000E-01	2.3352E-02	83.17%	13.14%	7.0409E-03	4.6346E-01	2.5883E-03	3.9000E-01	6.6367E-03	79.32%	1.89%	1.1600E+00	6.6367E-03	7.6986E-03	5.63%	76.99	1.1698E-02	0.55%	205.39
0.5	1.00E+17	60	1.00E+16	0.5	1.00E+17	SiO2	0.6000	1.00	0.37	9.00E+19	50	1.00E+20	15	1.00E+20	SiO2	1.00	2.4905E-02	0.6664E-01	1.7954E-02	7.6997E-01	2.3317E-02	83.11%	13.14%	7.0239E-03	4.6340E-01	2.5817E-03	3.9000E-01	6.6197E-03	79.32%	1.89%	1.1600E+00	6.6197E-03	7.6787E-03	5.62%	76.79	1.1675E-02	0.55%	205.25
0.5	1.00E+17	70	1.00E+16	0.5	1.00E+17	SiO2	0.6000	1.00	0.37	9.00E+19	50	1.00E+20	15	1.00E+20	SiO2	1.00	2.4904E-02	0.6661E-01	1.7974E-02	7.6997E-01	2.3343E-02	83.26%	13.16%	7.0249E-03	4.6341E-01	2.5829E-03	3.9000E-01	6.6222E-03	79.32%	1.89%	1.1600E+00	6.6222E-03	7.6822E-03	5.62%	76.82	1.1687E-02	0.56%	205.56
0.5	1.00E+17	80	1.00E+16	0.5	1.00E+17	SiO2	0.6000	1.00	0.37	9.00E+19	50	1.00E+20	15	1.00E+20	SiO2	1.00	2.4872E-02	0.6658E-01	1.7916E-02	7.7000E-01	2.3267E-02	83.12%	13.12%	7.0164E-03	4.6338E-01	2.5788E-03	3.9000E-01	6.6123E-03	79.32%	1.89%	1.1600E+00	6.6123E-03	7.6702E-03	5.62%	76.70	1.1653E-02	0.53%	204.95
0.5	1.00E+17	90	1.00E+16	0.5	1.00E+17	SiO2	0.6000	1.00	0.37	9.00E+19	50	1.00E+20	15	1.00E+20	SiO2	1.00	2.4904E-02	0.6654E-01	1.7977E-02	7.7000E-01	2.3347E-02	83.27%	13.16%	7.0105E-03	4.6337E-01	2.5735E-03	3.9000E-01	6.6116E-03	79.32%	1.89%	1.1600E+00	6.6116E-03	7.6695E-03	5.61%	76.69	1.1654E-02	0.55%	205.55
0.5	1.00E+17	100	1.00E+16	0.5	1.00E+17	SiO2	0.6000	1.00	0.37	9.00E+19	50	1.00E+20	15	1.00E+20	SiO2	1.00	2.4894E-02	0.6660E-01	1.7933E-02	7.7000E-01	2.3239E-02	83.11%	13.12%	7.0066E-03	4.6335E-01	2.5757E-03	3.9000E-01	6.6044E-03	79.32%	1.89%	1.1600E+00	6.6044E-03	7.6611E-03	5.61%	76.61	1.1658E-02	0.53%	205.00
0.5	1.00E+17	125	1.00E+16	0.5	1.00E+17	SiO2	0.6000	1.00	0.37	9.00E+19	50	1.00E+20	15	1.00E+20	SiO2	1.00	2.4905E-02	0.6661E-01	1.7934E-02	7.7000E-01	2.3293E-02	83.19%	13.13%	6.9933E-03	4.6331E-01	2.5717E-03	3.9000E-01	6.5942E-03	79.32%	1.88%	1.1600E+00	6.5942E-03	7.6492E-03	5.60%	76.49	1.1656E-02	0.53%	205.07
0.5	1.00E+17	150	1.00E+16	0.5	1.00E+17	SiO2	0.6000	1.00	0.37	9.00E+

SILVACO ATLAS Modelling Stats for Tandem GaAs (N-P-P+) GaSb (P-N-N+) solar cell (AM0)

Divs*:	10	Points:	4346	Triangles:	8424		High Doping																																
P-In	0.0366																																						
																																		Combined Results					
		Upper Cell (GaAs)								Lower Cell (GaSb)								Upper Cell								LowerCell								Dual Junction				Tandem	
N-t	N-d	P-t	P-d	BSF-t	BSF-d	ARC*	L-0	Gap-t	P-t	P-d	N-t	N-d	BSF-t	BSF-d	ARC*	L-0	Jsc	Voc	Pmax	Vmax	Imax	FF	Eff-u	Jsc	Voc	Pmax	Vmax	Imax	FF	Eff-l	V-t	I-t	P-t	Eff-t	W/m^2	P-t	Eff-t	W/m^2
0.00313	1.50E+18	0.01563	7.00E+17	0.00313	0.00E+18	SiO2	0.5000	0.10	0.37	9.00E+19	50	1.00E+20	0.37	1.00E+20	TiO2	0.00	4.1951E-04	8.6937E-01	4.1470E-04	7.5000E-01	5.5294E-04	76.99%	0.30%	2.1677E-02	4.9234E-01	8.5567E-03	4.2000E-01	2.0373E-02	80.18%	6.26%	1.1700E+00	5.5294E-04	6.4693E-04	0.47%	6.47	0.7089E-03	6.43%	99.71
0.00625	1.50E+18	0.03125	7.00E+17	0.00625	0.00E+18	SiO2	0.5000	0.10	0.37	9.00E+19	50	1.00E+20	0.37	1.00E+20	TiO2	0.00	9.0212E-04	8.6372E-01	5.9060E-04	7.4000E-01	7.9910E-04	75.74%	0.43%	2.1122E-02	4.9174E-01	8.3239E-03	4.2000E-01	1.9819E-02	80.14%	6.09%	1.1600E+00	7.9910E-04	9.2580E-04	0.68%	9.26	0.6594E-03	6.34%	99.14
0.0125	1.50E+18	0.0625	7.00E+17	0.0125	0.00E+18	SiO2	0.5000	0.10	0.37	9.00E+19	50	1.00E+20	0.37	1.00E+20	TiO2	0.00	1.0454E-02	8.9041E-01	7.4037E-03	7.4000E-01	9.8470E-03	80.30%	5.48%	2.0453E-02	4.9090E-01	7.9975E-03	4.2000E-01	1.9042E-02	80.00%	5.85%	1.1100E+00	9.8470E-03	1.1619E-02	0.91%	116.19	1.2133E-02	8.88%	154.01
0.025	1.50E+18	0.125	7.00E+17	0.025	0.00E+18	SiO2	0.5000	0.10	0.37	9.00E+19	50	1.00E+20	0.37	1.00E+20	TiO2	0.00	1.4399E-02	9.0370E-01	1.0342E-02	7.7000E-01	1.3451E-02	79.62%	7.59%	1.9302E-02	4.8965E-01	7.5590E-03	4.2000E-01	1.7998E-02	79.98%	5.53%	1.1900E+00	1.3451E-02	1.6016E-02	11.72%	160.14	1.6014E-02	11.72%	179.21
0.05	1.50E+18	0.25	7.00E+17	0.05	0.00E+18	SiO2	0.5000	0.10	0.37	9.00E+19	50	1.00E+20	0.37	1.00E+20	TiO2	0.00	1.9881E-02	9.1564E-01	1.3231E-02	7.8000E-01	1.6972E-02	79.92%	9.68%	1.8022E-02	4.8377E-01	7.0506E-03	4.1000E-01	1.7197E-02	79.55%	5.36%	1.1900E+00	1.6972E-02	2.0197E-02	14.79%	201.97	2.0197E-02	14.79%	202.09
0.0625	1.50E+18	0.2625	7.00E+17	0.0525	0.00E+18	SiO2	0.5000	0.10	0.37	9.00E+19	50	1.00E+20	0.37	1.00E+20	TiO2	0.00	1.8204E-02	9.1942E-01	1.3591E-02	7.9000E-01	1.7162E-02	80.32%	9.90%	1.7944E-02	4.8757E-01	7.0151E-03	4.1000E-01	1.7109E-02	79.95%	5.34%	1.2000E+00	1.7109E-02	2.0532E-02	15.43%	205.32	2.0532E-02	15.43%	205.34
0.075	1.50E+18	0.275	7.00E+17	0.075	0.00E+18	SiO2	0.5000	0.10	0.37	9.00E+19	50	1.00E+20	0.37	1.00E+20	TiO2	0.00	1.6517E-02	9.2223E-01	1.3703E-02	7.9000E-01	1.7347E-02	80.75%	10.09%	1.7912E-02	4.8744E-01	6.9814E-03	4.1000E-01	1.7021E-02	79.95%	5.31%	1.2000E+00	1.7021E-02	2.0433E-02	14.96%	204.33	2.0433E-02	14.96%	207.64
0.08	1.50E+18	0.3	7.00E+17	0.08	0.00E+18	SiO2	0.5000	0.10	0.37	9.00E+19	50	1.00E+20	0.37	1.00E+20	TiO2	0.00	1.4862E-02	9.2554E-01	1.4192E-02	7.9999E-01	1.7740E-02	81.29%	10.34%	1.7761E-02	4.8719E-01	6.9189E-03	4.1000E-01	1.6875E-02	79.96%	5.07%	1.2100E+00	1.6875E-02	2.0419E-02	14.95%	204.19	2.0419E-02	14.95%	211.11
0.1	1.50E+18	0.5	7.00E+17	0.1	0.00E+18	SiO2	0.5000	0.10	0.37	9.00E+19	50	1.00E+20	0.37	1.00E+20	TiO2	0.00	2.3323E-02	8.0431E-01	1.4320E-02	7.5000E-01	1.8340E-02	76.54%	10.34%	1.6933E-02	4.8591E-01	6.5794E-03	4.1000E-01	1.6047E-02	79.97%	4.82%	1.1600E+00	1.6047E-02	1.8615E-02	13.63%	186.15	1.8615E-02	13.63%	207.10
0.15	1.50E+18	0.75	7.00E+17	0.15	0.00E+18	SiO2	0.5000	0.10	0.37	9.00E+19	50	1.00E+20	0.37	1.00E+20	TiO2	0.00	2.0642E-02	9.3604E-01	1.5593E-02	8.0999E-01	1.9259E-02	80.70%	11.42%	1.6402E-02	4.8502E-01	6.3614E-03	4.1000E-01	1.5516E-02	79.97%	4.66%	1.2200E+00	1.5516E-02	1.8929E-02	13.86%	189.29	1.8929E-02	13.86%	219.55
0.175	1.50E+18	0.875	7.00E+17	0.175	0.00E+18	SiO2	0.5000	0.10	0.37	9.00E+19	50	1.00E+20	0.37	1.00E+20	TiO2	0.00	2.0578E-02	9.5167E-01	1.6459E-02	8.4997E-01	1.9244E-02	84.05%	12.05%	1.6237E-02	4.8476E-01	6.2940E-03	4.1000E-01	1.5351E-02	79.96%	4.61%	1.2400E+00	1.5351E-02	1.9342E-02	14.16%	193.42	1.9342E-02	14.16%	227.53
0.18	1.50E+18	0.9	7.00E+17	0.18	0.00E+18	SiO2	0.5000	0.10	0.37	9.00E+19	50	1.00E+20	0.37	1.00E+20	TiO2	0.00	2.0572E-02	9.5293E-01	1.6508E-02	8.5000E-01	1.9505E-02	84.87%	12.14%	1.6209E-02	4.8477E-01	6.2827E-03	4.1000E-01	1.5324E-02	79.96%	4.60%	1.2400E+00	1.5324E-02	1.9308E-02	14.13%	193.08	1.9308E-02	14.13%	228.62
0.185	1.50E+18	0.925	7.00E+17	0.185	0.00E+18	SiO2	0.5000	0.10	0.37	9.00E+19	50	1.00E+20	0.37	1.00E+20	TiO2	0.00	2.0562E-02	9.5292E-01	1.6444E-02	8.5965E-01	1.9339E-02	84.99%	12.20%	1.6183E-02	4.8467E-01	6.2719E-03	4.1000E-01	1.5297E-02	79.96%	4.59%	1.2497E+00	1.5297E-02	1.9422E-02	14.22%	194.22	1.9422E-02	14.22%	229.40
0.19	1.50E+18	0.95	7.00E+17	0.19	0.00E+18	SiO2	0.5000	0.10	0.37	9.00E+19	50	1.00E+20	0.37	1.00E+20	TiO2	0.00	2.0541E-02	9.5470E-01	1.6745E-02	8.5999E-01	1.9472E-02	85.36%	12.26%	1.6159E-02	4.8463E-01	6.2617E-03	4.1000E-01	1.5272E-02	79.96%	4.58%	1.2700E+00	1.5272E-02	1.9396E-02	14.20%	193.96	1.9396E-02	14.20%	230.07
0.195	1.50E+18	0.975	7.00E+17	0.195	0.00E+18	SiO2	0.5000	0.10	0.37	9.00E+19	50	1.00E+20	0.37	1.00E+20	TiO2	0.00	2.0342E-02	9.5516E-01	1.6679E-02	8.6000E-01	1.9294E-02	85.64%	12.21%	1.6135E-02	4.8459E-01	6.2520E-03	4.1000E-01	1.5249E-02	79.96%	4.58%	1.2700E+00	1.5249E-02	1.9364E-02	14.18%	193.64	1.9364E-02	14.18%	229.31
0.2	1.50E+18	1	7.00E+17	0.2	0.00E+18	SiO2	0.5000	0.10	0.37	9.00E+19	50	1.00E+20	0.37	1.00E+20	TiO2	0.00	2.0372E-02	9.5555E-01	1.6712E-02	8.6000E-01	1.9432E-02	85.85%	12.23%	1.6112E-02	4.8456E-01	6.2431E-03	4.1000E-01	1.5227E-02	79.96%	4.57%	1.2700E+00	1.5227E-02	1.9338E-02	14.16%	193.38	1.9338E-02	14.16%	229.55
0.21	1.50E+18	1.05	7.00E+17	0.21	0.00E+18	SiO2	0.5000	0.10	0.37	9.00E+19	50	1.00E+20	0.37	1.00E+20	TiO2	0.00	2.0328E-02	9.5615E-01	1.6734E-02	8.6000E-01	1.9414E-02	86.12%	12.25%	1.6071E-02	4.8449E-01	6.2260E-03	4.1000E-01	1.5185E-02	79.96%	4.54%	1.2700E+00	1.5185E-02	1.9285E-02	14.12%	192.85	1.9285E-02	14.12%	229.65
0.23	1.50E+18	1.15	7.00E+17	0.23	0.00E+18	SiO2	0.5000	0.10	0.37	9.00E+19	50	1.00E+20	0.37	1.00E+20	TiO2	0.00	2.0231E-02	9.5643E-01	1.6752E-02	8.6000E-01	1.9402E-02	86.35%	12.23%	1.6000E-02	4.8438E-01	6.1961E-03	4.1000E-01	1.5114E-02	79.96%	4.54%	1.2700E+00	1.5114E-02	1.9195E-02	14.05%	191.95	1.9195E-02	14.05%	229.09
0.25	1.50E+18	1.25	7.00E+17	0.25	0.00E+18	SiO2	0.5000	0.10	0.37	9.00E+19	50	1.00E+20	0.37	1.00E+20	TiO2	0.00	1.9904E-02	9.5630E-01	1.6485E-02	8.6000E-01	1.9107E-02	86.46%	12.05%	1.5941E-02	4.8424E-01	6.1727E-03	4.1000E-01	1.5055E-02	79.96%	4.52%	1.2700E+00	1.5055E-02	1.9120E-02	14.00%	191.20	1.9120E-02	14.00%	226.30
0.3	1.50E+18	1.5	7.00E+17	0.3	0.00E+18	SiO2	0.5000	0.10	0.37	9.00E+19	50	1.00E+20	0.37	1.00E+20	TiO2	0.00	1.9527E-02	9.5590E-01	1.6162E-02	8.6000E-01	1.8734E-02	86.39%	11.82%	1.5823E-02	4.8418E-01	6.1327E-03	4.1000E-01	1.4960E-02	79.96%	4.49%	1.2700E+00	1.4960E-02	1.8904E-02	13.96%	189.04	1.8904E-02	13.96%	222.91
0.4	1.50E+18	2	7.00E+17	0.4	0.00E+18	SiO2	0.5000	0.10	0.37	9.00E+19	50	1.00E+20	0.37	1.00E+20	TiO2	0.00	1.9103E-02	9.5391E-01	1.5801E-02	8.6000E-01	1.8345E-02	86.77%	10.99%	1.5717E-02	4.8392E-01	6.0807E-03	4.1000E-01	1.4831E-02	79.96%	4.45%	1.2700E+00	1.4831E-02	1.8835E-02	13.79%	188.35	1.8835E-02	13.79%	210.38
0.2	1.50E+18	1	7.00E+17	0.5	0.00E+18	SiO2	0.6000	0.50	0.37	9.00E+19	50	1.00E+20	15	1.00E+20	SiO2	1.00	2.0732E-02	9.5562E-01	1.6731E-02	8.5999E-01	1.9455E-02	85.96%	12.25%	7.2162E-03	4.6432E-01	2.6040E-03	3.9000E-01	6.6802E-03	79.33%	1.96%	1.2500E+00	6.6802E-03	8.6025E-03	6.39%	86.02	1.0271E-02	7.52%	194.15
0.2	1.50E+18	2	7.00E+17	0.5	0.00E+18	SiO2	0.6000	0.50	0.37	9.00E+19	50	1.00E+20	15	1.00E+20	SiO2	1.00	2.0748E-02	9.5359E-01	1.6494E-02	8.6000E-01	1.9279E-02	85.85%	12.07%	7.1150E-03	4.6297E-01	2.6445E-03	3.9000E-01	6.7808E-03	79.33%	1.94%	1.2500E+00	6.7808E-03	8.4760E-03	6.28%	84.76	1.0202E-02	7.47%	191.38
0.2	1.50E+18	3	7.00E+17	0.5	0.00E+18	SiO2	0.6000	0.50	0.37	9.00E+19	50	1.00E+20	15	1.00E+20	SiO2	1.00	2.0769E-02	9.5330E-01	1.6446E-02	8.6000E-01	1.9123E-02	85.79%	12.04%	7.1507E-03	4.6285E-01	2.6311E-03	3.9000E-01	6.7465E-03	79.33%	1.93%	1.2500E+00	6.7465E-03	8.4331E-03	6.17%	84.33	1.0089E-02	7.39%	190.77
0.2	1.50E+18	4	7.00E+17	0.5	0.00E+18	SiO2	0.6000	0.50	0.37	9.00E+19	50	1.00E+20	15	1.00E+20	SiO2	1.00	2.0784E-02	9.5242E-01	1.6455E-02	8.6000E-01	1.9134E-02	85.84%	12.05%	7.1358E-03	4.6279E-01	2.6253E-03	3.9000E-01	6.7316E-03	79.33%	1.92%	1.2500E+00	6.7316E-03	8.4145E-03	6.16%	84.14	1.0068E-02	7.38%	190.01
0.2	1.50E+18	5	7.00E+17	0.5	0.00E+18	SiO2	0.6000	0.50	0.37	9.00E+19	50	1.00E+20	15	1.00E+20	SiO2	1.00	2.0800E-02	9.5241E-01	1.6451E-02	8.5999E-01	1.9126E-02	85.84%	12.04%	7.1192E-03	4.6274E-01	2.6119E-03	3.9000E-01	6.7151E-03	79.32%	1.92%	1.2500E+00	6.7151E-03	8.3938E-03	6.14%	83.94	1.0079E-02	7.38%	190.70
0.2	1.50E+18	6	7.00E+17	0.5	0.00E+18	SiO2	0.6000	1.00	0.37	9.00E+19	50	1.00E+20	15	1.00E+20	SiO2	1.00	2.0810E-02	9.5241E-01	1.6452E-02	8.6000E-01	1.9124E-02	85.84%	12.04%	7.1024E-03	4.6275E-01	2.6204E-03	3.9000E-01	6.7194E-03	79.32%	1.92%	1.2500E+00	6.7194E-03	8.3993E-03	6.15%	83.99	1.0081E-02	7.38%	190.72
0.2	1.50E+18	10	7.00E+17	0.5	0.00E+18	SiO2	0.6000	1.00	0.37	9.00E+19	50	1.00E+20	15	1.00E+20	SiO2	1.00	2.0805E-02	9.5241E-01	1.6455E-02	8.6000E-01	1.9124E-02	85.85%	12.05%	7.1055E-03	4.6264E-01	2.6125E-03	3.9000E-01	6.7014E-03	79.32%	1.91%	1.2500E+00	6.7014E-03	8.3767E-03	6.13%	83.77	1.0074E-02	7.38%	190.49
0.2	1.50E+18	15	7.00E+17	0.5	0.00E+18	SiO2	0.6000	1.00	0.37	9.00E+19	50	1.00E+20	15	1.00E+20	SiO2	1.00	2.0797E-02	9.5417E-01	1.6530E-02	8.5999E-01	1.9221E-02	86.20%	12.10%	7.0803E-03	4.6263E-01	2.6068E-03	3.9000E-01	6.6841E-03	79.32%	1.91%	1.2500E+00	6.6841E-03	8.3591E-03	6.12%	83.59	1.0103E-02	7.40%	191.36
0.2	1.50E+18	20	7.00E+17	0.5	0.00E+18	SiO2	0.6000	1.00	0.37	9.00E+19	50	1.00E+20	15	1.00E+20	SiO2	1.00	2.0803E-02	9.5340E-01	1.6452E-02	8.6000E-01	1.9131E-02	85.84%	12.04%	7.0741E-03	4.6258E-01	2.6013E-03	3.9000E-01	6.6699E-03	79.32%	1.90%	1.2500E+00	6.6699E-03	8.3374E-03	6.10%	83.37	1.0062E-02	7.37%	190.54
0.2	1.50E+18	25	7.00E+17	0.5	0.00E+18	SiO2	0.6000	1.00	0.37	9.00E+19	50	1.00E+20	15	1.00E+20	SiO2	1.00	2.0813E-02	9.5264E-01	1.6405E-02	8.6000E-01	1.9075E-02	85.60%	12.01%	7.0695E-03	4.6256E-01	2.5995E-03	3.9000E-01	6.6653E-03	79.32%	1.90%	1.2500E+00	6.6653E-03	8.3316E-03	6.10%	83.32	1.0039E-02	7.35%	190.04
0.2	1.50E+18	30	7.00E+17	0.5	0.00E+18	SiO2	0.6000	1.00	0.37	9.00E+19	50	1.00E+20	15	1.00E+20	SiO2	1.00	2.0798E-02	9.5254E-01	1.6283E-02	8.6000E-01	1.9049E-02	85.53%	11.99%	7.0618E-03	4.6254E-01	2.5965E-03	3.9000E-01	6.6577E-03	79.32%	1.90%	1.2500E+00	6.6577E-03	8.3221E-03	6.09%	83.22	1.0024E-02	7.34%	189.79
0.2	1.50E+18	35	7.00E+17	0.5	0.00E+18	SiO2	0.6000	1.00	0.37	9.00E+19	50	1.00E+20	15	1.00E+20	SiO2	1.00	2.0819E-02	9.5249E-01	1.6290E-02	8.5999E-01	1.9058E-02	85.53%	12.00%	7.0556E-03	4.6250E-01	2.5925E-03	3.9000E-01	6.6474E-03	79.32%	1.90%	1.2500E+00	6.6474E-03	8.3091E-03	6.08%	83.09	1.0025E-02	7.34%	189.82
0.2	1.50E+18	40	7.00E+17	0.5	0.00E+18	SiO2	0.6000	1.00	0.37	9.00E+19	50	1.00E+20	15	1.00E+20	SiO2	1.00	2.0808E-02	9.5240E-01	1.6292E-02	8.6000E-01	1.9061E-02	85.59%	12.00%	7.0500E-03	4.6249E-01	2.5991E-03	3.9000E-01	6.6485E-03	79.32%	1.90%	1.2500E+00	6.6485E-03	8.3072E-03	6.08%	83.07	1.0026E-02	7.34%	189.84
0.2	1.50E+18	45	7.00E+17	0.5	0.00E+18	SiO2	0.6000	1.00	0.37	9.00E+19	50	1.00E+20	15	1.00E+20	SiO2	1.00	2.0809E-02	9.5250E-01	1.6297E-02	8.6000E-01	1.9064E-02	85.64%	12.00%	7.0385E-03	4.6248E-01	2.5972E-03	3.9000E-01	6.6343E-03	79.32%	1.89%	1.2500E+00	6.6343E-03	8.2929E-03	6.07%	82.93	1.0023E-02	7.34%	189.84
0.2	1.50E+18	50	7.00E+17	0.5	0.00E+18	SiO2	0.6000	1.00	0.37	9.00E+19	50	1.00E+20	15	1.00E+20	SiO2	1.00	2.0804E-02	9.5245E-01	1.6414E-02	8.6000E-01	1.9086E-02	85.78%	12.02%	7.0409E-03	4.6246E-01	2.5803E-03	3.9000E-01	6.6267E-03	79.32%	1.89%	1.2500E+00	6.6267E-03	8.2959E-03	6.07%	82.96	1.0032E-02	7.34%	190.02
0.2	1.50E+18	60	7.00E+17	0.5	0.00E+18	SiO2	0.6000	1.00	0.37	9.00E+19	50	1.00E+20	15	1.00E+20	SiO2	1.00	2.0799E-02	9.5203E-01	1.6428E-02	8.5999E-01	1.9103E-02	85.78%	12.02%	7.0314E-03	4.6240E-01	2.5846E-03	3.9000E-01	6.6273E-03	79.32%	1.89%	1.2500E+00	6.6273E-03	8.2839E-03	6.06%	82.84	1.0035E-02	7.35%	190.13
0.2	1.50E+18	70	7.00E+17	0.5	0.00E+18	SiO2	0.6000	1.00	0.37	9.00E+19	50	1.00E+20	15	1.00E+20	SiO2	1.00	2.0784E-02	9.5316E-01	1.6461E-02	8.5998E-01	1.9142E-02	85.86%	12.05%	7.0269E-03	4.6241E-01	2.5929E-03	3.9000E-01	6.6228E-03	79.32%	1.89%	1.2500E+00	6.6228E-03	8.2783E-03	6.06%	82.78	1.0048E-02	7.36%	190.44
0.2	1.50E+18	80	7.00E+17	0.5	0.00E+18	SiO2	0.6000	1.00	0.37	9.00E+19	50	1.00E+20	15	1.00E+20	SiO2	1.00	2.0803E-02	9.5322E-01	1.6460E-02	8.5999E-01	1.9140E-02	85.90%	12.05%	7.0175E-03	4.6238E-01	2.5792E-03	3.9000E-01	6.6134E-03	79.32%	1.89%	1.2500E+00	6.6134E-03	8.2667E-03	6.05%	82.67	1.0044E-02	7.35%	190.40
0.2	1.50E+18	90	7.00E+17	0.5	0.00E+18	SiO2	0.6000	1.00	0.37	9.00E+19	50	1.00E+20	15	1.00E+20	SiO2	1.00	2.0817E-02	9.5340E-01	1.6485E-02	8.6000E-01	1.9169E-02	85.94%	12.07%	7.0151E-03	4.6237E-01	2.5715E-03	3.9000E-01	6.6116E-03	79.32%	1.89%	1.2500E+00	6.6116E-03	8.2645E-03	6.05%	82.65	1.0054E-02	7.36%	190.63
0.2	1.50E+18	100	7.00E+17	0.5	0.00E+18	SiO2	0.6000	1.00	0.37	9.00E+19	50	1.00E+20	15	1.00E+20	SiO2	1.00	2.0802E-02	9.5342E-01	1.6472E-02	8.6000E-01	1.9153E-02	85.94%	12.06%	7.0033E-03	4.6233E-01	2.5739E-03	3.9000E-01	6.5996E-03	79.32%	1.88%	1.2500E+00	6.5996E-03	8.2496E-03	6.04%	82.50	1.0044E-02	7.35%	190.46
0.2	1.50E+18	125	7.00E+17	0.5	0.00E+18	SiO2	0.6000	1.00	0.37	9.00E+19	50	1.00E+20	15	1.00E+20	SiO2	1.00	2.0804E-02	9.5355E-01	1.6477E-02	8.5999E-01	1.9142E-02	85.96%	12.06%	6.9922E-03	4.6226E-01	2.5693E-03	3.9000E-01	6.5898E-03	79.32%	1.88%	1.2500E+00	6.5898E-03	8.2349E-03	6.03%	82.35	1.0043E-02	7.35%	190.49
0.2	1.50E+18	150	7.00E+17	0.5	0.00E+18	SiO2	0.6000	1.00	0.37	9.00E+19	50	1.00E+20	15	1.00E+20	SiO2	1.00	2.0805E-02	9.5355E-01	1.6477E-02	8.5999E-01	1.9154E-02	85.94%	12.06%	6.9900E-03	4.6228E-01	2.5685E-03	3.9000E-01	6.5859E-03	79.31%	1.88%	1.2500E+00	6.5859E-03	8.2322E-03	6.03%	82.32	1.0041E-02	7.35%	190.45
0.2	1.50E+18	175	7.00E+17	0.5	0.00E+18	SiO2	0.6000	1.00	0.37	9.00E+19	50	1.00E+20	15	1.00E+20	SiO2	1.00	2.0811E-02	9.5317E-01	1.6505E-02	8.6000E-01	1.9192E-02	86.08%	12.08%	6.9816E-03	4.6226E-01	2.5652E-03	3.9000E-01	6.5775E-03	79.31%	1.88%	1.2500E+00	6.5775E-03	8.2219E-03	6.02%	82.22	1.0050E-02	7.36%	190.70
0.2	1.50E+18	200	7.00E+17	0.5	0.00E+18	SiO2	0.6000	1.00	0.37	9.00E+19	50	1.00E+20	15	1.00E+20	SiO2	1.00	2.0808E-02	9.5371E-01	1.6487E-02	8.6000E-01	1.9178E-02	85.97%	12.07%	6.9678E-03	4.6226E-01	2.5598E-03	3.9000E-01	6.5637E-03	79.31%	1.87%	1.2500E+00	6.5637E-03	8.2046E-03	6.01%	82.05	1.0037E-02	7.35%	190.47
0.2	1.50E+18	225	7.00E+17	0.5	0.00E+18	SiO2	0.6000	1.00	0.37	9.00E+19	50	1.00E+20	15	1.00E+20	SiO2	1.00	2.0808E-02	9.5350E-01	1.6486E-02	8.5999E-01	1.9149E-02	85.89%	12.06%	6.9675E-03	4.6225E-01	2.5597E-03	3.9000E-01	6.5634E-03	79.31%	1.87%	1.2500E+00	6.5634E-03	8.2042E-03	6.01%	82.04	1.0028E-02	7.34%	190.27
0.2	1.50E+18	250	7.00E+17	0.5	0.00E+18	SiO2	0.6000	1.00	0.37	9.00E+19	50	1.00E+20	15	1.00E+20	SiO2	1.00	2.0810E-02	9.5371E-01	1.6487E-02	8.5999E-01	1.9171E-02	85.96%	12.07%	6.9516E-03	4.6217E-01	2.5562E-03	3.9000E-01	6.5544E-03	79.31%	1.87%	1.2500E+00	6.5544E-03	8.1930E-03	6.00%	81.93	1.0033E-02	7.34%	190.43
0.2	1.50E+18	275	7.00E+17	0.5	0.00E+18	SiO2	0.6000	1.00	0.37	9.00E+19	50	1.00E+20	15	1.00E+20	SiO2	1.00	2.0811E-02	9.5391E-01	1.6505E-02	8.6000E-01	1.9192E-02	86.08%	12.08%	6.9563E-03	4.6217E-01	2.5553E-03	3.9000E-01	6.5521E-03	79.31%	1.87%	1.2500E+00	6.5521E-03	8.1902E-03	6.00%	81.90	1.0040E-02	7.35%	190.61
0.2	1.50E+18	300	7.00E+17	0.5	0.00E+18	SiO2	0.6000	1.00	0.37	9.00E+19	50	1.00E+20	15	1.00E+20	SiO2	1.00	2.0809E-02	9.5360E-01	1.6474E-02	8.5999E-01	1.9159E-02	85.92%	12.06%	6.9515E-03	4.6216E-01	2.5534E-03	3.9000E-01	6.5473E-03	79.31%	1.87%	1.2500E+00	6.5473E-03	8.1845E-03	5.99%	81.84	1.0025E-02	7.34%	190.39
0.2	1.50E+18	325	7.00E+17	0.5	0.00E+18	SiO2	0.6000	1.00	0.37	9.00E+19	50	1.00E+20	15	1.00E+20	SiO2	1.00	2.0813E-02	9.5371E-01	1.6492E-02	8.6000E-01	1.9174E-02	85.97%	12.07%	6.9428E-03	4.6215E-01	2.5502E-03	3.9000E-01	6.5319E-03	79.31%	1.87%	1.2500E+00	6.5319E-03	8.1724E-03	5.98%	81.74	1.0029E-02	7.34%	190.42
0.2	1.50E+18	350	7.00E+17	0.5	0.00E+18	SiO2	0.6000	1.00

SILVACO ATLAS Modelling Stats for Tandem GaAs (N-P-P+) GaSb (P-N-N+) solar cell (2000 K Blackbody)

Divs': 10 Points: 4346 Triangles: 8424 Low Doping

P-In 90.725

Upper Cell (GaAs)									Lower Cell (GaSb)								Upper Cell							LowerCell							Combined Results: Dual Junction					Combined Results: Tandem		
N-t	N-d	P-t	P-d	BSF-t	BSF-d	ARC*	L-O	Gap-t	P-t	P-d	N-t	N-d	BSF-t	BSF-d	ARC*	L-O	Jsc	Voc	Pmax	Vmax	Imax	FF	Eff-u	Jsc	Voc	Pmax	Vmax	Imax	FF	Eff-l	V-t	I-t	P-t	Eff-t	W/m^2	P-t	Eff-t	W/m^2
0.5	1.00E+17	1	1.00E+16	0.5	1.00E+17	SiO2	0.50	0.10	0.37	9.80E+19	30	1.00E+20	0.37	1.00E+20	TiO2	0.00	1.1890E+00	1.6938E-11	1.0883E+00	9.0000E-01	1.1208E+00	2.1458E-12	1.14%	4.3807E+01	6.8940E-01	2.5485E+01	6.1000E-01	4.1779E+01	84.39%	28.08%	1.5100E+00	1.1208E+00	1.7419E+00	1.92%	17419.30	2.6189E+01	28.87%	269231.90
0.6	1.00E+17	1.2	1.00E+16	0.6	1.00E+17	SiO2	0.50	0.10	0.37	9.80E+19	30	1.00E+20	0.37	1.00E+20	TiO2	0.00	1.2100E+00	9.9972E-01	1.0446E+00	9.0000E-01	1.1610E+00	86.38%	1.15%	4.3784E+01	3.6894E+08	2.5477E+01	6.1000E-01	4.1765E+01	84.39%	28.08%	1.5100E+00	1.1610E+00	1.7550E+00	1.93%	17550.30	2.6185E+01	28.86%	269217.60
0.7	1.00E+17	1.4	1.00E+16	0.7	1.00E+17	SiO2	0.50	0.10	0.37	9.80E+19	30	1.00E+20	0.37	1.00E+20	TiO2	0.00	1.2168E+00	9.9642E-01	1.0485E+00	8.9998E-01	1.1661E+00	86.58%	1.16%	4.3785E+01	6.8938E-01	2.5471E+01	6.0999E-01	4.1757E+01	84.39%	28.08%	1.5100E+00	1.1661E+00	1.7608E+00	1.94%	17608.03	2.6183E+01	28.86%	269208.80
0.8	1.00E+17	1.6	1.00E+16	0.8	1.00E+17	SiO2	0.50	0.10	0.37	9.80E+19	30	1.00E+20	0.37	1.00E+20	TiO2	0.00	1.2139E+00	9.9357E-01	1.0428E+00	9.0000E-01	1.1586E+00	86.48%	1.15%	4.3779E+01	6.8938E-01	2.5468E+01	6.0999E-01	4.1751E+01	84.39%	28.07%	1.5100E+00	1.1586E+00	1.7485E+00	1.93%	17485.24	2.6174E+01	28.85%	269102.70
0.9	1.00E+17	1.8	1.00E+16	0.9	1.00E+17	SiO2	0.50	0.10	0.37	9.80E+19	30	1.00E+20	0.37	1.00E+20	TiO2	0.00	1.2044E+00	9.9096E-01	1.0386E+00	8.9998E-01	1.1557E+00	86.18%	1.15%	4.3774E+01	6.8937E-01	2.5463E+01	6.1000E-01	4.1745E+01	84.39%	28.07%	1.5000E+00	1.1557E+00	1.7336E+00	1.91%	17335.89	2.6170E+01	28.85%	264932.90
0.95	1.00E+17	1.9	1.00E+16	0.95	1.00E+17	SiO2	0.50	0.10	0.37	9.80E+19	30	1.00E+20	0.37	1.00E+20	TiO2	0.00	1.1978E+00	9.8999E-01	1.0368E+00	8.9998E-01	1.1498E+00	86.00%	1.12%	4.3772E+01	6.8937E-01	2.5464E+01	6.0999E-01	4.1744E+01	84.39%	28.07%	1.5000E+00	1.1498E+00	1.7184E+00	1.89%	17183.51	2.6162E+01	28.84%	264830.60
1	1.00E+17	2	1.00E+16	1	1.00E+17	SiO2	0.50	0.10	0.37	9.80E+19	30	1.00E+20	0.37	1.00E+20	TiO2	0.00	1.1803E+00	9.8818E-01	1.0100E+00	8.9000E-01	1.1348E+00	83.87%	1.11%	4.3770E+01	6.8937E-01	2.5463E+01	6.0999E-01	4.1742E+01	84.39%	28.07%	1.5000E+00	1.1348E+00	1.7002E+00	1.88%	17001.78	2.6155E+01	28.83%	264724.60
1.5	1.00E+17	3	1.00E+16	1.5	1.00E+17	SiO2	0.50	0.10	0.37	9.80E+19	30	1.00E+20	0.37	1.00E+20	TiO2	0.00	1.0814E+00	9.7903E-01	9.1617E-01	8.8000E-01	1.0411E+00	86.53%	1.01%	4.3760E+01	6.8936E-01	2.5456E+01	6.0999E-01	4.1732E+01	84.39%	28.06%	1.4800E+00	1.0411E+00	1.5512E+00	1.71%	15512.32	2.6091E+01	28.76%	263723.67
2	1.00E+17	4	1.00E+16	2	1.00E+17	SiO2	0.50	0.10	0.37	9.80E+19	30	1.00E+20	0.37	1.00E+20	TiO2	0.00	9.4703E-01	9.7228E-01	7.9798E-01	8.8000E-01	9.0680E-01	88.68%	0.88%	4.3736E+01	6.8936E-01	2.5435E+01	6.1000E-01	4.1727E+01	84.39%	28.06%	1.4800E+00	9.0680E-01	1.3211E+00	1.46%	13211.31	2.6006E+01	28.67%	262612.83
2.5	1.00E+17	5	1.00E+16	2.5	1.00E+17	SiO2	0.50	0.10	0.37	9.80E+19	30	1.00E+20	0.37	1.00E+20	TiO2	0.00	8.1085E-01	9.6640E-01	6.7840E-01	8.7000E-01	7.7977E-01	86.97%	0.75%	4.3732E+01	6.8936E-01	2.5431E+01	6.0998E-01	4.1724E+01	84.39%	28.05%	1.4800E+00	7.7977E-01	1.1340E+00	1.27%	11340.40	2.5927E+01	28.58%	261283.96
0.5	1.00E+17	5	1.00E+16	0.5	1.00E+17	SiO2	0.50	0.10	0.37	9.80E+19	30	1.00E+20	0.37	1.00E+20	TiO2	0.00	1.2672E+00	9.7795E-01	1.0585E+00	8.7998E-01	1.2028E+00	85.41%	1.17%	4.3760E+01	6.8936E-01	2.5456E+01	6.0999E-01	4.1732E+01	84.39%	28.06%	1.4800E+00	1.2028E+00	1.7922E+00	1.98%	17921.85	2.6190E+01	28.87%	269148.70
0.5	1.00E+17	10	1.00E+16	0.5	1.00E+17	SiO2	0.50	0.10	0.37	9.80E+19	30	1.00E+20	0.37	1.00E+20	TiO2	0.00	1.2564E+00	9.7462E-01	1.0431E+00	8.7998E-01	1.1854E+00	85.19%	1.15%	4.3750E+01	6.8936E-01	2.5450E+01	6.0999E-01	4.1722E+01	84.39%	28.05%	1.4800E+00	1.1854E+00	1.7661E+00	1.95%	17661.37	2.6173E+01	28.85%	264931.80
0.5	1.00E+17	15	1.00E+16	0.5	1.00E+17	SiO2	0.50	0.10	0.37	9.80E+19	30	1.00E+20	0.37	1.00E+20	TiO2	0.00	1.2551E+00	9.7438E-01	1.0404E+00	8.8000E-01	1.1823E+00	85.08%	1.15%	4.3744E+01	6.8935E-01	2.5446E+01	6.1000E-01	4.1716E+01	84.39%	28.05%	1.4800E+00	1.1823E+00	1.7617E+00	1.94%	17616.54	2.6168E+01	28.84%	264888.40
0.5	1.00E+17	20	1.00E+16	0.5	1.00E+17	SiO2	0.50	0.10	0.37	9.80E+19	30	1.00E+20	0.37	1.00E+20	TiO2	0.00	1.2548E+00	9.7435E-01	1.0388E+00	8.7000E-01	1.1938E+00	84.94%	1.14%	4.3739E+01	6.8935E-01	2.5443E+01	6.0999E-01	4.1713E+01	84.39%	28.04%	1.4800E+00	1.1938E+00	1.7668E+00	1.95%	17667.73	2.6172E+01	28.85%	264819.90
0.5	1.00E+17	25	1.00E+16	0.5	1.00E+17	SiO2	0.50	0.10	0.37	9.80E+19	30	1.00E+20	0.37	1.00E+20	TiO2	0.00	1.2548E+00	9.7427E-01	1.0373E+00	8.7000E-01	1.1923E+00	84.84%	1.14%	4.3735E+01	6.8935E-01	2.5441E+01	6.1000E-01	4.1707E+01	84.39%	28.04%	1.4800E+00	1.1923E+00	1.7646E+00	1.95%	17646.42	2.6168E+01	28.84%	264782.30
0.5	1.00E+17	30	1.00E+16	0.5	1.00E+17	SiO2	0.50	0.10	0.37	9.80E+19	30	1.00E+20	0.37	1.00E+20	TiO2	0.00	1.2547E+00	9.7446E-01	1.0302E+00	8.7000E-01	1.1842E+00	84.38%	1.14%	4.3726E+01	6.8934E-01	2.5432E+01	6.0999E-01	4.1692E+01	84.39%	28.03%	1.4800E+00	1.1842E+00	1.7525E+00	1.93%	17523.43	2.6164E+01	28.83%	264621.20
0.5	1.00E+17	100	1.00E+16	0.5	1.00E+17	SiO2	0.50	0.10	0.37	9.80E+19	30	1.00E+20	0.37	1.00E+20	TiO2	0.00	1.2544E+00	9.7435E-01	1.0154E+00	8.6000E-01	1.1807E+00	83.08%	1.12%	4.3525E+01	6.8920E-01	2.5118E+01	6.1000E-01	4.1497E+01	84.38%	27.90%	1.4700E+00	1.1807E+00	1.7397E+00	1.91%	17396.38	2.6033E+01	28.69%	263283.10
0.5	1.00E+17	200	1.00E+16	0.5	1.00E+17	SiO2	0.50	0.10	0.37	9.80E+19	30	1.00E+20	0.37	1.00E+20	TiO2	0.00	1.2538E+00	9.7462E-01	9.8638E-01	8.3000E-01	1.1884E+00	80.72%	1.09%	4.3508E+01	6.8919E-01	2.5302E+01	6.0999E-01	4.1480E+01	84.38%	27.89%	1.4400E+00	1.1884E+00	1.7113E+00	1.89%	17112.99	2.6027E+01	28.69%	262886.78

*Divisions: used as a measure of model complexity, a setting for the number of vertical and horizontal divisions for each region in the model (in the single cell models there are about 5 X-axis, and 10 Y-axis divisions, each subdivided by the "divs" number).

**ARC: thickness of ARC is dependent on Lambda-0 (optimal wavelength)and ARC refractive index --> arc_depth = Lambda-0 / (4*arc_refractive_index)

THIS PAGE INTENTIONALLY LEFT BLANK

APPENDIX B. SINGLE CELL DECKBUILD SCRIPT

```
############################################################
#        gaas cell test plots using Atlas                  #
#        Thomas, M: Aug 2015                               #
############################################################

go atlas

#############################################
## Parameters                               #
#############################################

# Cell Width (um)
set cell_width=10

# Dimensional multipliers (for realistic current and power numbers)
# Scaling up from set size to 1 square centimeter.
set full_width_mult=10000/$cell_width
set length_mult=10000
set J_mult=$full_width_mult*$length_mult

# Standard # of Divisions [for easy model scaling]
# An increase of one unit represents a unit squared increase in model complexity (at
least)
# Minimum successfully tested: 3 [only took a couple minutes -- 1 and 2 completed, but
produced strange model results].
# Maximum successfully tested: 30 [took about 34 minutes -- above that ran out of memory
or had too many triangles].
#                                [System Config: 8 core 2.4 GHz processor, 12 GB RAM]
set divs=10

# Contact (%)
set contact_percent=8

# Contact Specifications (cathode = upper contact, anode = lower contact)
set c_mat="Aluminum"
set a_mat="Aluminum"
set c_depth=0.3
set a_depth=0.3

set c_width=$cell_width*(0.01*$contact_percent)
#set c_width=$cell_width*0.99
set c_x_min=($cell_width/2)-($c_width/2)
set c_x_max=($cell_width/2)+($c_width/2)

set a_width=$cell_width*(0.01*$contact_percent)
#set a_width=$cell_width*0.99
set a_x_min=($cell_width/2)-($a_width/2)
set a_x_max=($cell_width/2)+($a_width/2)

#Anti-Reflective Coating (ARC) thickness
#Per pveducation.org: optimal AR coating thickness (d) = (wavelength) / (4*refractive
index)
#                                                    d  =  Lambda_0    / (4*n)
#   to minimize reflection at that wavelength (0.6 micron in this case).
#Per refractiveindex.info: n(SiO2) = 1.4585, n(TiO2) = 2.6142, n(ZrO2) = 2.1248, n(Al2O3)
= 1.7557
#   [for testing purposes, n for Air is 1.0002742
#Per IOPScience "Antireflection coatings for GaAs solar cell applications, ZrO2 and Al2O3
are
# components of a highly effective ARC for GaAs solar cells
set Lambda_0 = 0.6
```

```
set arc_mat="SiO2"
set arc_ref_index=1.7557
set arc_depth=$Lambda_0/(4*$arc_ref_index)

#ARC around contacts
set c_arc_width=($cell_width-$c_width)/2
set a_arc_width=($cell_width-$a_width)/2

#Material for gaps above ARC and next to Contacts
set gap_mat="Vacuum"

#GaAs (n, p, and bsf):

# N-Type layer
set n_mat="GaAs"
set n_depth=0.2
set n_dope=1.5000e+18

# P-Type layer
set p_mat="GaAs"
set p_depth=100
set p_dope=7.0000e+17

# BSF Layer
set bsf_mat="GaAs"
set bsf_depth=0.5
set bsf_dope=8.000e+18

#Upper and Lower cell limits (n, p, and bsf regions)
set j_depth=0
set l_top=$j_depth-$n_depth
set l_bot=$j_depth+$p_depth+$bsf_depth

##############################################
#Mesh specification                          #
##############################################

# The "scale_slide" values are used to dynamically adjust the density of the model
# in the substrate layer, p (for upper cell, n for lower cell) in this case.
# For very small values of layer depth (e.g. below 1 micron), these values can cause
# problems with the model, commenting them out here and where they're used in the
# y.mesh specifications can allow the model to run with fairly similar results.

set n_p_scale_slide=($n_depth/($p_depth/2))
set p_bsf_scale_slide=($bsf_depth/($p_depth/2))

# The width mulitplier for the mesh uses a combination of the multipliers for both
# width and length scaling; while this is not physically accurate, it results in
# correct values for amperage output (in A/cm^2).

mesh width=$J_mult

#-- X divisions
x.mesh loc=0.0                      s=$c_arc_width/$divs
x.mesh loc=$c_arc_width             s=$c_width/$divs
x.mesh loc=$c_arc_width+$c_width    s=$c_width/$divs
x.mesh loc=$cell_width              s=$c_arc_width/$divs
#-- Y divisions
y.mesh loc=$l_top-$c_depth            s=$c_depth/$arc_depth
y.mesh loc=$l_top-$arc_depth          s=$arc_depth
y.mesh loc=$l_top                     s=$n_depth/$divs
y.mesh loc=$j_depth                   s=$n_depth/$divs
y.mesh loc=$j_depth+$n_p_scale_slide  s=$n_depth/$divs
y.mesh loc=$j_depth+($p_depth/2)      s=$p_depth/$divs
y.mesh loc=$l_bot-$p_bsf_scale_slide  s=$bsf_depth/$divs
y.mesh loc=$l_bot                     s=$bsf_depth/$divs
y.mesh loc=$l_bot+$arc_depth          s=$a_depth/$arc_depth
y.mesh loc=$l_bot+$a_depth            s=$a_depth/$arc_depth
```

```
##Regions
region num=1   material=$gap_mat x.min=0.0            x.max=$c_x_min y.min=$l_top-
$c_depth   y.max=$l_top-$arc_depth
region num=2   material=$arc_mat x.min=0.0            x.max=$c_x_min y.min=$l_top-
$arc_depth y.max=$l_top
region num=3   material=$c_mat   x.min=$c_x_min x.max=$c_x_max y.min=$l_top-$c_depth
y.max=$l_top
region num=4   material=$arc_mat x.min=$c_x_max x.max=$cell_width    y.min=$l_top-
$arc_depth y.max=$l_top
region num=5   material=$gap_mat x.min=$c_x_max x.max=$cell_width    y.min=$l_top-
$c_depth   y.max=$l_top-$arc_depth
region num=6   material=$n_mat   x.min=0.0      x.max=$cell_width    y.min=$l_top
y.max=$j_depth
region num=7   material=$p_mat   x.min=0.0      x.max=$cell_width    y.min=$j_depth
y.max=$j_depth+$p_depth
region num=8   material=$bsf_mat x.min=0.0      x.max=$cell_width    y.min=$l_bot-
$bsf_depth y.max=$l_bot
region num=9   material=$gap_mat x.min=0.0      x.max=$a_x_min y.min=$l_bot+$arc_depth
y.max=$l_bot+$a_depth
region num=10  material=$arc_mat x.min=0.0      x.max=$a_x_min y.min=$l_bot
y.max=$l_bot+$arc_depth
region num=11  material=$a_mat   x.min=$a_x_min x.max=$a_x_max y.min=$l_bot
y.max=$l_bot+$a_depth
region num=12  material=$arc_mat x.min=$a_x_max x.max=$cell_width    y.min=$l_bot
y.max=$l_bot+$arc_depth
region num=13  material=$gap_mat x.min=$a_x_max x.max=$cell_width
y.min=$l_bot+$arc_depth y.max=$l_bot+$a_depth

##Electrodes
electrode num=1 name=anode   region=3  material=$c_mat x.min=$c_x_min x.max=$c_x_max
y.min=$l_top-$c_depth  y.max=$l_top
electrode num=2 name=cathode region=11 material=$a_mat x.min=$a_x_min x.max=$a_x_max
y.min=$l_bot           y.max=$l_bot+$a_depth

##Doping
#-- N
doping gaussian region=6  n.type conc=$n_dope
#-- P
doping gaussian region=7  p.type conc=$p_dope
#-- BSF
doping gaussian region=8  p.type conc=$bsf_dope

# set contact material to be opaque
material material=$c_mat imag.index=1000
material material=$a_mat imag.index=1000

# :T: Struct out after initial completion [for testing]
#structure outfile=gaas_test.str

###############################################
#Testing                                      #
###############################################

# Models
models conmob fldmob consrh print

# Method
method gummel newton trap atrap=0.8 maxtraps=20 climit=1e-4

# set light beam using inbuilt solar spectrum (AM1.5 or AM0)
#beam num=1 x.origin=$cell_width/2 y.origin=$l_top-10 angle=90 AM1.5 back.refl
beam num=1 x.origin=$cell_width/2 y.origin=$l_top-10 angle=90 AM0 back.refl

# ------------------
# test for IV curve:
# ------------------
```

```
solve init
solve previous

log outfile=gaas_test_iv.log
solve b1=1 beam=1 vcathode=-0.01 vstep=0.01 vfinal=1.0 name=cathode

#tonyplot gaas_test_iv.log -set iv_curve.set

# :T: Struct out after jsc, voc, iv curve tests to get photogeneration results [for
testing]
structure outfile=gaas_test.str

# ---------------------------
# test for spectral response:
# ---------------------------

solve init
solve previous

log outfile=gaas_test_sr.log
solve b1=1 beam=1 lambda=0.30 wstep=0.01 wfinal=1.2

#tonyplot gaas_test_sr.log -set spec_resp.set

# ------------------------------------------------
# calculate internal and external quantum efficiency:
# ------------------------------------------------
extract init inf="gaas_test_sr.log"
extract name="EQE" curve(elect."optical wavelength", -(i."cathode")/elect."source photo
current") outf="gaas_test_EQE.dat"
extract name="IQE" curve(elect."optical wavelength", -(i."cathode")/elect."available
photo current") outf="gaas_test_IQE.dat"

#tonyplot gaas_test_EQE.dat -overlay gaas_test_IQE.dat -set quant_eff.set

# ------------------------------------------------------------------
# calculate overall cell efficiency and general electrical parameters):
# ------------------------------------------------------------------
# The below is adapted from the SILVACO example solarex12
# input variables are appropriately adjusted for the init infile (e.g. cathode vice anode
--> whatever
# some variable names are adjusted for clarity as well (e.g. "Pm" --> "Pmax")

#Power in is based on integrated value of desired spectrum converted from W/m^2 -->
W/cm^2
#For reference: AM0 = 1366 W/m^2, AM1.5g (global) = 1000 W/m^2, AM1.5d (direct, for
concentrators) = 900 W/m^2
#set P_In = (900 / 10000)
#set P_In = (1000 / 10000)
set P_In = (1366 / 10000)

extract init infile="gaas_test_iv.log"
extract name="Jsc" y.val from curve(v."cathode", i."anode") where x.val=0.0
extract name="Voc" x.val from curve(v."cathode", i."anode") where y.val=0.0
extract name="P" curve(v."cathode", (v."cathode" * i."anode")) outf="gaas_test_P.dat"
extract name="Pmax" max(curve(v."cathode", (v."cathode" * i."anode")))
extract name="Vmax" x.val from curve(v."cathode", (v."cathode"*i."anode")) where
y.val=$"Pmax"
extract name="Imax" $"Pmax"/$"Vmax"
extract name="FF" $"Pmax"/($"Jsc"*$"Voc")*100
extract name="Eff" ($Pmax/$P_In)*100

#Real world GaAs (thin film, 0.9927 cm^2) stats for comparison (Jsc in mA/cm^2 -->
A/cm^2, Voc in V):
#Per "Solar cell efficiency tables (Version 45)", Green, et. al; Prog. Photovolt: Res.
Appl. 2015; 23: 1-9
set Jsc_realCell = (29.68/1000)
set Voc_realCell = 1.122
```

```
set FF_realCell  = 0.865*100
set Eff_realCell = 0.288*100

extract name ="Jsc_check" $Jsc / $Jsc_realCell
extract name ="Voc_check" $Voc / $Voc_realCell
extract name ="FF_check"  $FF  / $FF_realCell
extract name ="Eff_check" $Eff / $Eff_realCell

# :T: Struct out after all tests run [for testing]
#structure outfile=gaas_test.str

#tonyplot gaas_test.str
```

THIS PAGE INTENTIONALLY LEFT BLANK

APPENDIX C. TANDEM CELL DECKBUILD SCRIPT

```
############################################################
#      tandem gaas-gasb cell test plots using Atlas        #
#      Thomas, M: Aug 2015                                 #
############################################################

go atlas

#############################################
## Parameters                               #
#############################################

# Cell Width (um)
set cell_width=10

# Dimensional multipliers (for realistic current and power numbers)
# Scaling up from set size to 1 square centimeter.
set full_width_mult=10000/$cell_width
set length_mult=10000
set J_mult=$full_width_mult*$length_mult

# Standard # of Divisions [for easy model scaling]
# An increase of one unit represents a unit squared increase in model complexity (at
least)
# Minimum successfully tested: 3 [only took a couple minutes -- 1 and 2 completed, but
produced strange model results].
# Maximum successfully tested: 30 [took about 34 minutes -- above that ran out of memory
or had too many triangles].
#                                [System Config: 8 core 2.4 GHz processor, 12 GB RAM]
set divs=10

# Contact (%)
set contact_percent=8

# Contact Specifications (cathode = upper contact, anode = lower contact; u=upper cell,
l=lower cell)
set uc_mat="Aluminum"
set ua_mat="Aluminum"
set uc_depth=0.5
set ua_depth=0.5

set lc_mat="Aluminum"
set la_mat="Aluminum"
set lc_depth=0.5
set la_depth=0.5

set uc_width=$cell_width*(0.01*$contact_percent)
#set uc_width=$cell_width*0.99
set uc_x_min=($cell_width/2)-($uc_width/2)
set uc_x_max=($cell_width/2)+($uc_width/2)

set ua_width=$cell_width*(0.01*$contact_percent)
#set ua_width=$cell_width*0.99
set ua_x_min=($cell_width/2)-($ua_width/2)
set ua_x_max=($cell_width/2)+($ua_width/2)

set lc_width=$cell_width*(0.01*$contact_percent)
#set lc_width=$cell_width*0.99
set lc_x_min=($cell_width/2)-($lc_width/2)
set lc_x_max=($cell_width/2)+($lc_width/2)

#set la_width=$cell_width*(0.01*$contact_percent)
```

```
set la_width=$cell_width*0.99
set la_x_min=($cell_width/2)-($la_width/2)
set la_x_max=($cell_width/2)+($la_width/2)

#Anti-Reflective Coating (ARC) thickness
#Per pveducation.org: optimal AR coating thickness (d) = (wavelength) / (4*refractive
index)
#                                                    d  =  Lambda_0    / (4*n)
#   to minimize reflection at that wavelength (0.6 and 1.0 micron in this case).
#Per refractiveindex.info: n for SiO2 is 1.4585, n for TiO2 is 2.6142
#   [for testing purposes, n for Air is 1.0002742
#After testing SiO2, TiO2, and Air, SiO2 is an effective ARC for Silicon cells.

#Upper cell ARC
set u_Lambda_0 = 0.6
set uarc_mat="SiO2"
set uarc_ref_index=1.4585
set uarc_depth=$u_Lambda_0/(4*$uarc_ref_index)

# ARC around contacts
set uc_arc_width=($cell_width-$uc_width)/2
set ua_arc_width=($cell_width-$ua_width)/2

#Lower cell ARC
#set l_Lambda_0 = (1.0 - $u_Lambda_0)
set l_Lambda_0 = 1.0
set larc_mat="SiO2"
set larc_ref_index=1.4585
set larc_depth=($l_Lambda_0/(4*$larc_ref_index))

# ARC around contacts
set lc_arc_width=($cell_width-$lc_width)/2
set la_arc_width=($cell_width-$la_width)/2

#Material for gaps above ARC and next to Contacts
set gap_mat="Vacuum"

#Material and gap distance for between cells
set tgap_mat="TiO2"
set tgap_depth=0.5

#P, N, and BSF layers:

#Upper cell
#----------
# N-Type layer
set un_mat="GaAs"
set un_depth=0.2
set un_dope=1.5000e+18

# P-Type layer
set up_mat="GaAs"
set up_depth=1.0
set up_dope=7.0000e+17

# BSF Layer (P+)
set ubsf_mat="GaAs"
set ubsf_depth=0.5
set ubsf_dope=8.000e+18

#Lower cell
#----------
# P-Type layer
set lp_mat="GaSb"
set lp_depth=0.37
set lp_dope=9.8000e+19

# N-Type layer
```

```
set ln_mat="GaSb"
set ln_depth=45
set ln_dope=1.0000e+20

# BSF Layer (N+)
set lbsf_mat="GaSb"
set lbsf_depth=0.37
set lbsf_dope=1.0000e+20

#Upper and Lower cell limits (p, n, and bsf regions -- for some simpler / shorter math in
mesh statements)
set uj_depth=0
set u_top=$uj_depth-$un_depth
set u_bot=$uj_depth+$up_depth+$ubsf_depth

set lj_depth=$u_bot+$ua_depth+$tgap_depth+$lc_depth+$lp_depth
set l_top=$lj_depth-$lp_depth
set l_bot=$lj_depth+$ln_depth+$lbsf_depth

##############################################
#Mesh specification                          #
##############################################

# The "scale_slide" values are used to dynamically adjust the density of the model
# in the substrate layer, p (for upper cell, n for lower cell) in this case.
# For very small values of layer depth (e.g. below 1 micron), these values can cause
# problems with the model, commenting them out here and where they're used in the
# y.mesh specifications can allow the model to run with fairly similar results.

set un_p_scale_slide=($un_depth/($up_depth/2))
set up_bsf_scale_slide=($ubsf_depth/($up_depth/2))

set lp_n_scale_slide=($lp_depth/($ln_depth/2))
set ln_bsf_scale_slide=($lbsf_depth/($ln_depth/2))

# The width mulitplier for the mesh uses a combination of the multipliers for both
# width and length scaling; while this is not physically accurate, it results in
# correct values for amperage output (in A/cm^2).

mesh width=$J_mult

#-- X divisions
x.mesh loc=0.0                      s=$uc_arc_width/$divs
x.mesh loc=$uc_arc_width            s=$uc_width/$divs
x.mesh loc=$uc_arc_width+$uc_width  s=$uc_width/$divs
x.mesh loc=$cell_width              s=$uc_arc_width/$divs

#-- Y divisions
#----Upper Cell
y.mesh loc=$u_top-$uc_depth           s=$uc_depth/$uarc_depth
y.mesh loc=$u_top-$uarc_depth         s=$uarc_depth
y.mesh loc=$u_top                     s=$un_depth/$divs
y.mesh loc=$uj_depth                  s=$un_depth/$divs
y.mesh loc=$uj_depth+$un_p_scale_slide s=$un_depth/$divs
y.mesh loc=$uj_depth+($up_depth/2)    s=$up_depth/$divs
y.mesh loc=$u_bot-$up_bsf_scale_slide  s=$ubsf_depth/$divs
y.mesh loc=$u_bot                     s=$ubsf_depth/$divs
y.mesh loc=$u_bot+$uarc_depth         s=$ua_depth/$uarc_depth
y.mesh loc=$u_bot+$ua_depth           s=$ua_depth/$uarc_depth

#----Tandem Cell Gap: average between bottom of top and top of bottom cells
y.mesh loc=(($u_bot+$ua_depth)+($l_top-$lc_depth))/2 s=$tgap_depth/$divs

#----Lower Cell
y.mesh loc=$l_top-$lc_depth           s=$lc_depth/$larc_depth
y.mesh loc=$l_top-$larc_depth         s=$larc_depth
y.mesh loc=$l_top                     s=$lp_depth/$divs
y.mesh loc=$lj_depth                  s=$lp_depth/$divs
```

```
y.mesh loc=$lj_depth+$lp_n_scale_slide s=$lp_depth/$divs
y.mesh loc=$lj_depth+($ln_depth/2)     s=$ln_depth/$divs
y.mesh loc=$l_bot-$ln_bsf_scale_slide  s=$lbsf_depth/$divs
y.mesh loc=$l_bot                      s=$lbsf_depth/$divs
y.mesh loc=$l_bot+$larc_depth          s=$la_depth/$larc_depth
y.mesh loc=$l_bot+$la_depth            s=$la_depth/$larc_depth

##Regions
#--Upper Cell
region num=1   material=$gap_mat  x.min=0.0       x.max=$uc_x_min   y.min=$u_top-
$uc_depth   y.max=$u_top-$uarc_depth
region num=2   material=$uarc_mat x.min=0.0       x.max=$uc_x_min   y.min=$u_top-
$uarc_depth y.max=$u_top
region num=3   material=$uc_mat   x.min=$uc_x_min x.max=$uc_x_max   y.min=$u_top-
$uc_depth   y.max=$u_top
region num=4   material=$uarc_mat x.min=$uc_x_max x.max=$cell_width y.min=$u_top-
$uarc_depth y.max=$u_top
region num=5   material=$gap_mat  x.min=$uc_x_max x.max=$cell_width y.min=$u_top-
$uc_depth   y.max=$u_top-$uarc_depth
region num=6   material=$un_mat   x.min=0.0       x.max=$cell_width y.min=$u_top
y.max=$uj_depth
region num=7   material=$up_mat   x.min=0.0       x.max=$cell_width y.min=$uj_depth
y.max=$uj_depth+$up_depth
region num=8   material=$ubsf_mat x.min=0.0       x.max=$cell_width y.min=$u_bot-
$ubsf_depth y.max=$u_bot
region num=9   material=$tgap_mat x.min=0.0       x.max=$ua_x_min
y.min=$u_bot+$uarc_depth y.max=$u_bot+$ua_depth
region num=10  material=$uarc_mat x.min=0.0       x.max=$ua_x_min   y.min=$u_bot
y.max=$u_bot+$uarc_depth
region num=11  material=$ua_mat   x.min=$ua_x_min x.max=$ua_x_max   y.min=$u_bot
y.max=$u_bot+$ua_depth
region num=12  material=$uarc_mat x.min=$ua_x_max x.max=$cell_width y.min=$u_bot
y.max=$u_bot+$uarc_depth
region num=13  material=$tgap_mat x.min=$ua_x_max x.max=$cell_width
y.min=$u_bot+$uarc_depth y.max=$u_bot+$ua_depth

#--Tandem Cell Gap
region num=14  material=$tgap_mat x.min=0.0     x.max=$cell_width
y.min=$u_bot+$ua_depth y.max=$l_top-$lc_depth

#--Lower Cell
region num=15  material=$tgap_mat x.min=0.0       x.max=$lc_x_min   y.min=$l_top-
$lc_depth   y.max=$l_top-$larc_depth
region num=16  material=$larc_mat x.min=0.0       x.max=$lc_x_min   y.min=$l_top-
$larc_depth y.max=$l_top
region num=17  material=$lc_mat   x.min=$lc_x_min x.max=$lc_x_max   y.min=$l_top-
$lc_depth   y.max=$l_top
region num=18  material=$larc_mat x.min=$lc_x_max x.max=$cell_width y.min=$l_top-
$larc_depth y.max=$l_top
region num=19  material=$tgap_mat x.min=$lc_x_max x.max=$cell_width y.min=$l_top-
$lc_depth   y.max=$l_top-$larc_depth
region num=20  material=$lp_mat   x.min=0.0       x.max=$cell_width y.min=$l_top
y.max=$lj_depth
region num=21  material=$ln_mat   x.min=0.0       x.max=$cell_width y.min=$lj_depth
y.max=$lj_depth+$ln_depth
region num=22  material=$lbsf_mat x.min=0.0       x.max=$cell_width y.min=$l_bot-
$lbsf_depth y.max=$l_bot
region num=23  material=$gap_mat  x.min=0.0       x.max=$la_x_min
y.min=$l_bot+$larc_depth y.max=$l_bot+$la_depth
region num=24  material=$larc_mat x.min=0.0       x.max=$la_x_min   y.min=$l_bot
y.max=$l_bot+$larc_depth
region num=25  material=$la_mat   x.min=$la_x_min x.max=$la_x_max   y.min=$l_bot
y.max=$l_bot+$la_depth
region num=26  material=$larc_mat x.min=$la_x_max x.max=$cell_width y.min=$l_bot
y.max=$l_bot+$larc_depth
region num=27  material=$gap_mat  x.min=$la_x_max x.max=$cell_width
y.min=$l_bot+$larc_depth y.max=$l_bot+$la_depth
```

```
##Electrodes (actual contact names set here -- adjust here if necessary, not in mesh
specification)
electrode num=1 name=anode     region=3  material=$uc_mat x.min=$uc_x_min x.max=$uc_x_max
y.min=$u_top-$uc_depth y.max=$u_top
electrode num=2 name=cathode   region=11 material=$ua_mat x.min=$ua_x_min x.max=$ua_x_max
y.min=$u_bot           y.max=$u_bot+$ua_depth

electrode num=3 name=collector region=17 material=$lc_mat x.min=$lc_x_min x.max=$lc_x_max
y.min=$l_top-$lc_depth y.max=$l_top
electrode num=4 name=emitter   region=25 material=$la_mat x.min=$la_x_min x.max=$la_x_max
y.min=$l_bot           y.max=$l_bot+$la_depth

##Doping
#-- Upper Cell: GaAs (N on P on P+)
#---- N
doping gaussian region=6  n.type conc=$un_dope
#---- P
doping gaussian region=7  p.type conc=$up_dope
#---- BSF
doping gaussian region=8  p.type conc=$ubsf_dope

#-- Lower Cell: GaSb (P on N on N+)
#---- P
doping gaussian region=20 p.type conc=$lp_dope
#---- N
doping gaussian region=21 n.type conc=$ln_dope
#---- BSF
doping gaussian region=22 n.type conc=$lbsf_dope

# set contact material to be opaque
material material=$uc_mat imag.index=1000
material material=$ua_mat imag.index=1000
material material=$lc_mat imag.index=1000
material material=$la_mat imag.index=1000

# :T: Struct out after initial completion [for testing]
structure outfile=gaas_gasb_tandem.str

################################################
#Testing                                       #
################################################

# Models
models conmob fldmob consrh print

# Method
method gummel newton trap atrap=0.8 maxtraps=20 climit=1e-4

# set light beam using solar spectrum from external file
#beam num=1 x.origin=$cell_width/2 y.origin=$u_top-100 angle=90 AM1.5 back.refl
beam num=1 x.origin=$cell_width/2 y.origin=$u_top-100 angle=90 AM0 back.refl

# ------------------
# test for IV curve:
# ------------------

#--Upper cell
solve init
solve previous

log outfile=gaas_gasb_tandem_iv_u.log
solve b1=1 beam=1 vcathode=-0.01 vstep=0.01 vfinal=1.0 name=cathode

#--Lower cell
solve init
solve previous

log outfile=gaas_gasb_tandem_iv_l.log
```

```
solve b1=1 beam=1 vcollector=-0.01 vstep=0.01 vfinal=1.0 name=collector

#tonyplot gaas_gasb_tandem_iv_u.log -overlay gaas_gasb_tandem_iv_l -set iv_curve.set

# :T: Struct out after jsc, voc, iv curve tests to get photogeneration results [for
testing]
structure outfile=gaas_gasb_tandem.str

# --------------------------
# test for spectral response:
# --------------------------

solve init
solve previous

log outfile=gaas_gasb_tandem_sr.log
solve b1=1 beam=1 lambda=0.30 wstep=0.01 wfinal=2.0

#tonyplot gaas_gasb_tandem_sr.log -set spec_resp.set

# ------------------------------------------------
# calculate internal and external quantum efficiency:
# ------------------------------------------------
extract init inf="gaas_gasb_tandem_sr.log"
extract name="EQE_u" curve(elect."optical wavelength", (i."anode")/elect."source photo
current") outf="gaas_gasb_tandem_EQE_u.dat"
extract name="IQE_u" curve(elect."optical wavelength", (i."anode")/elect."available photo
current") outf="gaas_gasb_tandem_IQE_u.dat"
extract name="EQE_l" curve(elect."optical wavelength", (i."emitter")/elect."source photo
current") outf="gaas_gasb_tandem_EQE_l.dat"
extract name="IQE_l" curve(elect."optical wavelength", (i."emitter")/elect."available
photo current") outf="gaas_gasb_tandem_IQE_l.dat"
extract name="EQE_t" curve(elect."optical wavelength", (i."anode" +
i."emitter")/elect."source photo current") outf="gaas_gasb_tandem_EQE_t.dat"
extract name="IQE_t" curve(elect."optical wavelength", (i."anode" +
i."emitter")/elect."available photo current") outf="gaas_gasb_tandem_IQE_t.dat"

#tonyplot gaas_gasb_tandem_EQE_u.dat -overlay gaas_gasb_tandem_IQE_u.dat \
# -overlay gaas_gasb_tandem_IQE_l.dat -overlay gaas_gasb_tandem_IQE_l.dat \
# -overlay gaas_gasb_tandem_IQE_t.dat -overlay gaas_gasb_tandem_IQE_t.dat -set
quant_eff.set

# ---------------------------------------------------------------------
# calculate overall cell efficiency and general electrical parameters):
# ---------------------------------------------------------------------
# The below is adapted from the SILVACO example solarex12
# input variables are appropriately adjusted for the init infile (e.g. cathode vice anode
--> whatever
# some variable names are adjusted for clarity as well (e.g. "Pm" --> "Pmax")

#Power in is based on integrated value of desired spectrum converted from W/m^2 -->
W/cm^2
#For reference: AM0 = 1366 W/m^2, AM1.5g (global) = 1000 W/m^2, AM1.5d (direct, for
concentrators) = 900 W/m^2
#set P_In = (900 / 10000)
#set P_In = (1000 / 10000)
set P_In = (1366 / 10000)

#-------------------------------#
#  Calculations for upper cell  #
#-------------------------------#
extract init infile="gaas_gasb_tandem_iv_u.log"
extract name="uJsc" y.val from curve(v."cathode", i."anode") where x.val=0.0
extract name="uVoc" x.val from curve(v."cathode", i."anode") where y.val=0.0
extract name="uP" curve(v."cathode", (v."cathode" * i."anode"))
outf="gaas_gasb_tandem_uP.dat"
extract name="uPmax" max(curve(v."cathode", (v."cathode" * i."anode")))
```

```
extract name="uVmax" x.val from curve(v."cathode", (v."cathode"*i."anode")) where
y.val=$"uPmax"
extract name="uImax" $"uPmax"/$"uVmax"
extract name="uFF" $"uPmax"/($"uJsc"*$"uVoc")*100
extract name="uEff" ($uPmax/$P_In)*100

#Real world GaAs (thin film, 0.9927 cm^2) stats for comparison (Jsc in mA/cm^2 -->
A/cm^2, Voc in V):
#Per "Solar cell efficiency tables (Version 45)", Green, et. al; Prog. Photovolt: Res.
Appl. 2015; 23: 1-9
set Jsc_realCellu = (29.68/1000)
set Voc_realCellu = 1.122
set FF_realCellu  = 0.865*100
set Eff_realCellu = 0.288*100

extract name ="Jsc_check" $uJsc / $Jsc_realCellu
extract name ="Voc_check" $uVoc / $Voc_realCellu
extract name ="FF_check"  $uFF  / $FF_realCellu
extract name ="Eff_check" $uEff / $Eff_realCellu

#-----------------------------#
#  Calculations for lower cell #
#-----------------------------#
extract init infile="gaas_gasb_tandem_iv_l.log"
extract name="lJsc" y.val from curve(v."collector", i."emitter") where x.val=0.0
extract name="lVoc" x.val from curve(v."collector", i."emitter") where y.val=0.0
extract name="lP" curve(v."emitter", (v."collector" * i."emitter"))
outf="gaas_gasb_tandem_lP.dat"
extract name="lPmax" max(curve(v."collector", (v."collector" * i."emitter")))
extract name="lVmax" x.val from curve(v."collector", (v."collector"*i."emitter")) where
y.val=$"lPmax"
extract name="lImax" $"lPmax"/$"lVmax"
extract name="lFF" $"lPmax"/($"lJsc"*$"lVoc")*100
extract name="lEff" ($lPmax/$P_In)*100

#Real world GaSb stats for comparison (Jsc in A/cm^2, Voc in V):
#Per "Fundamental Characterization Studies of GaSb Solar Cells," Fraas et. al; Boeing
High Technology Center, Seattle, WA.
set Jsc_realCelll = (5.5/1000)
set Voc_realCelll = 0.491
set FF_realCelll  = 0.813*100
set Eff_realCelll = 0.07*100

extract name ="Jsc_check" $lJsc / $Jsc_realCelll
extract name ="Voc_check" $lVoc / $Voc_realCelll
extract name ="FF_check"  $lFF  / $FF_realCelll
extract name ="Eff_check" $lEff / $Eff_realCelll

#---------------------------------------------------------------#
#  Results for combined cell performance, as dual-junction or    #
#  tandem design, were calculated in an external application     #
#  (e.g. Microsoft Excel) based on upper and lower cell outputs. #
#---------------------------------------------------------------#

# :T: Struct out after all tests run [for testing]
#structure outfile=gaas_gasb_tandem.str

#tonyplot gaas_gasb_tandem.str

quit
```

THIS PAGE INTENTIONALLY LEFT BLANK

LIST OF REFERENCES

[1] Best research-cell efficiencies. (2015). National Renewable Energy Lab. [Online]. Available: http://www.nrel.gov/ncpv/images/efficiency_chart.jpg

[2] M. Bellis. (2015). History: Photovoltaics timeline. [Online]. Available: http://inventors.about.com/od/timelines/a/Photovoltaics.htm

[3] The KamLAND Collaboration. (2011, Jul. 17). Partial radiogenic heat model for Earth revealed through geoneutrino measurements. *Nature Geoscience.* [Online]. *4.* pp. 647–651. Available: http://www.nature.com/articles/ngeo1205.epdf?referrer_access_token=-NVJSaMhiU6T6MV45gIS1NRgN0jAjWel9jnR3ZoTv0NgMR9T2UiKWCSyJgTHai0B-2JL8iFJTjGuIP3NmtF8lip3_6tcDCRi-CHHTcuZqk3AKySIcgm-TVfNYCsRO7k04Kk0KMZBdARXIuvNAIros3txWeLzQF6hUpukMrof-FCDXoN1aXmCxVR44_jYeVs9fR5dYyD6DTLd7tZx0yp3fe2rA-BW7wWHKTvqAsU_CWVs54087y3AxMdPTJusvdKW&tracking_referrer=*physicsworld*.com

[4] R. C. Langham. "Feasibility study and system architecture of radioisotope thermoelectric generation power systems for USMC forward operating bases.," M.S. thesis, Dept. Sys. Eng., Naval Postgraduate School, Monterey, CA, 2013.

[5] B. Davenport, "Advanced thermophotovoltaic cells modeling, optimized for use in radioisotope thermoelectric generators (RTGs) for Mars and deep space missions," M.S. thesis, Dept. of Elect. and Comp. Eng., Naval Postgraduate School, Monterey, CA, 2004.

[6] J. F. Vogt, "A review of thermoelectric materials used in radioisotope thermoelectric generators," M.S. thesis, Dept. of Nuclear Eng, Pennsylvania State University, State College, PA, 1976.

[7] J.P. Reason. "A comparative study of nuclear technology and direct energy conversion methods for space power systems," M.S. thesis, Dept. of Astro. Eng., Naval Postgraduate School, Monterey, CA, 1997.

[8] K. Tate. (2011, Nov. 21). Nuclear generators power NASA deep space probes (infographic). [Online]. Available: http://www.space.com/13702-nuclear-generators-rtg-power-nasa-planetary-probes-infographic.html

[9] New Horizons. (n.d.) NASA. [Online]. Available: http://www.nasa.gov/mission_pages/newhorizons/main/index.html. Accessed Jun. 23, 2015.

[10] "Solar Cells," class notes for EC3240: Renewable Energy At Military Bases and for the Warfighter, Dept. of Elect. and Comp. Eng., Naval Postgraduate School, Monterey, CA, Summer/2014.

[11] M. A. Green, K. Emery, Y. Hishikawa, W. Warta, and E. D. Dunlop. "Solar cell efficiency tables (Version 45), *Prog. Photovolt: Res. Appl.*, vol. 23 no. 1-9, 2015.

[12] Shockley-Queisser limit. (n.d.). *Wikipedia*. Available: https://en.wikipedia.org/wiki/Shockley%E2%80%93Queisser_limit. Accessed June 25, 2015.

[13] Thermoelectric effect. (n.d.) *Wikipedia.*Available: http://en.wikipedia.org/wiki/Thermoelectric_effect. Accessed February 18, 2015.

[14] "Radioisotope thermoelectric generators of the U.S. Navy," USN, Naval Power Unit, Port Hueneme, CA. Jul. 1978.

[15] S. O'Halloran and M. Rodriguez. Power and efficiency measurement in a thermoelectric generator. [Online]. American Society for Engineering Education,, 2012. Available: http://www.asee.org/public/conferences/8/papers/3976/view

[16] A. L. Presby. "Thermophotovoltaic energy conversion in space nuclear reactor power systems," M.S. thesis, Dept. of Mech. and Astro. Eng., Naval Postgraduate School, Monterey, CA, 2004.

[17] E. Nefzaoui, J. Drevillon, and K. Joulain. (2012 Apr. 27). Selective emitters design and optimization for thermophotovoltaic applications. *American Institute of Physics*, [Online]. vol. 111. Available: http://scitation.aip.org/content/aip/journal/jap/111/8/10.1063/1.4705363

[18] About Us. (n.d.). SILVACO. [Online]. Available: http://www.silvaco.com/company/profile/profile.html. Accessed 26 June, 2015.

[19] P. Michalapoulos. "A novel approach for the development and optimization of state-of-the-art photovoltaic devices using Silvaco," M.S. thesis, Depts. of Com. Sci. and Elec. and Comp. Eng., Naval Postgraduate School, Monterey, CA, 2002.

[20] B. J. Canfield. "Advanced modeling of high temperature performance of indium gallium arsenide thermophotovoltaic cells." M.S. thesis, Dept. of Mech. and Astro. Eng., Naval Postgraduate School, Monterey, CA, 2005.

[21] J. Utsler. "Genetic algorithm based optimization of advanced solar cell designs modeled in Silvaco Atlas." M.S. thesis, Dept. of Elect. and Comp. Eng., Naval Postgraduate School, Monterey, CA, 2006.

[22] Atlas. (n.d.). SILVACO. [Online]. Available: http://www.silvaco.com/products/tcad/device_simulation/atlas/atlas.html. Accessed 26 June, 2015.

[23] Atlas User's Manual: Device Simulation Software. Santa Clara, CA: SILVACO, Inc., 2014.

[24] V.M. Andreev, S.V. Sorokina, N. K. Timoshina, V. P. Khvostikov, and M.Z. Shvarts. "Solar cells based on gallium antimonide," *Phys. of Semiconductor Devices*, vol. 43, no. 5, pp. 668–671, 2009.

[25] Innovation starts here – the Alta difference. (n.d.). Alta Devices. [Online]. Available: http://www.altadevices.com/technology-overview/

THIS PAGE INTENTIONALLY LEFT BLANK

INITIAL DISTRIBUTION LIST

1. Defense Technical Information Center
   Ft. Belvoir, Virginia

2. Dudley Knox Library
   Naval Postgraduate School
   Monterey, California